AD-A081 953 NORTHROP CORP HAWTHORNE CA AIRCRAFT GROUP F/G 20/4
HYBRID COMPUTER ERRORS IN ENGINEERING FLIGHT SIMULATION.(U)
AUG 79 R A WEEKS F33615-78-C-3608
UNCLASSIFIED NOR 79-89 AFFDL-TR-79-3091 NL

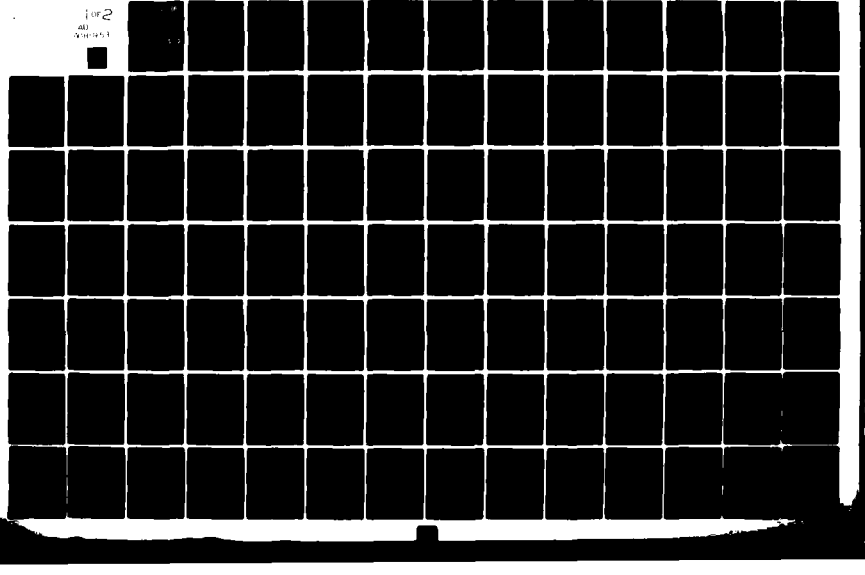

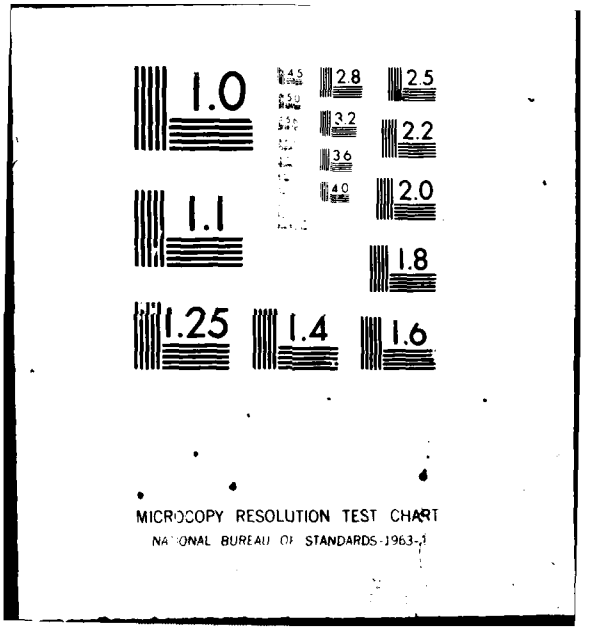
1.0
1.1
1.25
1.4
1.6
1.8
2.0
2.2
2.5
2.8
3.2
3.6
4.0
MICROCOPY RESOLUTION TEST CHART
NATIONAL BUREAU OF STANDARDS-1963-A

LEVEL II

AFFDL-TR-79-3091

HYBRID COMPUTER ERRORS IN ENGINEERING FLIGHT SIMULATION

Richard A. Weeks
Northrop Corporation - Aircraft Group
3901 W. Broadway
Hawthorne, California 90250

August 1979
TECHNICAL REPORT AFFDL-TR-79-3091
Final Report: May 1978 - August 1979

Approved for public release; distribution unlimited

AIR FORCE FLIGHT DYNAMICS LABORATORY
AIR FORCE WRIGHT AERONAUTICAL LABORATORIES
AIR FORCE SYSTEMS COMMAND
WRIGHT-PATTERSON AIR FORCE BASE, OHIO 45433

NOTICE

When Government drawings, specifications, or other data are used for any purpose other than in connection with a definitely related Government procurement operation, the United States Government thereby incurs no responsibility nor any obligation whatsoever; and the fact that the government may have formulated, furnished, or in any way supplied the said drawings, specifications, or other data, is not to be regarded by implication or otherwise as in any manner licensing the holder or any other person or corporation, or conveying any rights or permission to manufacture, use, or sell any patented invention that may in any way be related thereto.

This report has been reviewed by the Information Office (OI) and is releasable to the National Technical Information Service (NTIS). At NTIS, it will be available to the general public, including foreign nations.

This technical report has been reviewed and is approved for publication.

_____ _____

FOR THE COMMANDER

_____

"If your address has changed, if you wish to be removed from our mailing list, or if the addressee is no longer employed by your organization please notify _____,W-PAFB, OH 45433 to help us maintain a current mailing list".

Copies of this report should not be returned unless return is required by security considerations, contractual obligations, or notice on a specific document.

UNCLASSIFIED

SECURITY CLASSIFICATION OF THIS PAGE (When Data Entered)

REPORT DOCUMENTATION PAGE	READ INSTRUCTIONS BEFORE COMPLETING FORM
1. REPORT NUMBER: AFFDL-TR-79-3091	2. GOVT ACCESSION NO. / 3. RECIPIENT'S CATALOG NUMBER
4. TITLE (and Subtitle): HYBRID COMPUTER ERRORS IN ENGINEERING FLIGHT SIMULATION	5. TYPE OF REPORT & PERIOD COVERED: Final Report, May [illegible]78 - Aug [illegible]79
	6. PERFORMING ORG. REPORT NUMBER: NOR 79-89
7. AUTHOR(s): Richard A. Weeks	8. CONTRACT OR GRANT NUMBER(s): F33615-78-C-3608
9. PERFORMING ORGANIZATION NAME AND ADDRESS: Northrop Corporation-Aircraft Group, 3901 W. Broadway, Hawthorne, California 90250	10. PROGRAM ELEMENT, PROJECT, TASK AREA & WORK UNIT NUMBERS: Project 2307
11. CONTROLLING OFFICE NAME AND ADDRESS: Air Force Flight Dynamics Laboratory, Air Force Wright Aeronautical Laboratories, Air Force Systems Command, Wright Patterson Air Force Base, Ohio 45433	12. REPORT DATE: Aug [illegible]79
	13. NUMBER OF PAGES: 118
14. MONITORING AGENCY NAME & ADDRESS (if different from Controlling Office)	15. SECURITY CLASS. (of this report): Unclassified
	15a. DECLASSIFICATION/DOWNGRADING SCHEDULE

16. DISTRIBUTION STATEMENT (of this Report)

Approved for public release; distribution unlimited

17. DISTRIBUTION STATEMENT (of the abstract entered in Block 20, if different from Report)

18. SUPPLEMENTARY NOTES

19. KEY WORDS (Continue on reverse side if necessary and identify by block number)

Error Analysis	Digital Simulation
Flight Simulation	Hybrid Simulation
Mathematical Modeling	Analog Simulation
Real Time	Numerical Integration
Equations of Motion	Power Spectral Density

20. ABSTRACT (Continue on reverse side if necessary and identify by block number)

A real time airframe simulation was constructed with an all analog, hybrid-single Central Processing Unit (CPU), hybrid-dual CPUs with shared common memory, hybrid-dual CPUs with an Input/Output serial link, and all digital computer configurations so as to investigate the effects of various computer error sources on solution accuracy. The airframe simulation represented three degrees-of-freedom of longitudinal motion such that effects of error sources on both short period and phugoid motion could be observed. The error analysis utilized Fast Fourier Transforms which showed how the Power

DD FORM 1 JAN 73 1473 EDITION OF 1 NOV 65 IS OBSOLETE 4-20-175 (over)

SECURITY CLASSIFICATION OF THIS PAGE (When Data Entered)

20. continued

Spectra of the transient airframe response distorted (relative to a theoretical response) when contaminated with error sources.

FOREWORD

This report was prepared for the United States Air Force by the Northrop Corporation - Aircraft Group, 3901 W. Broadway, Hawthorne, California, 90250. It covers work performed during the 15-month program under Air Force Contract F33615-78-C-3608, Project 2307. The work was performed from 15 May 1978 to 15 August 1979.

The studies described in this report were performed by Northrop, in the Flight Simulation Laboratory under the management of Mr. Douglas W. Linder. The Principal Investigator was Mr. Richard A. Weeks and the Air Force Project Engineer was Mr. John J. Bankovskis. The author wishes to acknowledge the contributions of Mr. Paul S. Tsutsui, Mr. Jorge E. Galvis and Mrs. Lonnie Holmes.

TABLE OF CONTENTS

Section			Page
1.	INTRODUCTION		1
2.	SUMMARY		3
3.	REAL TIME COMPUTER ERRORS-ANALYTICAL CONSIDERATIONS		9
	3.1	Literature Survey	9
	3.2	Analog Configuration	10
	3.3	Hybrid-Single Central Processing Unit Configuration	14
	3.4	Hybrid-Multiple CPUs With Shared Memory Configuration	28
	3.5	Hybrid-Multiple CPUs With Input/Output Link Configuration	32
4.	REAL TIME COMPUTER ERRORS-AIRFRAME SIMULATION		35
	4.1	Experimental Investigations	35
	4.2	Airframe Mathematical Model	39
	4.3	Analog Configuration	44
	4.4	Hybrid-Single CPU Configuration	49
	4.5	Hybrid-Dual CPUs With Shared Common Memory Configuration	54
	4.6	Hybrid-Dual CPUs With Input/Output Link Configuration	62
	4.7	Concluding Remarks	66
5.	EFFECTS OF DIGITAL COMPUTER FRAME TIME		67
6.	ERROR ACCUMULATION		82
7.	CONCLUSIONS AND RECOMMENDATIONS		91
	REFERENCES		92
APPENDIX A.	THEORETICAL AIRFRAME		102
APPENDIX B.	SIGNAL ANALYSIS FOR THE INVESTIGATION OF COMPUTER ERRORS		116

LIST OF ILLUSTRATIONS

Figure		Page
1.	General Computer Configuration	4
2.	Effects of Amplifier Bandwidth And Capacitor Dielectric Absorption	14
3.	Hybrid-Single CPU Configuration	15
4.	Relationship Between Truncation And Roundoff Errors	18
5.	Signal Aliasing	21
6.	Quantized Signal	23
7.	Quantizing Characteristic	24
8.	Quantizing Error Characteristic	25
9.	Effect Of A/D And D/A Converter Time Delay	26
10.	Data Reconstruction Hold Circuits	27
11.	Hybrid-Multiple CPUs With Shared Common Memory Configuration	29
12.	Timing Chart	31
13.	Hybrid-Multiple CPUs With I/O Link Configuration	33
14.	I/O Link Diagram	33
15.	Power Spectrum Of A 3 Bit And 15 Bit Quantizer	37
16.	Quantizer Map	38
17.	Typical Pitch Attitude Power Spectral Density	43
18.	Analog Configuration	44
19.	Analog Test Results-Pitch Attitude	46
20.	Analog Test Results-Angle Of Attack	47
21.	Analog Test Results-Forward Velocity	48

LIST OF ILLUSTRATIONS (continued)

Figure		Page
22.	Hybrid-Single CPU Configuration	49
23.	Effects Of Time Delay Due To Hybrid Linkage	51
24.	Effects Of Linkage Word Length	52
25.	Effects Of Frame Time	54
26.	Hybrid-Dual CPUs With Shared Common Memory Configuration	55
27.	Effects Of Time Delay Due To Hybrid Linkage	57
28.	Effects Of Quantization Resolution	57
29.	Peak Power Magnitude Shift Due To Frame Time	59
30.	Reference Frequency Shift Due To Frame Time	59
31.	Airframe Mechanization Timing Chart	60
32.	Effects Of Asynchronous Frame Times	62
33.	Hybrid-Dual CPUs With I/O Link Configuration	63
34.	Peak Power Magnitude Shift Due To Frame Time	65
35.	Effects Of Quantization Resolution	65
36.	Variation In Bode Gain Due To Frame Time	69
37.	Variation In Bode Phase Angle Due To Frame Time	71
38.	Bode Gain For Forward Velocity, Frame Time = 0.1 Seconds	72
39.	Bode Phase Angle For Forward Velocity, Frame Time = 0.1 Seconds	73
40.	Bode Gain For Angle Of Attack, Frame Time = 0.1 Seconds	74
41.	Bode Phase Angle For Angle Of Attack, Frame Time = 0.1 Seconds	76

LIST OF ILLUSTRATIONS (continued)

Figure		Page
42.	Accuracy Chart - Pitch Attitude, Frame Time = 0.00833 Seconds	77
43.	Accuracy Chart - Pitch Attitude, Frame Time = 0.025 Seconds	78
44.	Accuracy Chart - Pitch Attitude, Frame Time = 0.05 Seconds	79
45.	Accuracy Chart - Pitch Attitude, Frame Time = 0.1 Seconds	81
46.	Analog Configuration Error Accumulation	86
47.	Hybrid-Single CPU Error Accumulation	87
48.	Hybrid-Dual CPUs With Shared Common Memory Error Accumulation	88
49.	Hybrid-Dual CPUs With I/O Link Error Accumulation	90

1. INTRODUCTION

Man-in-the-loop real time simulation, with a sophisticated simulator, requires a large computation facility to provide the capability for effective and detailed mathematical modeling of the air vehicle and its subsystems, as well as provide the medium for execution of simulator hardware (motion, visual and instrument) drives. Analog computers offer simultaneous real time solution of equations and maintain a continuous solution which makes this method of computation attractive, especially for modern high-speed fighter aircraft flight control system mechanizations. The flight control systems typically involve frequencies which are a decade higher than the airframe. However, as an analog simulation grows in size and becomes more complex, checkout and setup become lengthy. Also, more sophisticated flight control systems usually require gain scheduling which then tends to require straight line function generation approximations on the analog computer.

Digital computation, on the other hand, allows for rapid setup and repeatable results, and although function generation is still straight line approximation, many orders of magnitude increases in data points are achieved. Digital computation also allows for detailed airframe modeling through extensive nonlinear aerodynamic data tables. However, digital computers require finite time intervals for computation resulting from the serial processing of information. Simultaneity can be achieved in the digital computer through iterative solutions, but would require larger computational time intervals which may have a more adverse effect on the solution accuracy than the serial solution. This is particularly true when numerical integrations are required during the computational cycle. Many large simulation mechanizations run in a hybrid fashion, where both analog and digital computing methods are employed. In operating a hybrid computer configuration, the best features of both analog and digital computation are utilized; however, errors and problems associated with both, and the communication link between them, must also be addressed.

The objective of this study was to investigate error sources that are inherent in analog, hybrid, and digital computation. An extensive evaluation of existing literature was accomplished for identification of computer error sources, whether hardware or numerical in nature. Initially, error sources were examined analytically for source and expected magnitude. These possible sources of error were then evaluated for the determination of primary sources and subsequent determination of controllable sources. A controllable error source is one which might be deliberately induced or altered for experimental evaluation.

Once the controlled error sources were identified, they were evaluated dynamically with computer mechanizations. Four mathematical models of an airframe were constructed. One was an all analog configuration and the other three were various hybrid configurations. The controlled error sources were then injected into the problem such that their effects on the simulated (numerical) airframe response could be examined. In all evaluations, the numerical response was related to a closed-form solution of the equations-of-motion representing the airframe.

An additional all-digital airframe mechanization was developed which utilized an accurate high-order predictor/corrector integration technique. This computer configuration was utilized solely to evaluate the effects of digital computer frame time on the dynamic response of the simulated airframe. Error accumulation was also addressed in this study from the concept of a particular computer configuration's ability to maintain a steady-state condition.

Section 2 of this report presents a summary and overview of the study, Section 3 then discusses the analytical evaluation of error sources characteristic to particular computer configurations while Section 4 presents the effects of these error sources on the dynamic accuracy of an airframe simulation. Effects of digital computer frame time and error accumulation are discussed in Sections 5 and 6, respectively.

2. SUMMARY

The investigation of hybrid computer errors in engineering flight simulation was accomplished at the Northrop Corporation-Aircraft Group, Flight Simulation Laboratory in Hawthorne, California. Although many error sources are stochastic or random in nature rather than deterministic, and obviously many error sources are directly a function of the computer hardware and its maintained condition, certain types of errors which are present in hybrid simulations can be catagorized due to the specific computer configuration utilized.

In this study, four separate computer configurations were mechanized for the investigation of the effects of error sources on a typical man-in-the-loop aerospace simulation problem. Since it has been shown that even if the complete nonlinear equations are solved on the computer, simplified linearized equations adequately represent the dynamic equations being solved which offer insight into potential computer solution errors (see Reference 53). For this reason, a linear airframe model was utilized for the investigation of the effects of error sources on solution accuracy. Furthermore, as presented in Reference 53, it has been shown that short period airframe dynamics tend to be the most critical to the effects of computer errors.

This conclusion indicates that only a two-degree-of-freedom longitudinal airframe need be simulated to investigate hybrid computer errors. However, since it was desired to examine the effects of hybrid computer errors relative to both high and low frequency equations, a three-degree-of-freedom longitudinal airframe mechanization was maintained. Henceforth, the forward, pitch, and vertical acceleration airframe equations were mechanized. Since the airframe pitch attitude is greatly affected by both the short period dynamics and phugoid motion of the airframe, this variable was utilized extensively throughout the report to indicate results.

Before proceeding with a summary of results, it is worthwhile to describe the computer hardware which was utilized in the study. Since both

analog and hybrid tests were required as well as several types of hybrid configurations with dual CPUs, shared common memory and a digital Input/ Output (I/O) link, specialized and versatile computing equipment was required to support this study. A small portion of the Northrop Corporation Flight Simulation Laboratory's computer facility was utilized to meet this requirement. As shown in Figure 1, three separate Harris Slash 4 digital computers, a shared common memory between two of the Slash 4 computers, an I/O link between two of the Slash 4 computers, digital computer peripherals, an Electronic Associates Incorporated (EAI) hybrid linkage, and a Comcor 5000 analog computer were utilized in the study.

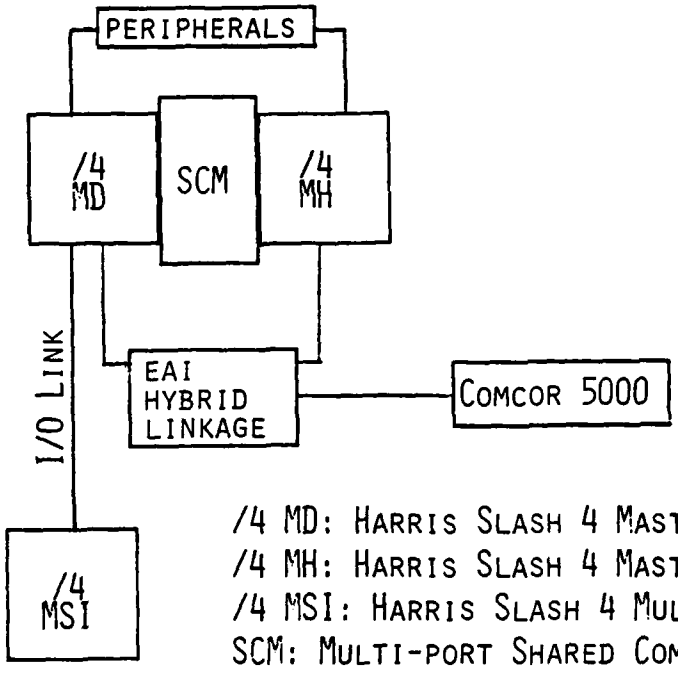

/4 MD: HARRIS SLASH 4 MASTER DIGITAL, 56KW
/4 MH: HARRIS SLASH 4 MASTER HYBRID, 24KW
/4 MSI: HARRIS SLASH 4 MULTIPLE SYSTEM INTERFACE, 96KW
SCM: MULTI-PORT SHARED COMMON MEMORY
EAI HYBRID LINKAGE: 64 A/D, 192 D/A, 96 CONTROL LINES, 96 SENSE LINES
COMCOR 5000: COMCOR ANALOG, 400 AMPS

FIGURE 1. GENERAL COMPUTER CONFIGURATION

The first computer configuration studied utilized the Comcor 5000 analog computer as a stand alone computing system. The second computer configuration examined was a simple hybrid arrangement with a single Central Processing Unit (CPU), the Comcor 5000 and the EAI hybrid linkage. The Master Digital Slash 4 CPU and Master Hybrid Slash 4 CPU, shared common memory, EAI linkage, and Comcor 5000 computer constructed the third computer configuration. Finally, the fourth computer equipment setup utilized the Master Digital Slash 4, the Multiple System Interface Slash 4, an I/O link EAI hybrid linkage, and Comcor 5000 analog computer. All computer configurations utilized a magnetic (Mag) tape unit peripheral to the Master Digital/ Hybrid Slash 4 computers. This was even true of the all analog case described earlier. The Mag tape unit was required for purposes of recording data for a subsequent Power Spectral Density (PSD) analysis.

One of the best methods for investigating error sources is to artificially increase known errors and then measure their effects. Therefore, during the testing for the effects of hybrid computer errors on simulated airframe solution accuracy, a predetermined controlled error scurce configuration was injected into the problem. The influence of the controlled error source could then be noted.

For the majority of the analysis, a PSD approach was utilized. The power spectra of a simulated airframe response was generated for airframe pitch attitude, forward velocity, and angle of attack. This power spectra was then related to the theoretical PSD. After a theoretical reference frequency was established, the shift in reference frequency and power magnitude shift at the reference frequency was measured for the airframe variables mentioned above.

In the analog configuration runs, it was found that if the potentiometer settings were set higher than nominal, the pitch attitude power at the reference frequency would drop. Also, the reference frequency would

shift to a higher value. A previous study (Reference 83) showed that a shift in power spectra magnitude denotes the presence of time delay. Furthermore, it was found that for high tolerance potentiometer values, the angle of attack variable and forward velocity variables increased power at the reference frequency.

Investigations with the hybrid-single CPU runs indicated a sensitivity of the short period and phugoid mode dynamics to time delay associated with the hybrid linkage operation. The effect of the hybrid linkage quantization resolution was found to increase the reference frequency power for pitch attitude while decreasing power for forward velocity when the linkage word size was decreased to coarser values. Digital computer frame time influences tend to increase the reference frequency power with increasing frame time. Furthermore, as the frame time increases, the reference frequency tends to increase in value while the phugoid mode period decreases in value. In all runs for this computer configuration, the hybrid linkage greatly effects the low frequency dynamics as a substantial increase in phugoid frequency of the simulated airframe was observed.

When dual CPUs (Master Hybrid and Master Digital) were utilized with a shared common memory, it was found that the hybrid linkage word length had a large effect on the forward velocity response. This was due to the integration of the forward acceleration equation on the analog computer (Section 4 details the exact configuration). The results indicated an improvement with lower quantization resolutions. Since the pitch and vertical acceleration equations were computed and integrated in the digital computer, the effects of quantization resolution and time delay due to the hybrid linkage were very slight. Small changes in reference frequency power were observed due to the change in analog elevator surface inputs through the linkage.

It was found that when the Master Hybrid frame time was held constant, an increase in the Master Digital frame time produced a decrease in the reference frequency power. When the Master Hybrid frame time was increased with a constant Master Digital frame time, the power change at the reference frequency increased slightly up to a certain point. A further increase in the Master Hybrid frame time, however, offered improved results. The effects of numerical integration technique on solution accuracy tend to increase both the reference frequency power and location.

For the hybrid-dual CPU (Master Digital and MSI) with an I/O link configuration, it was found that for nearly all integration techniques, the power shift at the reference frequency increases negatively as the frame time increases. The one exception was for an Open Euler method. However, this method resulted in a reference frequency shift, whereas the other techniques examined did not distort the system frequency appreciably. The 2nd Order Runge Kutta method appeared impressive for real time numerical integration with the airframe model utilized in the study. Effects of the hybrid linkage word length, in this computer configuration, tended to increase the power frequency magnitude as the quantization coarseness increased. This trend existed for all numerical integration methods examined.

Effects of digital computer frame time were studied by constructing an all digital-single CPU (Master Digital) airframe model with 4th order Runge Kutta numerical integrations. Results showed that frame time had virtually no effect on the forward velocity variable while angle of attack and pitch attitude were greatly influenced by computer frame time.

Error accumulation for the analog and three hybrid computer configurations was investigated by observing the ability of the simulated airframe (in each unique computer configuration) to maintain a given steady-state trim condition. The net effect of accumulated error was to reposition the airframe at a new steady-state trim point. This repositioning occurred for all variables (forward velocity, pitch attitude and angle of attack).

The above discussions presented a brief overview of the results of this study. Besides presenting the analytical aspects of hybrid computer errors, the following sections describe in detail and justify the aforementioned results, as well as present the exact test conditions and computer configurations utilized.

3. REAL TIME COMPUTER ERRORS - ANALYTICAL CONSIDERATIONS

3.1 Literature Survey

An extensive literature search was made from the Defense Documentation Center (DDC) data banks at the Los Angeles facility. This is a user interactive (on-line) computer retrieval system to correlate requested subject areas and identify pertinent documents. The strategy utilized for this study provided for three levels of correlated search. The terms below were searched by the DDC computer (terms preceded by the asterisk denote weighted retrieval terms).

FIRST LEVEL SEARCH TERMS

Analog Simulation
*Computer Applications
Computer Program Reliability
Computer Program Verification
*Computer Programming
*Computer Programs
*Computerized Simulation
Digital Simulation
Hybrid Simulation
*Mathematical Models
Numerical Integration
Numerical Methods and Procedures
Runge Kutta Method

SECOND LEVEL SEARCH TERMS

Algorithms
Computer Errors
Corrections
Difference Equations
Differential Equations
Error Analysis
Errors

THIRD LEVEL SEARCH TERMS

Real Time
Stability
Time Dependence
Time Domain
Time Intervals
Time Lag Theory

From this search strategy, a total of 307 documents were identified as being pertinent to this study by the DDC Computer. Abstracts of these documents were requested and reviewed, from which 50 were eventually selected as being required research literature for this study. In addition to these references, an additional 286 documents were reviewed for relevancy to this study. These latter documents are a part of the reference library in the Northrop Flight Simulation Laboratory.

There appears to be an extreme amount of literature on numerical techniques associated with digital computation relative to that available on analog techniques. This indicates the trend and interest in the use of digital computers to simulate detailed large-scale systems with a minimum amount of computer hardware. Most analog references examined were generated in the 1950's and 1960's, indicating the earlier use of this method of computation. As with the digital computation references, errors associated with hybrid methods are extensively discussed, again denoting the desirability and interest in the use of digital computers for detailed simulations requiring mass data storage, function generation, or decision logic. In general, there is a lack of documented literature on the use of parallel digital computers with communication through a shared common memory. This is also true of the case of multiple digital computers communicating through an Input/Output link, although this case can almost be treated as a single processor if proper data-block transfer methods are employed.

3.2 Analog Configuration

An analog computer performs computations, memorizes , and makes logical decisions on variables in a continuous parallel manner. Therefore, analog computers are especially suited to the solution of differential equations (i.e., performing integration). There seems

to be agreement within the literature that under ideal laboratory conditions, the accuracy of the analog computer can approach 0.01 percent of full scale voltage. However, the accuracy of typical analog computers commercially available tends to range between 0.1 percent and 5 percent of the maximum variation of the variables of interest.

Analog components in the computer have a poor memory capability since machine variables can only be retained for the period of time that capacitors associated with the integrating components can retain them. Another limitation of this type of computer results from the fact that variables must be scaled. Scaling is the procedure of properly setting the attenuator (potentiometer) and amplifier gains. The goal is to provide an adequately large output signal, to reduce the effects of noise, while preventing saturation of the system.

With the analog computer, solution accuracy is directly a function of the accuracy of the computing components. Analog computer errors can be divided into two classes: static and dynamic. Static errors are those caused by misalignments, component imbalance and tolerance, incorrect pot settings and equipment malfunctions to name a few. Dynamic errors are caused by inadequate dynamic characteristics of the equipment which include noise (instantaneous disturbances) and component transfer functions. The net effect is that the computer solution is relative to a machine equation rather than the actual equation. These machine equations produce shifts in the characteristic roots of the differential equation being solved.

Errors occur in operational amplifiers (Op Amps) when the voltage from grid-to-ground differs from zero. Normally, Op Amp grid voltage and current are assumed to be zero. However, amplifiers do not have an infinite open-loop gain and some grid voltage is required to have

the desired output. Also, if the amplifier is not perfectly linear there will be some curvature to the grid voltage in output voltage characteristics, equivalent to a variation in gain. The grid voltage may also have an offset due to drift.

An Op Amp, when used as a summer, will also have a dynamic error since the amplifier has a finite bandwidth. Some studies, as presented in Reference 74, found that an error of 1 percent can occur when the adder bandwidth is 2000 times the highest frequency in the differential equation solution. This dynamic error can be described as having the frequency response characteristic of a first order lag transfer function, or:

$$\frac{E_{out}}{E_{in}} = \frac{K_s}{\tau_s s+1} \tag{3.1}$$

The principal component of the time constant (τ_s) is the lag due to the capacitance from the output to input in parallel with the feedback resistance. Also, there will be a small component due to a lag in the amplifier forward loop which is dependent on the closed loop gain K_s. The summer time constant can be determined experimentally by measuring the phase shift of a sine wave buffered by an Op Amp relative to the pure input sine wave. The ratio of the phase shift to the input sine wave frequency will then determine τ_s. This procedure is described in detail in Reference 13.

For the integrator, as in the case of the Op Amp, grid voltage may occur due to finite amplifier gain, non-linearity, or changes in the effective bias of the amplifier. Grid voltage may also come from feedback capacitor leakage resistance. Grid voltages due to above causes will generally exceed the short-term drift, and will be comparable in magnitude to the long-term drift. Regardless of the cause, the overall

effect of integrator grid voltage is to limit the available computing time for a desired accuracy. In general, the number of computing elements should be minimized and d-c amplifier gains should be kept as low as possible so as to minimize the effects of noise and drift.

One method for determining the drift characteristics of an integrator is to construct an integrator from an Op Amp and then measure the output with a grounded input. Reference 13 documents drift values of 3-5 millivolts/hour (mv/hr) are typically obtained for non-stabilized amplifiers. However, tests on 16 integrators run prior to the airframe simulation reported in Section 4, drift values ranging from 10 mv/hr to 820 mv/hr were obtained. The integrators tested were picked at random and were not intentionally calibrated for the test. Pre-test calibrated integrators most likely would have produced the improved results as presented in Reference 13.

The analysis of the effects of the feedback capacitor utilized in constructing an integrator is complex. The permittivity or dielectric constant of the material used in capacitors is not constant, but rather is a function of temperature and frequency. Therefore, the feedback capacitance used with an Op Amp to construct an integrator should be considered a variable. Reference 24 presents a model for complex capacitance and also considers transient current effects and capacitor voltage recovery. Capacitor dielectric absorption has the effect of inducing damping in the solution and changes the frequency of oscillation of the solution. The damping ratio induced by dielectric absorption is a function of frequency. The solution of a neutrally damped simple harmonic motion ordinary differential equation is well suited to study this phenomenon since any phase shift in the computing components will cause either a decay or an increase in the desired constant amplitude sinusoidal computer solution.

An analog amplifier/integrator test was performed in order to investigate amplifier/integrator bandwidth and capacitor dielectric absorption.

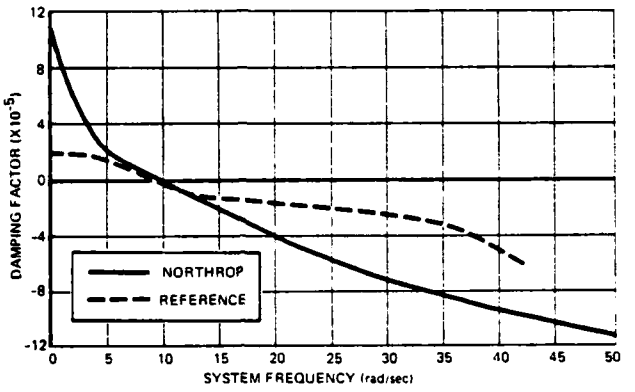

FIGURE 2. EFFECTS OF AMPLIFIER BANDWIDTH AND CAPACITOR DIELECTRIC ABSORPTION

Results of the Northrop test are shown in Figure 2 along with results of tests presented in Reference 24. The tests at Northrop were performed on a Comcor 5000 Analog Computer running in real time, and solved a simple, neutrally damped harmonic motion differential equation. As can be seen in Figure 2, the trends are identical with the Reference 24 findings although the damping factor magnitude tends to differ somewhat between the two tests. This is attributed to slight differences in component characteristics of different computers. It was also found that different amplifiers/integrators in the same computer yield different result magnitudes.

3.3 Hybrid - Single Central Processing Unit Configuration

The hybrid - single central processing unit (CPU) configuration, as typified in Figure 3, provides for the best features of both analog

and digital computation to be utilized. However, errors associated with both methods of computation are encountered as well as the introduction of new error sources generated by the analog/digital and digital/analog communications link (hybrid linkage).

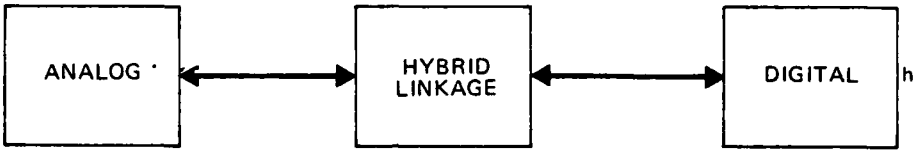

FIGURE 3. HYBRID-SINGLE CPU CONFIGURATION

Errors associated with analog computers were previously discussed in Section 3.2. In contrast to the analog computer, which perform continuous computation, digital computers perform computation, memorization, and logical decisions in terms of variables which appear in discrete form as serial data sequences.

Basically, there are two sources of error in the digital solution of differential equations:

1) Truncation Errors
2) Roundoff Errors

Truncation errors develop from the truncation of an infinite process to give a finite difference approximation to the differential equations being solved. Roundoff errors arise from the limited precision (due to word length) with which arithmetic operations are carried out in the digital computer.

Truncation errors are the result of numerical integration tech-

niques and digital computer frame time. A numerical integration formula transforms a differential equation into a difference equation. In the process of this transformation, many of the higher order terms of the Taylor's Series expansion representing the integration technique are neglected or truncated. This procedure specifies the order of the truncation error which is a function of the digital computer frame time. If the higher derivatives of the series are assumed to be small, the truncation error is then decreased by the use of a smaller frame time. If the frame time is too long to handle the highest frequencies in the modeled system, amplitude and phase errors arise as well as spectral folding or aliasing. In general, a sampling interval of at least twice the frequency of the system being sampled is required (Nyquist or Shannon frequency) although a sampling frequency of 10 to 100 times the system frequency is desirable. Truncation error may sometimes be decreased by using higher-order integration methods. In most cases, the execution time required for digital computation determines the frame time. However, since higher-order integration methods take longer to execute, an appropriate compromise must be reached between the order of the integration algorithm and the frame time.

Many different types of numerical integration techniques are available which include:

1) Single- and Multi-Step prediction methods
2) Predictor - Corrector methods
   a) Iterative methods
   b) Modified methods
   c) Predictor - single corrector methods
3) Single-Step methods

Specific examples of these types of methods are discussed in Section 4, as they apply to real time airframe simulation. Most numerical methods become unstable if the frame time is made too large in relation to the time constants of the system being modeled. However, up to the time where instability occurs, the methods may be computing with the required accuracy, but a further slight increase in step-length into the region of instability results in the generation of completely erroneous solutions. Therefore, the significant difference between the stability of a solution and the accuracy of that solution is when a solution becomes computatively unstable, the errors increase in an unbounded fashion and the result has no physical meaning. However, in a computatively stable solution, the errors are bounded and the results might appear reasonable. This appearance can be extremely deceptive in that the results obtained might not be accurate at all.

There seems to be an absence of discussions in the literature on the absolute effects of roundoff error. Generally, roundoff error effects are treated in a statistical fashion, in order to generate the bounds of their effects. Although truncation errors are more amenable to study, occasionally these errors do not dominate. Many simulations are rendered inaccurate because the roundoff error dominates. This is particularly true in single precision computations in which high frequency response systems are modeled.

Theoretically, it is possible to drive the truncation error to zero as the digital computer frame time is driven to zero. Decreasing the frame time, however, increases the number of computations and thereby increases the roundoff error. As the frame time approaches zero, the roundoff error dominates and the solution becomes unstable. This phenomenon of how the truncation and roundoff error behave in a

converse manner is shown in Figure 4. Unfortunately, the optimum selection of the frame time based on truncation and roundoff error considerations is quite difficult to determine in advance and becomes a matter of trial and error with the modeled system.

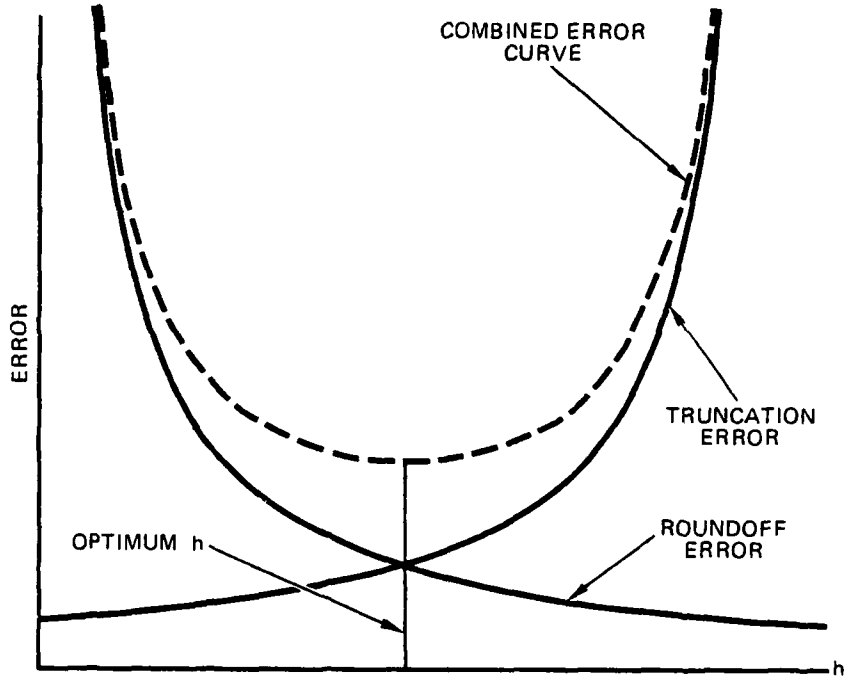

FIGURE 4. RELATIONSHIP BETWEEN TRUNCATION AND ROUNDOFF ERRORS

As shown in Figure 3, the hybrid linkage serves as the communications link between the analog and digital computers. For the purpose

of this study, the hybrid linkage refers to analog-to-digital (A/D), data transfer and digital-to-analog (D/A) data transfer. In A/D conversion, the major system components comprising this part of the hybrid loop include:

1) Multiplexer
2) Sampler
3) Quantizer

For D/A conversion, the system components considered include:

1) Digital-Analog Converter
2) Analog Hold Circuits

The most serious error associated with hybrid computing systems is time delay. This time delay is a result of the D/A and A/D conversion process and the time required for digital computation. Computing time required for digital computation is a direct function of the problem complexity which is not the case with analog computation. This is due to the serial processing of information in the digital computer.

Multiplexing is the process of allowing a single A/D converter (quantizer) to be time shared among a number of analog channels. Errors associated with multiplexers include zero offsets, noninfinite backward resistance, nonzero forward resistance, crosstalk, common-mode pickup, electro-magnetic interference and time delay for switch closure. Many of these errors are associated with the hardware components utilized in the multiplexer. Others are associated with the method or fashion in which the hardware is configured or interfaced. The most influential error source, as previously mentioned, is time delay. This time delay is commonly referred to as skewing.

As a result of skewing in the multiplex unit, the data received by the digital computer represent two different instances in time. One technique for avoiding this problem is to sample and hold all multiplexer inputs. In this manner, all analog channels are sampled simultaneously and then these sampled signals are multiplexed. However, these multiplexed signals now refer to or reflect the same instant in time.

Sampling is unavoidable in a hybrid simulation, since at some instant in time, the continuous analog variables must be converted into a sequence of digital words. Sampling is usually a synchronous process with successive samples being equally spaced in time. Errors in sampling occur due to the sampling operation and the sampler hardware itself. The sampler hardware can induce switching transients and noise into the analog sample. These errors, along with electronic cross-talk, can be eliminated with a signal conditioner such as a low-pass filter. However, this filtering can induce phase shifts into the sampled signals. Another sampler error is jitter, which is a variation in the length of time for the sampling switch to become enabled. Since the sampler switch remains closed for a finite time interval (known as aperture time), and the analog signal undergoes significant change during this time, some uncertainty exists as to the significance of the output of the A/D converter relative to the time continuum being sampled

In sampling theory, a fundamental theorem of sampling was established by C. E. Shannon which concluded that the sampling frequency must be at least twice the frequency of the highest Fourier component of the analog signal being sampled. In other words, two samples per cycle are required to indicate a signal's presence. However, this sample is subject to 100 percent amplitude error under these conditions. If this criteria is not met, spectral folding or aliasing occurs. In general, aliasing errors occur when the time-varying signal being sampled undergoes significant change between samples. Two frequencies are said to be

aliases of each other if sampled data points on their corresponding sinusoids cannot be distinguished. An example of aliasing is shown in Figure 5.

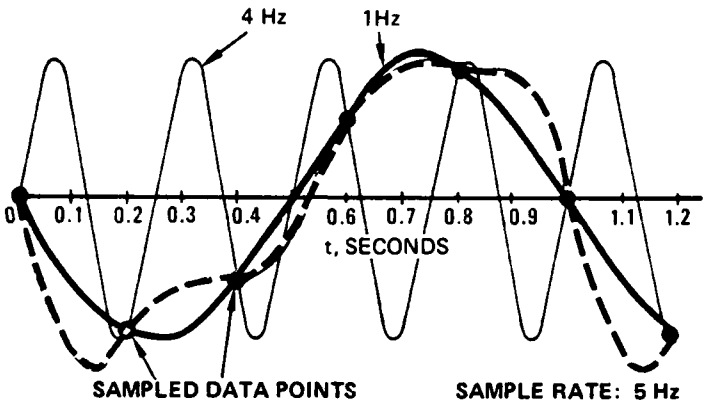

FIGURE 5. SIGNAL ALIASING

In Figure 5, two sinusoidal signals are sampled at a rate of 5 Hertz (Hz). The sampled data points of the 4 Hz sine wave are indistinguishable from those sampled data points of the 1 Hz sine wave. The dashed line represents a third signal (nonsinusoidal) which has the identical sampled output as the 1 Hz and 4 Hz sine waves. An anti-aliasing filter can be used in front of the A/D converter to attenuate the aliases; however if filter parameters are not properly specified, significant gain, phase, and offset errors may be induced.

After an analog quantity is sampled, it undergoes a conversion to a digital word format. This process is known as quantizing. Analog hardware errors associated with quantizing include component tolerance, zero off-sets, and drift. Digital oriented errors include roundoff errors due to word length and digital coding technique. Reference 5 presents an example of how the specific digital code utilized in the quantizer affects the quantizer output. In this example, a pure binary code is employed where a binary digit change from a 0 to 1 condition

occurs more rapidly than the change from a 1 to 0. Now, for example, if an analog value is to change from a magnitude of 3 to 4, the corresponding binary equivalent output from the A/D converter would change from 011 to 100. However, if the 0 to 1 condition changes more rapidly than the 1 to 0 condition, for brief instant in time the A/D converter output would be 111. This would produce an erroneous converter output during the conversion process. This type of error can be eliminated by conversion complete pulse timing. Another method of avoiding digital coding error is to employ special binary codes in which the change from a number to the next smaller or larger number never involves more than a single binary digit at a time.

A major error source in the quantizing process is due to word length employed in the quantizer. Typical word lengths can range from 4 bits to 15 bits, with sign included. The quantizer word length determines the input analog level requirement for the A/D converter output to discretely jump to the next quantum level, q. The quantum level (or grain) q is defined as:

$$q = \frac{E_{fs}}{2^{n-1}} \qquad (3\text{-}2)$$

where:

E_{fs} = full scale analog input
n = quantizer word length (in bits) with sign included.

Quantization errors become significant when it is impractical to utilize a sufficiently large number of bits in characterizing the continuous input.

An example of a quantized signal is shown in Figure 6. The signal being sampled is a smoothly varying continuous function of time. The

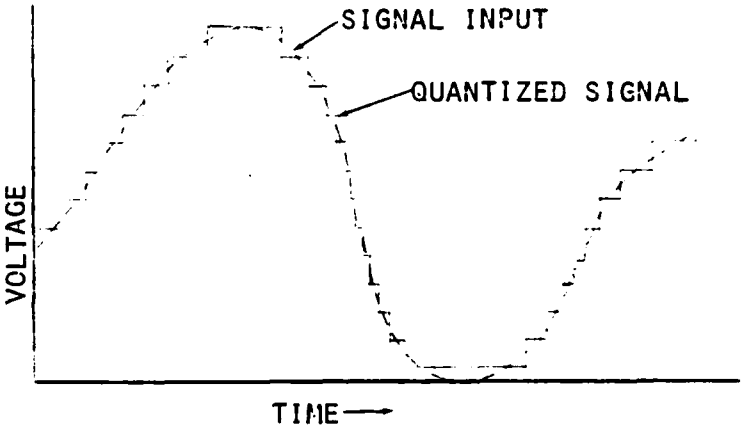

FIGURE 6. QUANTIZED SIGNAL

quantizer output, however, remains constant while the input signal remains within the boundaries of a quantum level and then changes abruptly by one full level when the signal crosses the boundary. The distortion or error consists of the difference between the input and output signals. The maximum instantaneous value of error is one half of one quantum level while the total range of variation is from negative half level to a positive half level. This error is sometimes referred to as a per-step quantizer error.

Since at any given instant of time an input signal might be rapidly crossing back and forth over a quantum level boundary, the distortion caused by quantizing errors produces an effect similar to that of an independent source of noise. Therefore, due to the stochastic nature of the quantizer output, most error analyses of quantization takes a statistical approach. Furthermore, as can be seen in Figure 6, quantization is a highly nonlinear process. Incorporation of such a process within a system makes the entire system nonlinear and therefore difficult to analyze analytically. However, a statistical approach greatly reduces the problem complexity by giving average results. Statistical descriptions of quantization turn out to be fairly straight forward and easy to obtain since the quantizer output density distribution is obtained

by a linear sampling process operating upon the input distribution density.

Assuming a unit ramp input to the quantizer, the quantizing characteristic is that as shown in Figure 7.

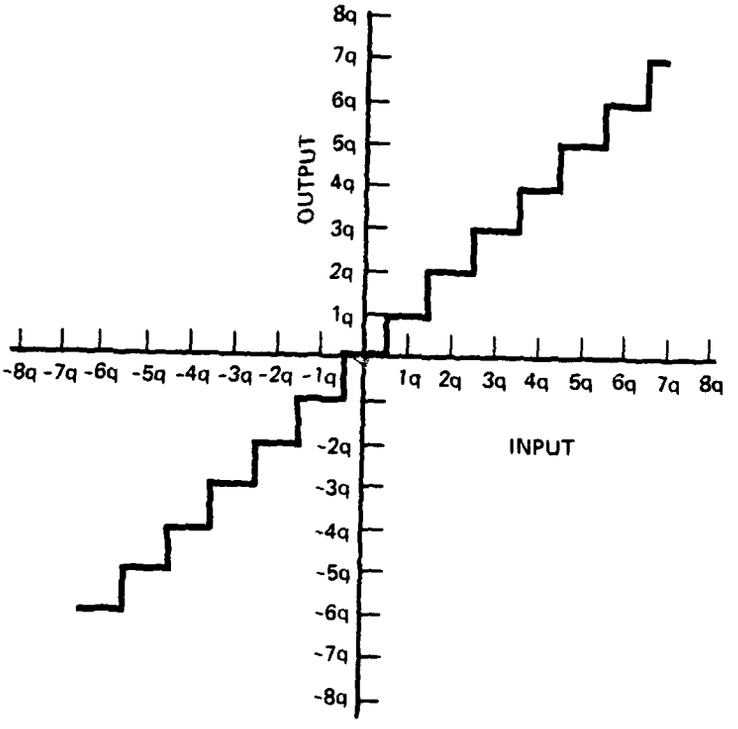

FIGURE 7. QUANTIZING CHARACTERISTIC

The corresponding quantizing error is therefore characterized by the sawtooth signal shown in Figure 8. From the error characteristic shown in Figure 8, the mean square error of the quantizer can be computed as one twelfth of the square of the quantum level magnitude. The accuracy is always improved by decreasing either the sampling rate or quantization grain, or both. However, for course quantization, a rather high increase in sampling rate is required to improve performance. For this case, a small decrease in quantization grain is much more effective.

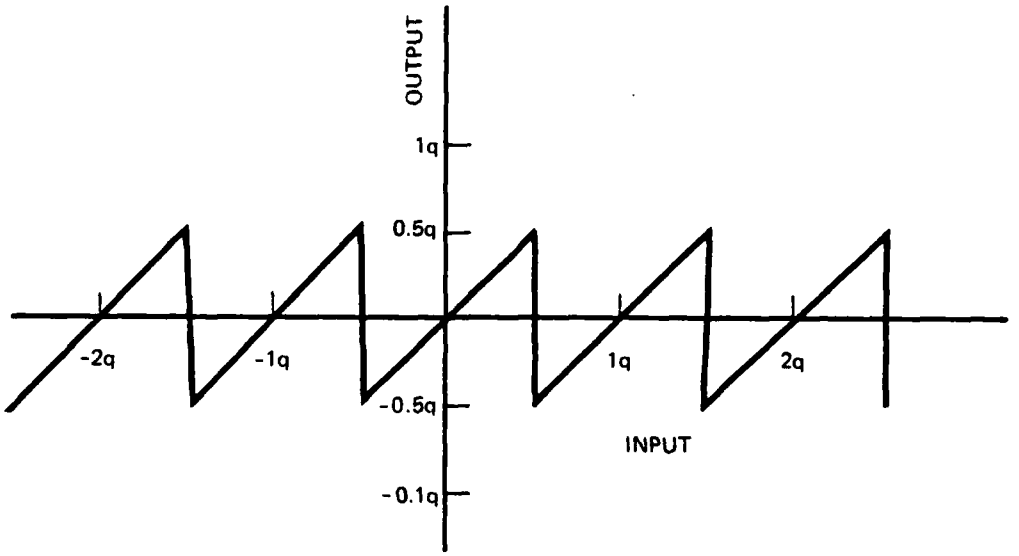

FIGURE 8. QUANTIZING ERROR CHARACTERISTIC

On the other hand, if the quantization grain is fine and a further decrease in grain size offers little improvement, only by an increase in sampling rate would a significant improvement be achieved.

As previously mentioned, time delay is a major source of error in the A/D conversion and D/A conversion processes. A series of tests were run to demonstrate the effects of hybrid linkage time delay on solution accuracy. A linear, second-order, simple harmonic ordinary differential equation (whose theoretical solution is neutrally damped sinusoid) was mechanized. This type of equation is particularly well-suited to this method of investigation, since any time delay induced into the mechanization will change the damping characteristics of the modeled system. The digital processor was free running, and was used only to read the A/D converter and output to the D/A converter. Therefore, time delay in the hybrid solution would be primarily due to the hybrid linkage. The system frequency and number of A/D and D/A channels were varied to investigate the time delay effects. The results of the test are shown in Figure 9.

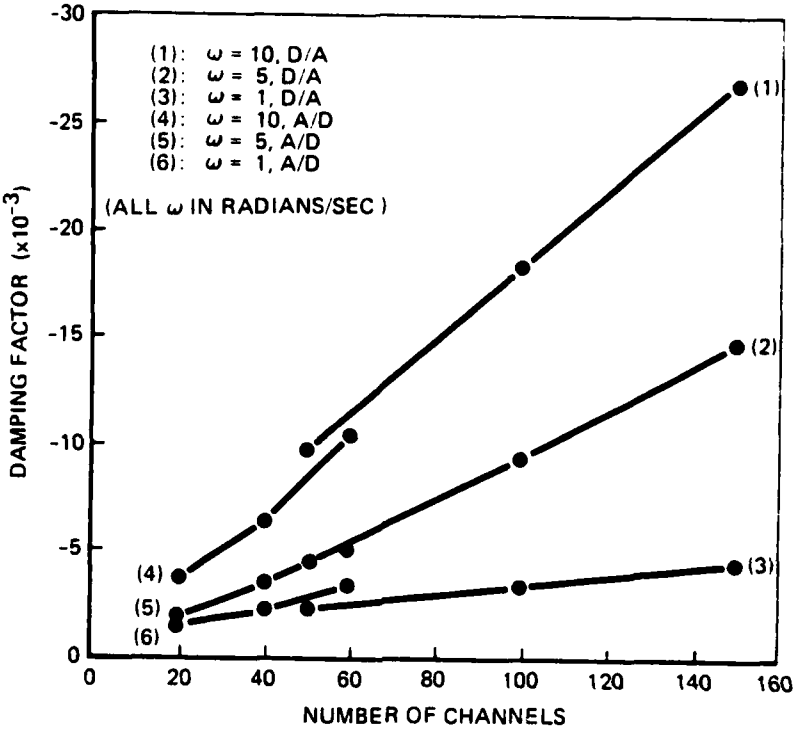

FIGURE 9. EFFECT OF A/D AND D/A CONVERTER TIME DELAY

As can be seen in Figure 9, the simple harmonic frequency was varied between 1 and 10 radians per second. Numbers of A/D channels examined were from 20 to 60 whereas 50 to 150 D/A channels were examined. For a D/A test, only a single A/D channel was utilized; whereas, for an A/D test test, only one D/A channel was used. The measure of time delay was in the effective damping factor of the hybrid solution. Note in Figure 9 how the solution consistently diverges for all test conditions examined (again, the theoretical solution is neutral stability). System frequencies were kept below 10 radians per second since analog bandwidth/ capacitor dielectric absorption tests described earlier showed similar (but with less magnitude) trends at higher frequencies.

The purpose of the D/A converter portion of the hybrid linkage

system is to translate the sequence of words produced in the digital computer into continuous analog voltages. Electronic analog errors induced by the D/A converter are typified by zero off-sets, jitter, and component tolerances. Besides the serious errors induced by linkage time delay (as discussed in the previous few paragraphs) another major error source in the process is due to the data reconstruction method (hold circuits).

Several types of hold circuits, as shown in Figure 10, are available for hybrid linkage systems.

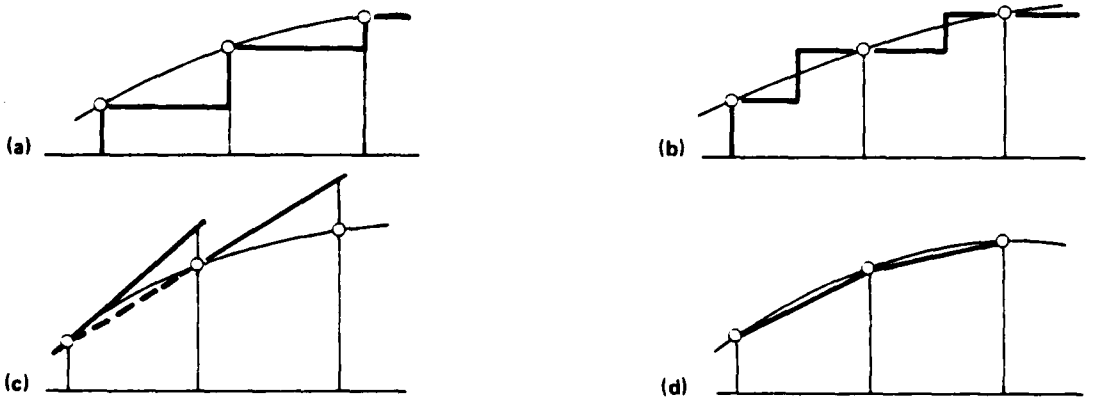

FIGURE 10. DATA RECONSTRUCTION HOLD CIRCUITS

In Figure 10 the following hold circuits are depicted:

(a) Zero-order hold
(b) Zero-order hold with data predicted one-half frame time ahead
(c) First-order hold
(d) First-order polygonal hold

The zero-order hold output from a D/A converter represents the recon-

structed analog variable which is correct at the beginning of each hold period. Furthermore, at this time the reconstructed data usually represent a delayed output due to hybrid linkage time delay. Although the output is delayed, the zero-order hold circuit causes no phase distortion. Smoothing with a low pass filter may help but will induce phase shift. For better data reconstruction, analog circuits can be built up to generate extrapolation polynominals to match successive data points. The simplest is the first-order hold which implements a linear extrapolation from the last two data points. This type of hold circuit, however, causes distortion of the sampled data signals with respect to magnitude and phase. Linear interpolation between the last and next new data point is desirable, but the next data point is in the future and can only be predicted. Exact reconstruction can be achieved with an n-th order polynominal extrapolation if the desired signal is a polynomial of degree less than or equal to n.

3.4 Hybrid-Multiple CPUs With Shared Common Memory Configuration

The hybrid-multiple CPU configuration, with communication between the digital computers through a common area in core, is shown in Figure 11. In this configuration, error sources inherent in the single CPU-hybrid configuration, as discussed in Section 3.3, are experienced as well as some unique errors due to the common memory usage. In this configuration, it is assumed that only one of the digital processors accesses the hybrid linkage.

The most significant additional error source of the computer configuration shown in Figure 11, relative to the hybrid-single CPU case, is due to common memory skewing. Common memory skewing is caused by the free access and modification of the common area of memory by multiple uninterrupted CPUs. When multiple CPUs are used in a parallel uninterrupted fashion, a variable in common memory might be accessed or modified prematurely while attempting to maintain continuity between the parallel processors for a given instant in time. A simple example exemplifies this phenomenon.

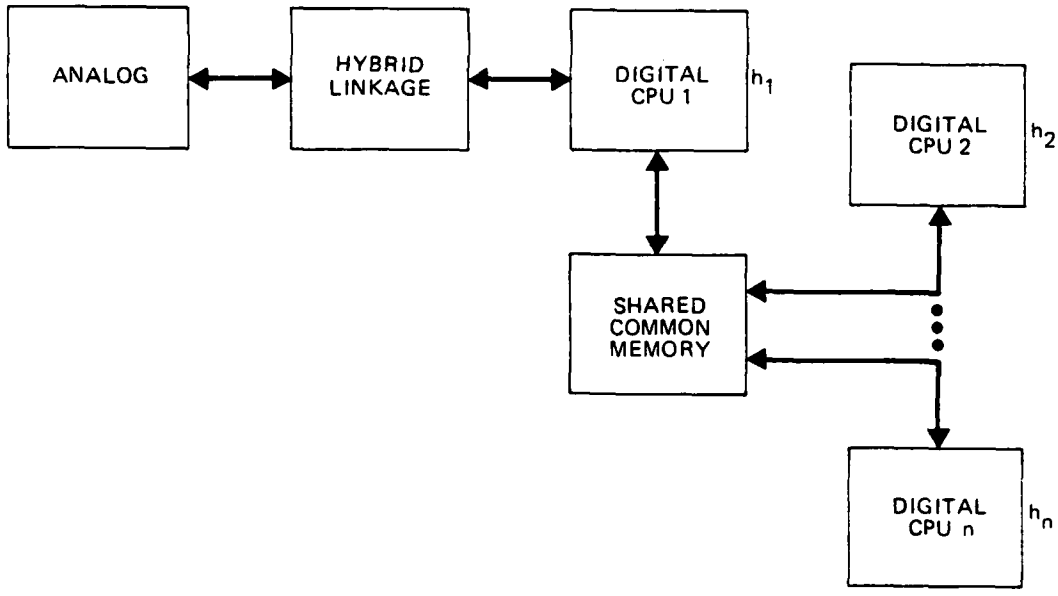

FIGURE 11. HYBRID-MULTIPLE CPUS WITH SHARED COMMON MEMORY CONFIGURATION

Two CPUs are operating at different frame times. CPU No. 1 computes aerodynamic data (table lookup) and executes at 20 milliseconds (msec) while CPU No. 2 computes the aero angles (angle of attack and sideslip angle) and executes at 10 msec. Assume that all of the scheduled time is required for these computations. At the top of the frame, both CPUs start their executions. CPU No. 1 begins aero data generation as a function of angle of attack and sideslip while CPU No. 2 begins generating more current values for the aero angles (say, due to gusts). Now at the end of CPU No. 2's frame, CPU No. 2 updates angle of attack and sideslip. However, CPU No. 1 continues generating aero data, only now it is reading new and different values for the aero angles relative to those read at the top of its frame. This timing mismatch can cause considerable error for fast moving variables.

Another example (of a more complex problem) shows how parallel uninterrupted processing can require significant timing considerations. Assume that a linearized airframe simulation is comprised of 6 major program modules and is allocated into 2 CPUs which operate at the same frame time. Module 1 (ADC) is where all pilot inputs are read in from the A/D converters. Module 2 (AERO) comprises the aerodynamic data and force/moment buildup which is a function of airframe surface positions (from the Flight Control System), angle of attack and sideslip angle. Module 3 (EOM) computes the airframe equations-of-motion as well as the angle of attack and sideslip angle based on the forces and moments generated in the AERO module and Euler angles from the aircraft's direction cosines. Module 4 (ENGINE) performs computations relative to the aircraft engine model based on A/D conversion readings of throttle position, while Module 5 (CONT SYS) performs the digital flight control system computations relative to the pilot inputs brought in by the ADC module. The last module, number 6 (DC), computes the Euler rates based on the airframe body rates as computed in the EOM module and determines the aircraft inertial orientation. For this example, it is assumed that the variables computed in each module are not transferred to common memory until the end of the module's computation and that all inputs are required at the top of module. The following computation times for each module are assumed:

1) Module 1 (ADC) = 2 milliseconds
2) Module 2 (AERO) = 6 milliseconds
3) Module 3 (EOM) = 2 milliseconds
4) Module 4 (ENGINE)= 3 milliseconds
5) Module 5 (CONT SYS) = 4 milliseconds
6) Module 6 (DC) = 3 milliseconds

To aid in the understanding of the significance of common memory skewing, a "timing diagram" of the airframe simulation example is constructed as shown in Figure 12. It might be noted that in a timing diagram, the module lengths are drawn and scaled proportionately to the actual time required to perform the computations of that module. It is in this fashion that module synchronization between parallel digital computers can be established.

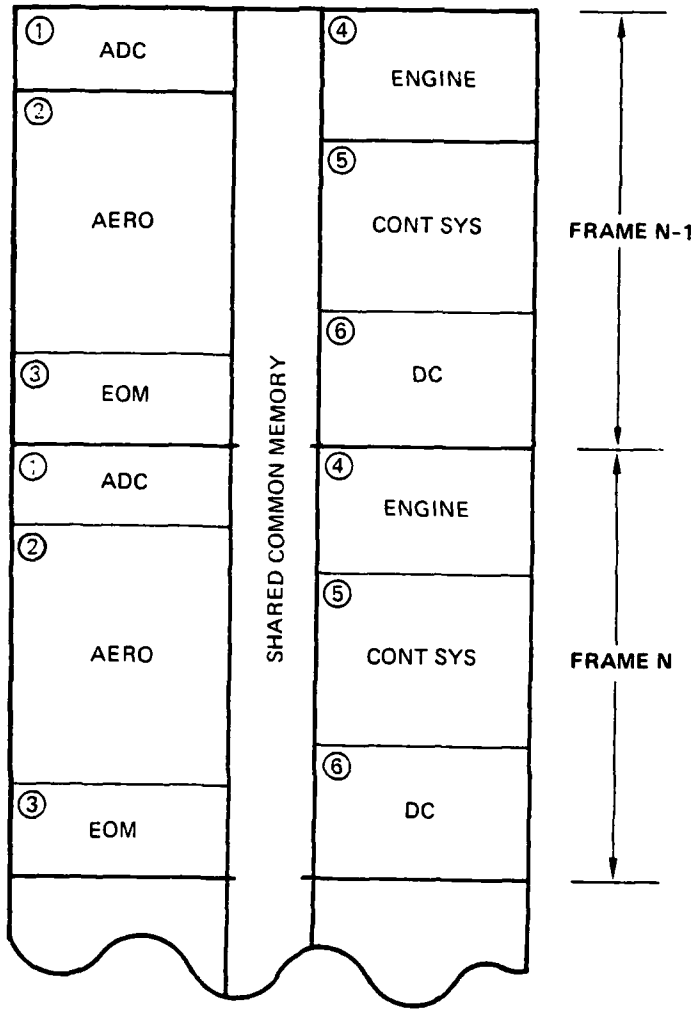

FIGURE 12. TIMING CHART

From timing diagram shown in Figure 12, the following conclusions about "Frame n" can be made:

1) ENGINE (Module 4) uses Frame n-1 and Frame n ADC data
2) CONT SYS (Module 5) uses Frame n ADC data
3) AERO (Module 2) uses Frame n-1 EOM and CONT SYS data and Frame n CONT SYS data
4) EOM (Module 3) uses Frame n AERO and ENGINE data and Frame n-1 DC data
5) DC (Module 6) uses Frame n-1 EOM data

As can be seen from the above conclusions, during a typical frame in the parallel processors, current computations use a combination of previous frame results as well as current frame results. The severity of this common memory skewing is dependent solely on the relative magnitudes of the frame times of all processors accessing common memory and the time requested to perform the various computations.

3.5 Hybrid-Multiple CPUs With Input/Output Link Configuration

For the configuration shown in Figure 13, multiple digital processors communicate through a serial data Input/Output device. For uninterrupted CPUs, a similar error to shared common memory skewing occurs. This error, termed I/O link skewing, is best explained by an example. If the six modules described in the linear airframe mechanization in Section 3.4 are configured in separate CPUs and all operate at the same frame time, the I/O link skewing effect is evident by the Link diagram shown in Figure 14. It is assumed that the I/O line data transfer occurs at the end of the frame. As can be seen by this example, all modules utilize past data. Since this example represents the configuration for the solution of coupled sets of equations, the required cross-talk within the link causes a four frame time delay in the computation of the aircraft attitude due to a pilot input (the numbers in parenthesis in Figure 14 count out the paths of transport delay cycles).

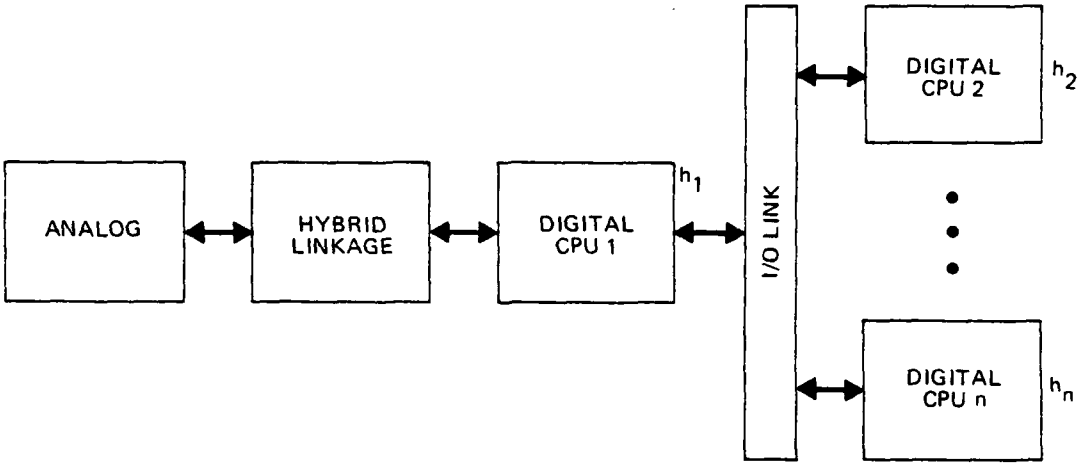

FIGURE 13. HYBRID-MULTIPLE CPUS WITH I/O LINK CONFIGURATION

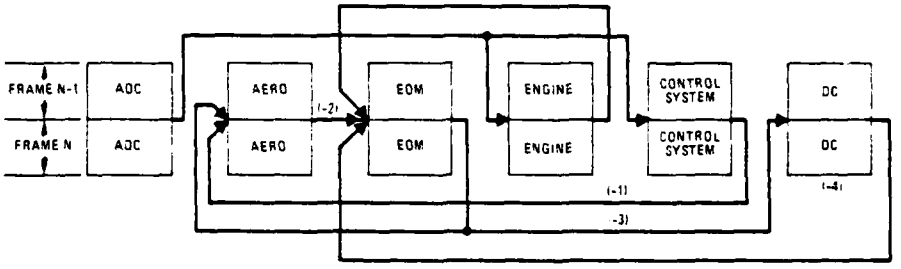

FIGURE 14. I/O LINK DIAGRAM

Although the effect of I/O link skewing appears quite severe, typically this type of communication is used for solutions of uncoupled sets of equations. However, this type of computation is attractive with use of special purpose high-speed digital computers such as Array Processors. When Array Processors are utilized, an I/O Link to that processor can be established several times during the normal frame of an executive CPU. When the Array Processor is accessed, the linking CPU is put into a hold mode since the Array Processor executes at much higher rates. This type of arrangement works quite well when large nonlinear aerodynamic data packages are required and allows the overall structure of the executive CPU to process information in a more serial unskewed fashion.

4. REAL TIME COMPUTER ERRORS - AIRFRAME SIMULATION

4.1 Experimental Investigations

As described in Section 3, several preliminary investigations into the characteristics of certain error sources were accomplished. The effects of the following error sources were evaluated:

1) Analog integrator drift
2) Analog amplifier/integrator error due to bandwidth and capacitor dielectric absorption
3) D/A conversion skewing
4) A/D conversion skewing
5) Hybrid linkage quantization coarseness (word length)

For the analog integrator drift test, an arbitrary sample of 16 integrators was utilized. The integrator inputs were grounded with a unity gain and it was found that drift voltages from 10 millivolts to as high as 820 millivolts occurred in one hour. The results of the analog amplifier/integrator bandwidth and capacitor dielectric absorption test were presented in Section 3.2. Briefly, the test showed how the analog solution of a linear second-order simple harmonic motion differential equation (whose theoretical solution is a neutrally stable sinusoid) tends to damp itself out at lower system frequencies. However, as the system frequency is increased, the solution tends toward the exact solution but then diverges with respect to time with a further increase in frequency.

Results of the D/A and A/D conversion skewing tests were described in Section 3.3. The simple harmonic motion differential equation described above was mechanized in a hybrid-single CPU configuration where the digital processor was unscheduled and free running. The digital

computer was utilized only to read in an analog variable and then immediately output the same variable through the hybrid linkage. The number of channels of A/D and D/A conversions were varied so as to examine the effect of hybrid linkage skewing. The magnitude of induced instability by the linkage skewing was found to be a direct function of the numbers of I/O link channels utilized. The instabilities are caused by time delay induced into the system, but however, leave the power spectral content of the system unaltered in frequency.

The hybrid linkage quantization coarseness test investigated the effects of A/D and D/A converter word length. A simple sine wave was processed through a single A/D channel and was immediately converted back to an analog wave form through a single D/A channel. Therefore, any distortion in the sine wave would be predominately due to the hybrid linkage word-length and not linkage time delay. Figure 15 compares the Power Spectral Densities of a quantized 10 radian/second sine wave for 15 bit and 3 bit resolutions (sign included). As can be seen in Figure 15 (B), the 3 bit quantization generated a d-c biased wave form in the time domain and produces harmonic spikes in the power spectrum. The 10 radian/second natural frequency, however, remains as the predominate power in the frequency domain. For the 15 bit resolution, no distortion of the time history or power spectrum is observed.

As noted during the 3 bit quantization coarseness test, the wave form output had obtained a d-c bias. A resulting level by level map of a 3 bit quantizer (sign not included) showed that this bias was inherent in the quantizer hardware. Figure 16 shows this quantizer map. As shown in Figure 16, an input level of 12.5 volts is required to jump to the first quantum level in the positive direction. However, in the negative direction, any voltage in that direction results in an immediate jump to the first negative quantum level. This accounts for the d-c bias described earlier.

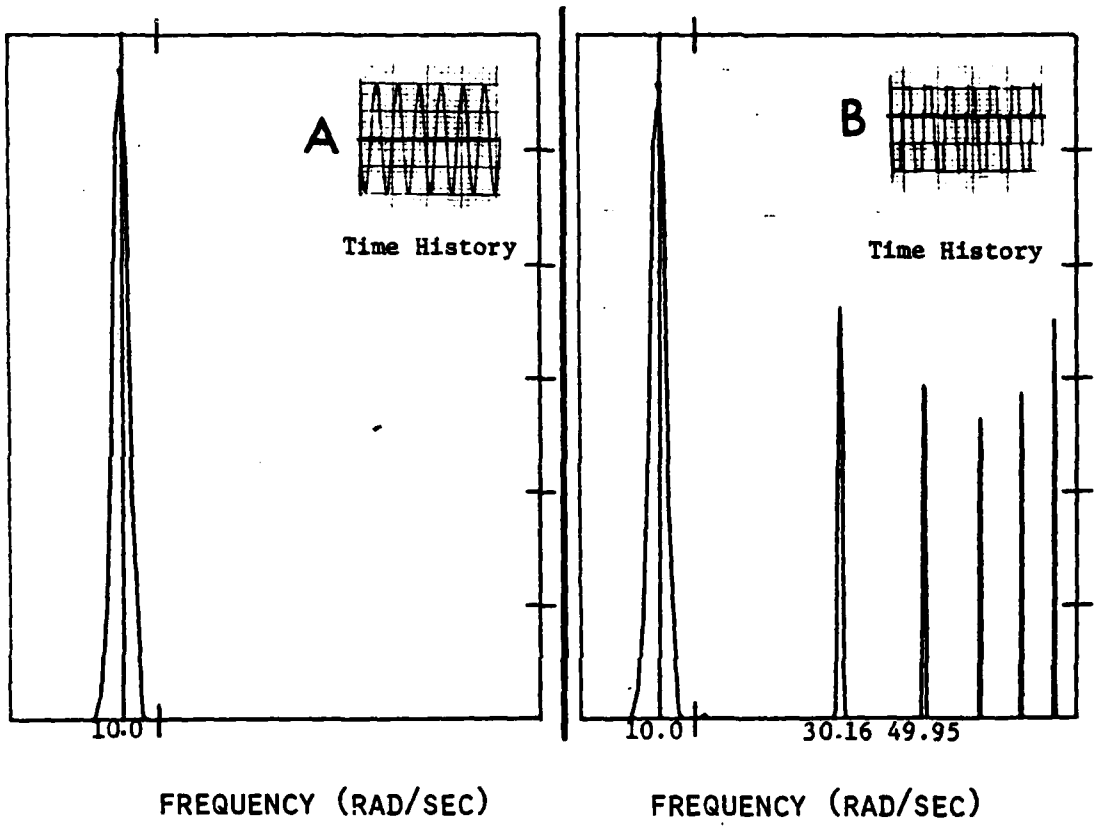

FIGURE 15. POWER SPECTRUM OF A 3 BIT AND 15 BIT QUANTIZER

Subsequent to the preliminary tests, which investigated the characteristics of predominate errors in the hybrid loop, a full scale analysis of the effects of hybrid computer errors on the accuracy of a typical flight simulation mathematical model was accomplished. The following sections detail the mechanizations, analysis, and results of this investigation.

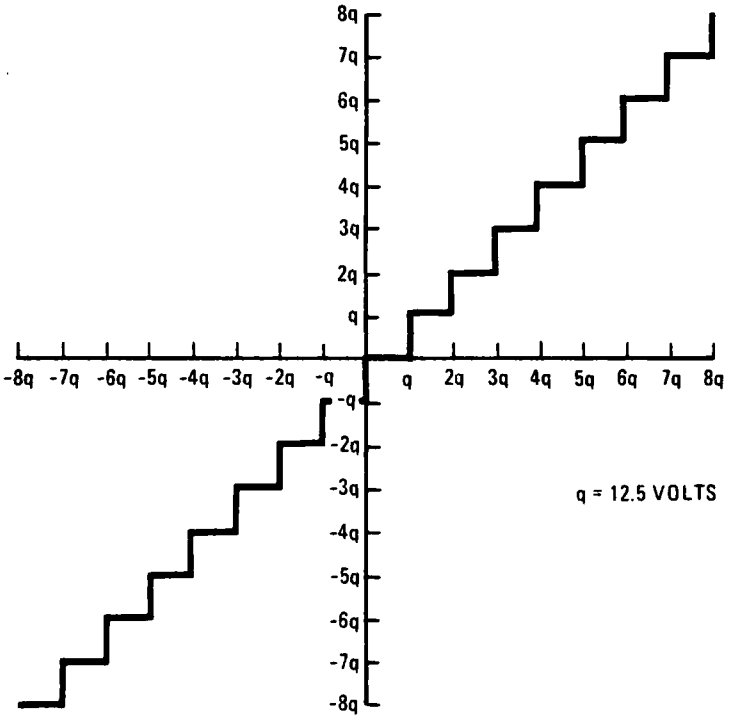

FIGURE 16. QUANTIZER MAP

4.2 Airframe Mathematical Model

The mathematical model utilized in this portion of the study was the coupled equations-of-motion representing the longitudinal motion of an airframe. These equations incorporated three-degree-of-freedom and were linearized for small perturbations. The equations-of-motion mechanized were:

$$\dot{u} = X_w w + X_u u - g\theta \tag{4-1}$$

$$\dot{w} = Z_w w + Z_u u + U_o q + Z_{\delta e}\delta e \tag{4-2}$$

$$\dot{q} = M_u u + M_{\dot{w}}\dot{w} + M_w w + M_q q + M_{\delta e}\delta e \tag{4-3}$$

where:

$w \equiv$ vertical velocity
$u \equiv$ forward velocity
$\theta \equiv$ pitch attitude
$q \equiv$ pitch rate
$U_o \equiv$ true airspeed
$\delta_e \equiv$ elevator (surface) command

The form of these equations provides for the use of nonlinear aerodynamic data. However, as described in Section 2, since the effects of error sources on solution accuracy can be demonstrated more easily with a linear mechanization, linear aerodynamic data were utilized. Listed below are the aerodynamic and flight condition data utilized with the above equations-of-motion.

$$\left.\begin{aligned} X_w &= 0.0016 \\ X_u &= -0.0097 \\ Z_w &= -1.43 \end{aligned}\right|$$

$$
\left.
\begin{aligned}
Z_u &= -0.0955 \\
Z_{\delta_e} &= 69.8 \\
M_u &= 0.0 \\
M_w &= -0.0235 \\
M_q &= -1.92 \\
M_{\delta_e} &= 26.1 \\
M_{\dot{w}} &= -0.0013 \\
U_o &= 660.0 \\
g &= 32.174
\end{aligned}
\right\} \qquad (4\text{-}4)
$$

Substitutuion of equations 4-4 into 4-1 through 4-3 yield:

$$\dot{u} = 0.0016w - 0.0097u - 32.174\theta \qquad (4\text{-}5)$$

$$\dot{w} = -1.43w - 0.0955u + 660q + 69.8\delta e \qquad (4\text{-}6)$$

$$\dot{q} = -0.0235w - 0.0013\dot{w} - 1.92q + 26.1\delta e \qquad (4\text{-}7)$$

Equation 4-5 represents the forward acceleration response of the airframe model while equations 4-6 and 4-7 represent the vertical acceleration and pitch acceleration response of the airframe, respectively. These responses yield perturbations from the trim conditions, which were assumed to be zero for this study. Solution of equations 4-5 through 4-7 is accomplished by straight forward integration with respect to time, or:

$$u = \int_o^t \dot{u} dt \qquad (4\text{-}8)$$

$$w = \int_o^t \dot{w} dt \qquad (4\text{-}9)$$

$$q = \int_o^t \dot{q} dt \tag{4-10}$$

The pitch attitude response, which is required to complete the solution of equation 4-5, is computed by integrating equation 4-10 with respect to time (assumes small angles), or:

$$\theta = \int_o^t q dt \tag{4-11}$$

Another variable of interest is the airframe angle of attack which, for small angles, is simply defined as:

$$\alpha = \frac{w}{U_o} \tag{4-12}$$

The elevator surface input utilized in the investigation of the effects of error sources on airframe solution accuracy was an exponential forcing function as defined by:

$$\delta_e = K_i e^{-ft} \tag{4-13}$$

In all investigations involving the aforementioned airframe model, the system of equations defining the airframe response (equations 4-5 through 4-7) were solved in real time by the computer which is referred to as the numerical or computer set-up solution. At the same time, in real time, a theoretical solution was computed which is referred to as the analytical or theoretical solution. The theoretical solution is the closed form solution to equations 4-5 through 4-7. A detailed theoretical solution development is presented in Appendix A.

Four separate computer configurations were utilized in mechanizing the longitudinal airframe mathematical model to investigate the effects of error sources on solution accuracy. Those configurations examined were all analog, hybrid-single CPU, hybrid-dual CPUs with shared common memory, and hybrid-dual CPUs with an I/O link. In all mechanizations it was assumed that the forcing function was an analog variable. A typical test would include a controlled error source configuration with the particular computer setup being examined. After the computers were placed into operation, the airframe was disturbed by the elevator surface command at which time a magnetic tape, peripheral to the digital computer, would start data collection in real time. This magnetic tape would store all computer setup solutions as well as the analytical solutions. Relative error between the computer setup and analytical solutions were also computed and stored on the magnetic tape in real time.

The following four sections describe the experimental analysis and results of the error effect investigations on the various computer configurations described above. The accuracy of the computer solution was always related to the theoretical solution. In the frequency domain, the theoretical pitch attitude Power Spectral Density exhibited a slight power concentration or peak at a frequency of 3.3 radians per second, as shown in Figure 17. Therefore, many of the results presented in the following sections are referenced to this peak power reference frequency in terms of a decibel (db) increase or decrease (Δdb), or to a shift in the reference frequency (Δf_{ref}).

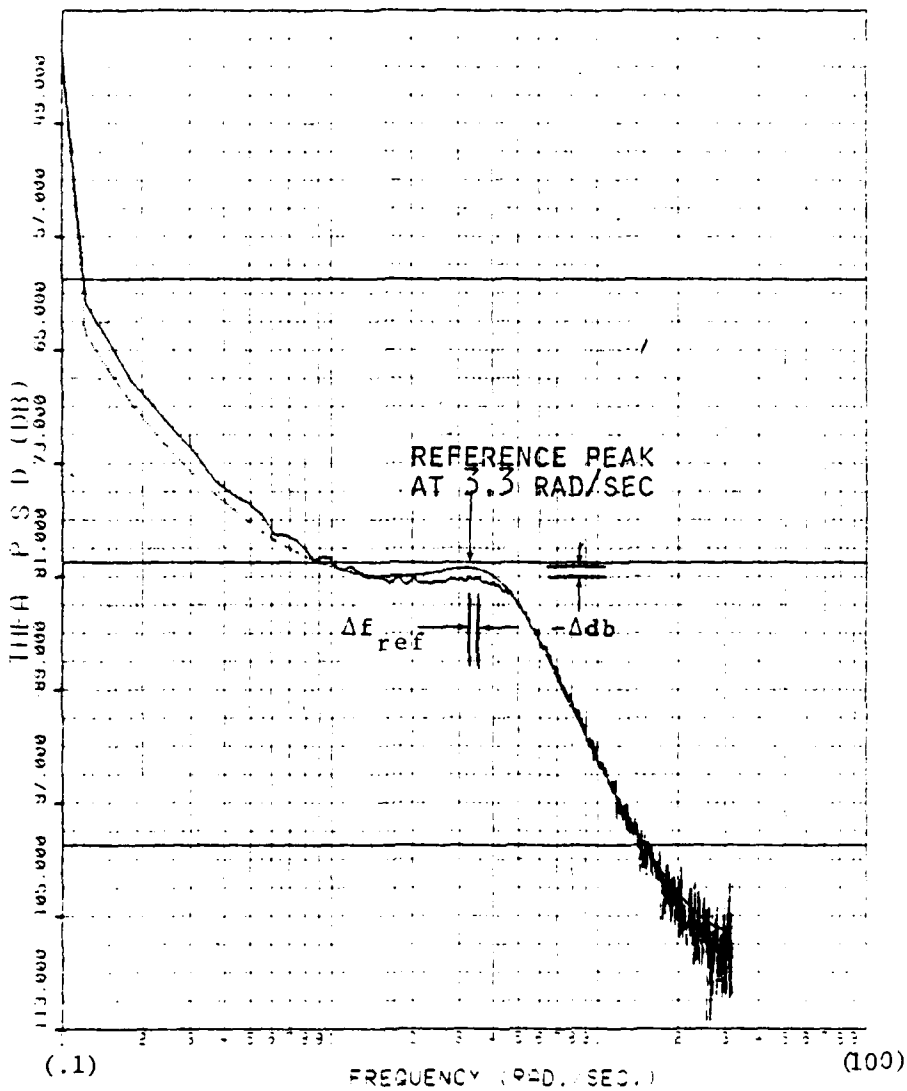

FIGURE 17. TYPICAL PITCH ATTITUDE POWER SPECTRAL DENSITY

4.3 Analog Configuration

The mechanization of the longitudinal airframe mathematical model in an all analog configuration is shown in Figure 18.

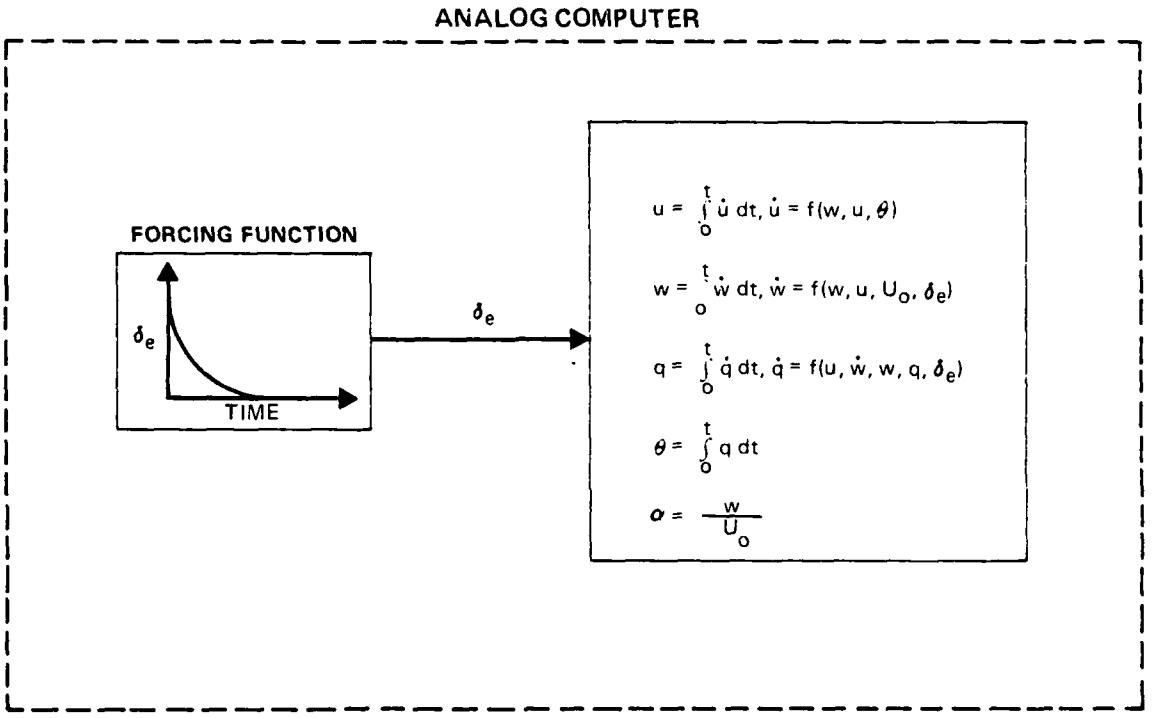

FIGURE 18. ANALOG CONFIGURATION

In this configuration, the elevator surface forcing function, as well as the aerodynamic buildup and integration of the equations-of-motion are accomplished on the Comcor 5000 analog computer which was described in Section 2. The only digital interface was for Power Spectral Density (PSD) analysis purposes.

The main variables of interest in this configuration was parameter scaling and pot tolerance. Eight distinct test cases were established:

Test 1 - Nominal parameter scaling
Test 2 - Reduced scaling by a factor of 10
Test 3 - Reduced scaling by a factor of 100
Test 4 - Increased scaling by a factor of 2.5
Test 5 - Pot settings 5% high
Test 6 - Pot settings 5% low
Test 7 - Pot settings 10% high
Test 8 - Pot setting 10% low

As previously described, a peak power frequency was utilized for referencing the results of the tests. For this purpose, the variable Δdb is defined as the power change, at the characteristic frequency of 3.3 radians per second, of the computer solution relative to the theoretical solution.

Figure 19 shows the results of the analog tests for the pitch attitude response of the airframe. As can be seen, a decrease in system power (at 3.3 radians per second) is experienced for pots which are set at the high tolerance values. This power change increases negatively as the tolerance value increases. Similarly, for low tolerance values, an increase in power concentration occurs and increases as the negative tolerance value increases. Also, as was detected in the PSD analysis, as the positive tolerance value increases, the peak power frequency tends to shift towards the higher frequencies. The relative value of this frequency shift relative to the theoretical 3.3 radian per second standard is depicted in Figure 19 by the value adjacent to the data point. A positive direction denotes an increase in peak frequency. Negative value peak

frequency shifts are shown for the negative tolerance values.

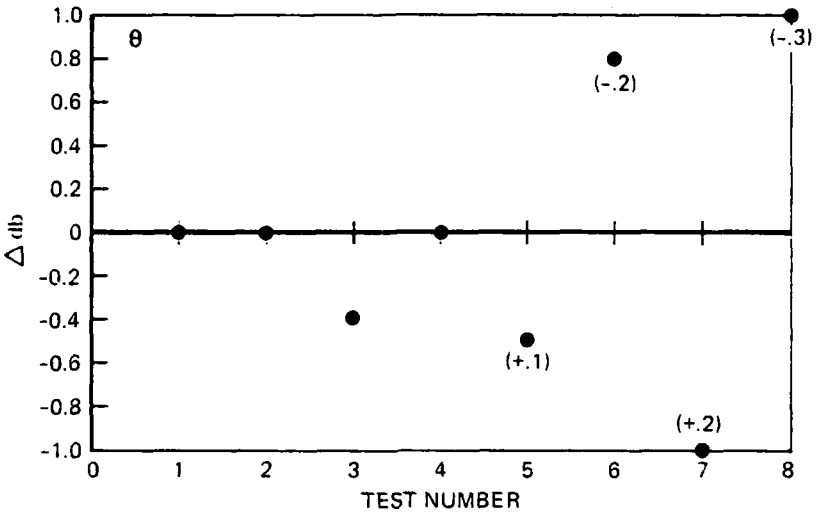

FIGURE 19. ANALOG TEST RESULTS-PITCH ATTITUDE

The effects of parameter scaling are not quite as profound as the effects due to pot tolerance. However, a negative shift in power frequency magnitude was observed when the scaling was reduced by a factor of 100 from the nominal values.

For angle-of-attack, the effects of pot tolerance are nearly identical to pitch attitude except that a positive tolerance trend causes a positive shift in Δdb and vice-versa for a negative tolerance trend. as can be seen in Figure 20. Also the effect of parameter

scaling is observed when the scaling factor is increased by 2.5 rather than decreased by 100, as was the case with pitch attitude.

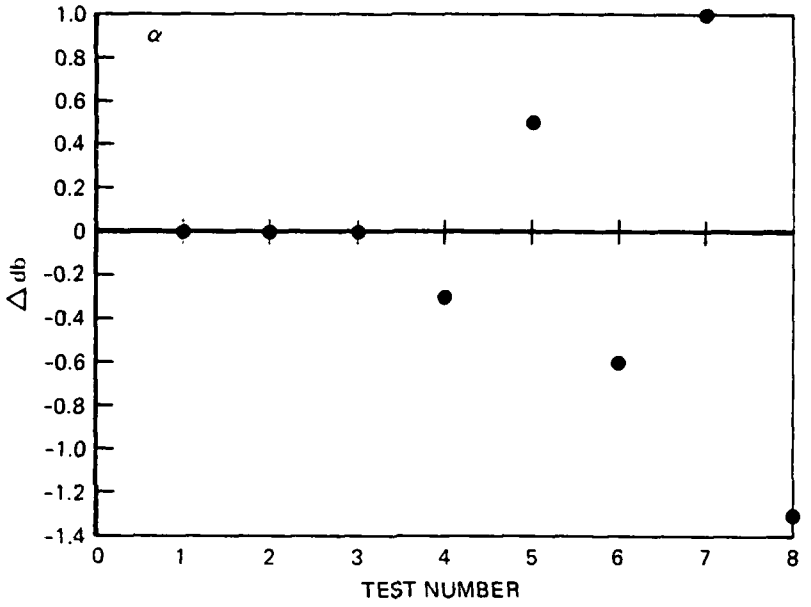

FIGURE 20. ANALOG TEST RESULTS-ANGLE OF ATTACK

Figure 21 shows the power change in the forward velocity response at 3.3 radians per second as a result of the controlled analog error sources. Note how the power change is much more adverse for this variable relative to pitch attitude and angle-of-attack. This variable is predominated by the phugoid motion of the free airframe rather than the short period, where the accuracy measure frequency of 3.3 radians per second resides. In Figure 21, the values in the parenthesis pertain to a period shift (in seconds) of the forward velocity time history relative to the theoretical time history response. A negative shift denotes an increased

frequency in the phugoid motion.

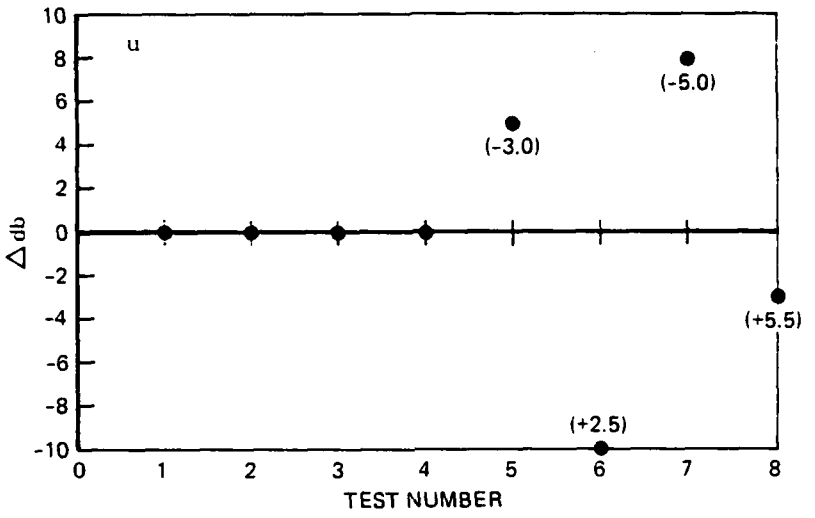

FIGURE 21. ANALOG TEST RESULTS-FORWARD VELOCITY

The test 8 results for forward velocity show an improved Δdb. This result is misleading as the PSD plot for this test case, where the pots were set at the 10% low tolerance values, exhibited an inconsistent trend relative to the theoretical PSD. Typically a smooth mean falloff in power is observed as the frequency increases. For this case, however, the power gradient changes rapidly resulting in dips and nonuniformities in the power spectra. These distortions and irregularities create difficulties in deriving the significance of the results, especially when relating them to well behaved power spectra.

4.4 Hybrid-Single CPU Configuration

In the hybrid-single CPU configuration, as shown in Figure 22, the elevator surface forcing function and integration of the equations-of-motion were accomplished on the analog computer. The aerodynamic buildup was computed in the Master Hybrid (MH) digital computer.

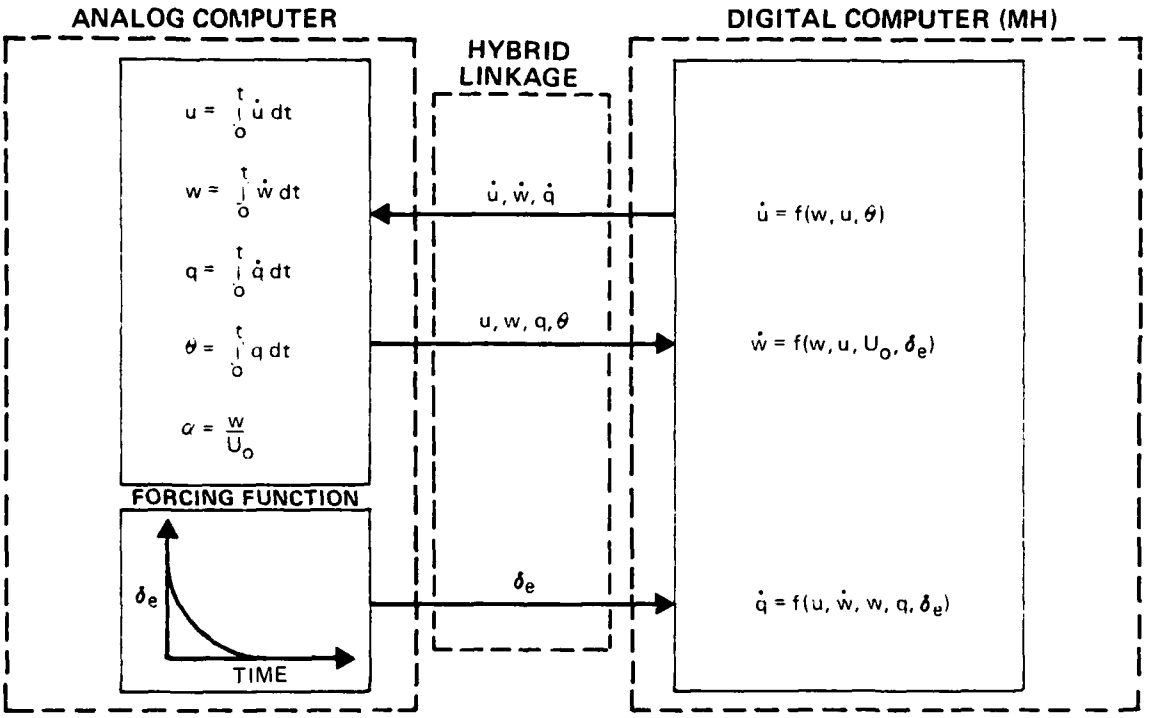

FIGURE 22. HYBRID-SINGLE CPU CONFIGURATION

In this configuration, controlled error sources included:

1) Linkage time delay
2) Quantization resolution
3) Digital computer frame time, h

The effects of hybrid linkage time delay were generated by altering the number of A/D and D/A channels to be read or set. The numbers of channels to be utilized was specified from a data card which was read into the digital computer.

At least 6 A/D channels were always utilized. These channels were for the elevator surface input, forward velocity, vertical velocity, pitch rate, pitch attitude, and angle of attack. All but the angle of attack channel were required for the aerodynamic buildup. Angle of attack was brought into the digital computer such that it could be recorded and utilized in the PSD analysis. Three D/A channels were always required, from which the airframe accelerations (resulting from the aerodynamic buildup) were made available to the analog computer for integration.

Since earlier preliminary tests (Section 4.1) showed that the effects of time delay due to A/D and D/A conversion were essentially the same, the number of A/D channels was primarily fixed at the nominal value of 6, while the number of D/A channels was varied from 50 to 150. When 50 D/A channels were utilized, 0.6 milliseconds was required for the conversion process. For 100 and 150 D/A channel cases, 2.05 and 3.2 milliseconds, respectively, were required.

The shift in the peak power frequency at 3.3 radians per second, due to hybrid linkage time delay, was best exhibited by the angle of attack results. As can be seen in Figure 23, for frame times of 0.00833 and 0.05 seconds, a noticeable increase in power frequency magnitude is experienced for both 15 and 12 bit linkage word lengths. For the 0.1 second frame time case, the effect is less noticeable, although the trend is identical with the other frame time cases.

For the pitch attitude response, the effect shown in Figure 23 is obtained, only with less magnitude.

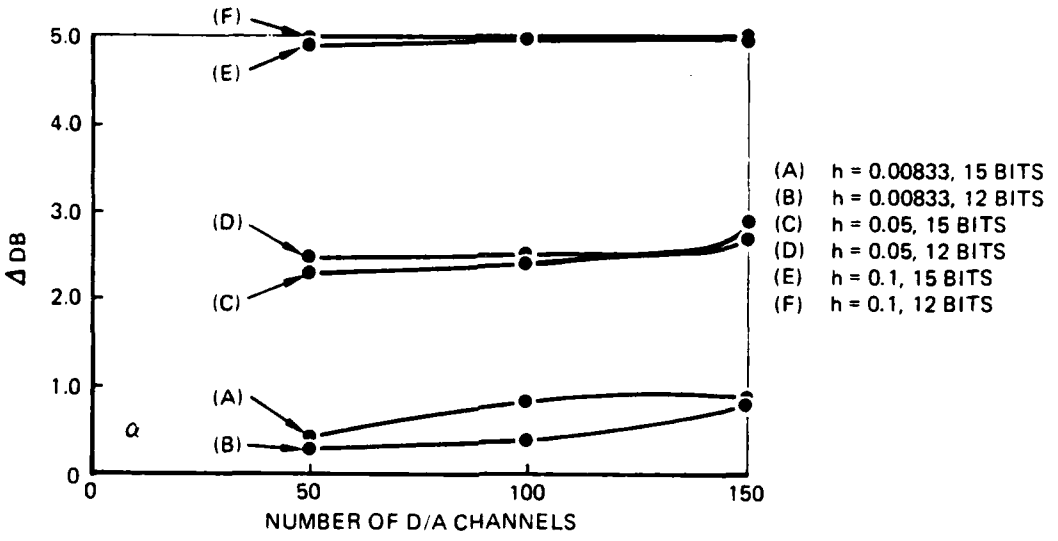

FIGURE 23. EFFECTS OF TIME DELAY DUE TO HYBRID LINKAGE

For example, at the 15 bit 8.33 millisecond test case, the angle of attack power undergoes a 0.5 db change in magnitude at the 150 D/A channels condition relative to the 50 D/A channel condition. However, for pitch attitude, under the same test conditions, only a 0.2 db change in power was observed for the time delay associated with 150 D/A channels relative to 50 D/A channels.

For forward velocity, there was virtually no change in peak power magnitude due to the linkage time delay. It can be concluded, that in this hybrid single CPU configuration, for a given frame time

and linkage word length the time delay associated with the hybrid linkage adversely affects the high frequency equations to a greater degree relative to the low frequency equations. This was demonstrated by the fact that the accuracy of the angle-of-attack results (which are almost exclusively related to the short period dynamics) were more adversely affected than the forward velocity results (which are predominately phugoid motion related).

The effects of linkage word length on solution accuracy is exhibited in Figure 24.

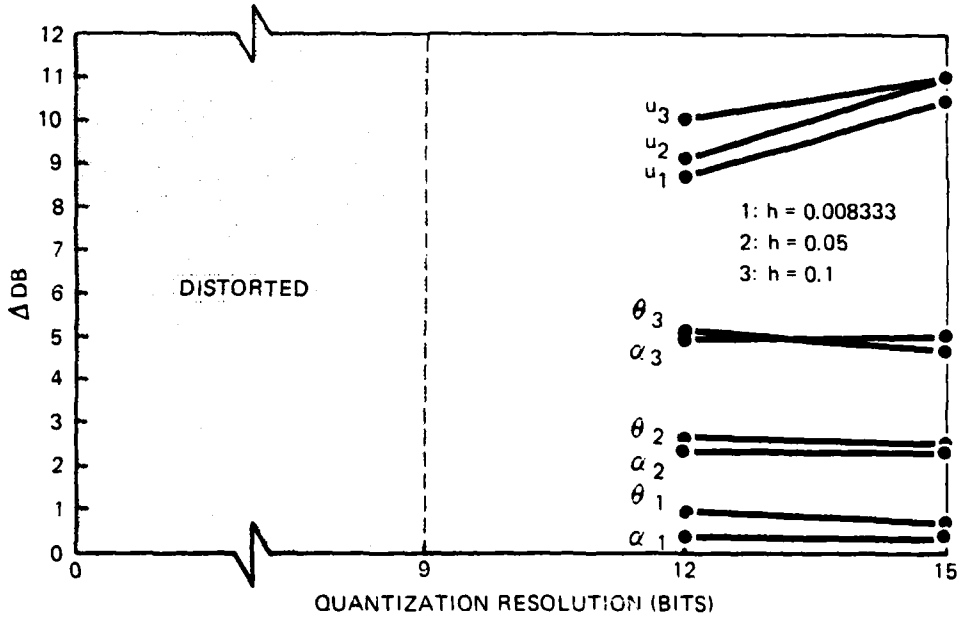

FIGURE 24. EFFECTS OF LINKAGE WORD LENGTH

As shown in this figure, for each frame time examined, decreasing the digital linkage word length to the 9 bit condition causes extreme distortion in the results to an unacceptable level. For pitch attitude, the solution accuracy decreases as the word length decreases. This is shown in Figure 24 as a decrease in peak power magnitude change (relative to theory) with increasing word length. The effects of quantization resolution are virtually non-existent for the angle-of-attack responses as no appreciable change in power magnitude at the 3.3 radians per second reference condition is experienced.

For forward velocity, the accuracy of the solution actually improved with a decreasing quantization resolution up to the 12 bit word length. These results can be attributed to the fact that the lower word lengths offer larger steps to the analog computer which tends to compensate the time delayed digital solution.

The effects of frame time were observed in both Figures 23 and 24. As shown in these figures, for nearly any combination of hybrid linkage word length and channel quantity, increasing the frame time increases the peak power magnitude change at the reference frequency. Furthermore, a shift in the reference frequency (Δf_{ref}) was observed as the frame time was increased. This effect is shown in Figure 25 for the pitch attitude response with 3 D/A and 6 A/D converter channels at a 15 bit word length.

Results for the forward velocity response, however, show an improvement in the phugoid motion time history as the frame time is increased. The cause of this effect is believed to be similar to the lower linkage word length effects described earlier. The fact that fewer updates are received by the analog computer implies that the updates are transmitted in larger steps. This aids in compensating the digital computation.

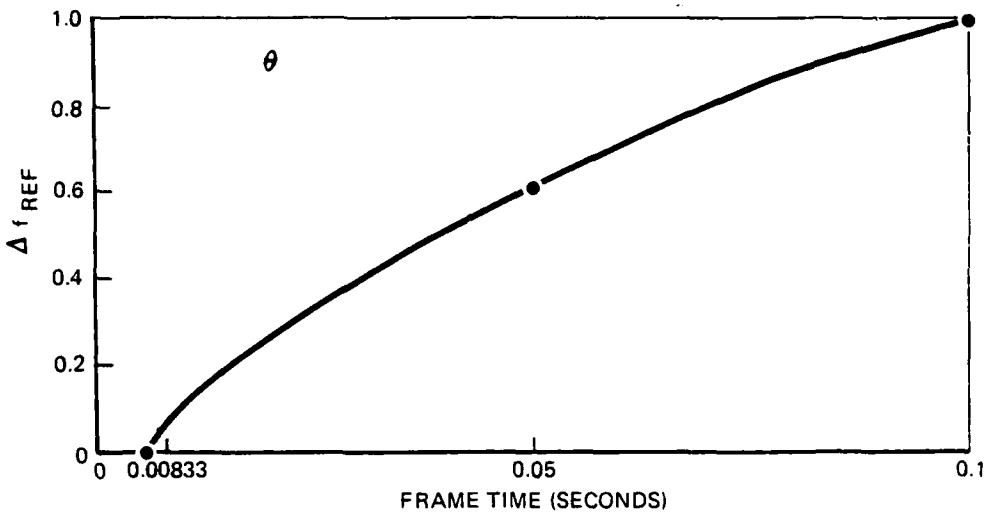

FIGURE 25. EFFECTS OF FRAME TIME

4.5 Hybrid-Dual CPUs With Shared Common Memory Configuration

In the hybrid-dual CPUs with shared common memory configuration shown in Figure 26, the aerodynamic buildup is accomplished in the Master Hybrid digital computer. The computed airframe accelerations are stored in common memory where they are retrieved by the Master Digital computer. In this computer, the vertical acceleration, pitch acceleration and pitch rate equations are numerically integrated. Angle of attack is also computed in this processor. The results of these computations are then passed back to and stored

in common memory where they are utilized in the next aerodynamic buildup computation. In this configuration, the analog computer is utilized for the generation of the elevator surface forcing function and the integration of the forward acceleration equation.

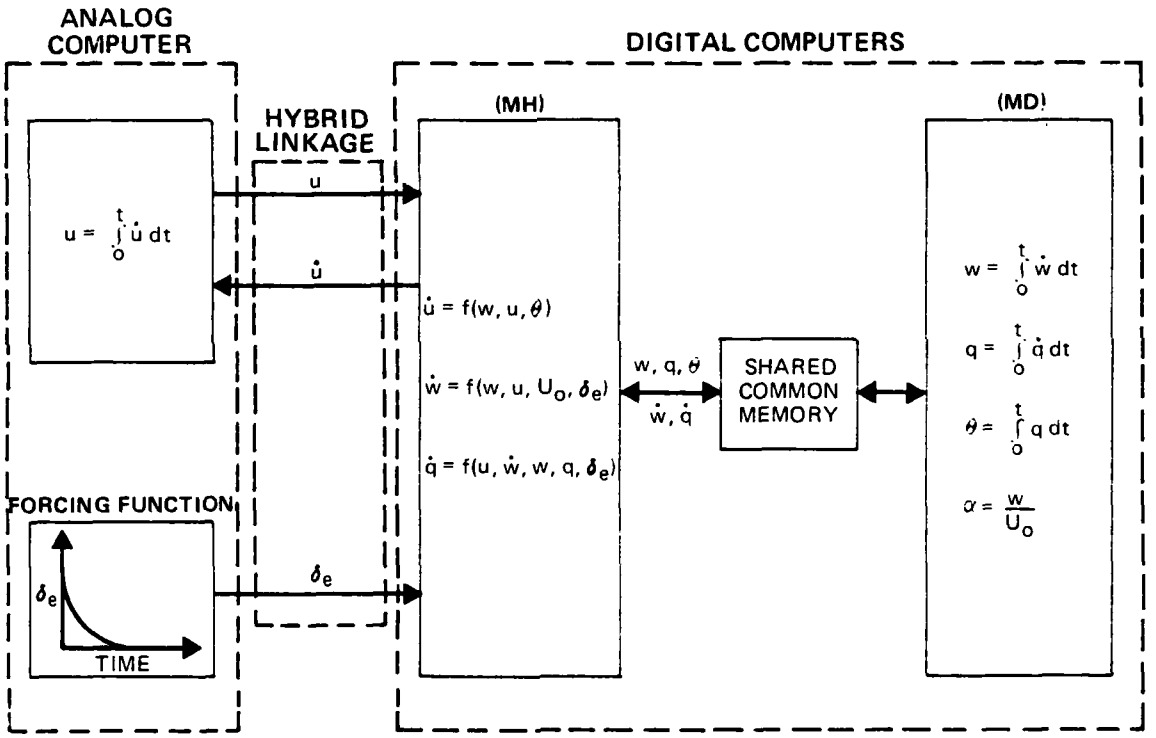

FIGURE 26. HYBRID-DUAL CPUS WITH SHARED COMMON MEMORY CONFIGURATION

Controlled error sources examined with this computer configuration included:

1) Linkage time delay
2) Quantization resolution
3) Master digital frame time, h_{MD}
4) Master hybrid frame time, h_{MH}
5) Numerical integration technique

The effects of hybrid linkage time delay were studied in the same fashion as the hybrid configuration discussed in the previous section. In summary, there is virtually no effect of linkage time delay in this configuration since most of the computations are contained in the digital computers. The one integral computation contained on the analog is the forward velocity integration. This variable, however, was found to be insensitive to hybrid linkage time delay in the hybrid-single CPU tests earlier. To illustrate these results, Figure 27 shows the flat Δdb response for varying numbers of D/A converter channels.

The effects of quantization resolution are shown in Figure 28. For the pitch attitude and angle of attack variables, which depend on the hybrid linkage mainly for the elevator surface forcing function, the effect of lower linkage word lengths is not that pronounced. For forward velocity, however, the effect is quite adverse as severe spectral distortion is observed at the 9 bit condition. This is due to the fact that the forward acceleration is passed through the hybrid linkage for analog integration. This large forward velocity power magnitude shift at 9 bits causes the larger pitch attitude power increase at the 9 bit condition, relative to angle of attack case which is virtually unaffected by forward velocity effects.

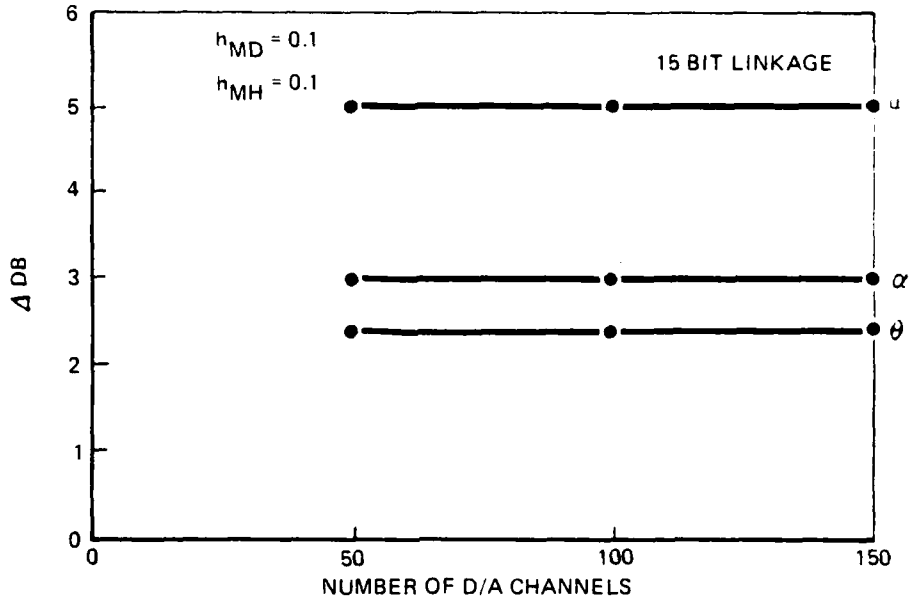

FIGURE 27. EFFECTS OF TIME DELAY DUE TO HYBRID LINKAGE

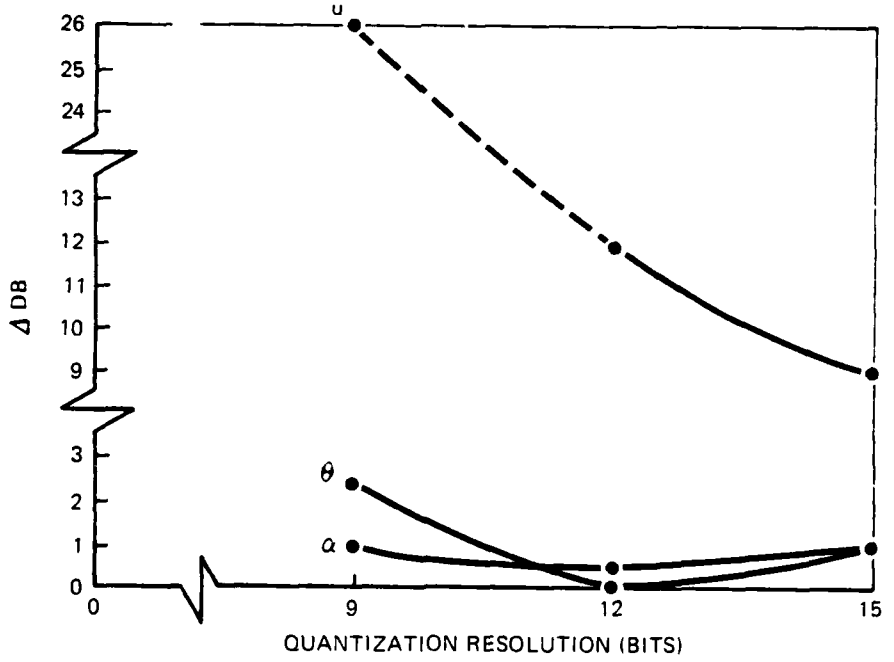

FIGURE 28. EFFECTS OF QUANTIZATION RESOLUTION

In digital computation, the airframe equations-of-motion are usually numerically integrated by recursion formulas. These formulas are of at least the same order as the equations-of-motion. Any integration technique of order greater than the order of the equations-of-motion introduces extraneous or spurious roots into the solution. To investigate the effects of numerical integration technique, 3 different methods of different orders, were employed: Open Euler, Second Order Adams Bashforth, and Mod Gurk (third order). All three methods are open or explicit methods which utilized only past available data. No predictions or corrections must be made in these integration methods. The integration algorithms representing these methods are:

1) Open Euler (OE):

$$y_{n+1} = y_n + h\dot{y}_n \tag{4-14}$$

2) Adams Bashforth (AB):

$$y_{n+1} = y_n + \frac{h}{2}(3\dot{y}_n - \dot{y}_{n-1}) \tag{4-15}$$

3) Mod Gurk (MG):

$$y_{n+1} = 1.1462084y_n - 0.2010870y_{n-1} + 0.0548787y_{n-2} + h(1.6415864\dot{y}_n - 1.0080130\dot{y}_{n-1} + 0.2750971\dot{y}_{n-2}) \tag{4-16}$$

Solution accuracy is degraded with an increase in frame time with numerical integrations. This result is shown in Figure 29 for pitch attitude. The data presented in Figure 29 are for the case when the time delay due to the hybrid linkage is at a minimum with quantization resolution at 15 bits. Also, the frame times of the Master Digital and Master Hybrid computers were maintained at the same values. As can be seen in Figure 29, the Open Euler method goes unstable for the simulated airframe as the frame time pushed past 0.05 seconds. It appears that the Second Order Adams Bashforth

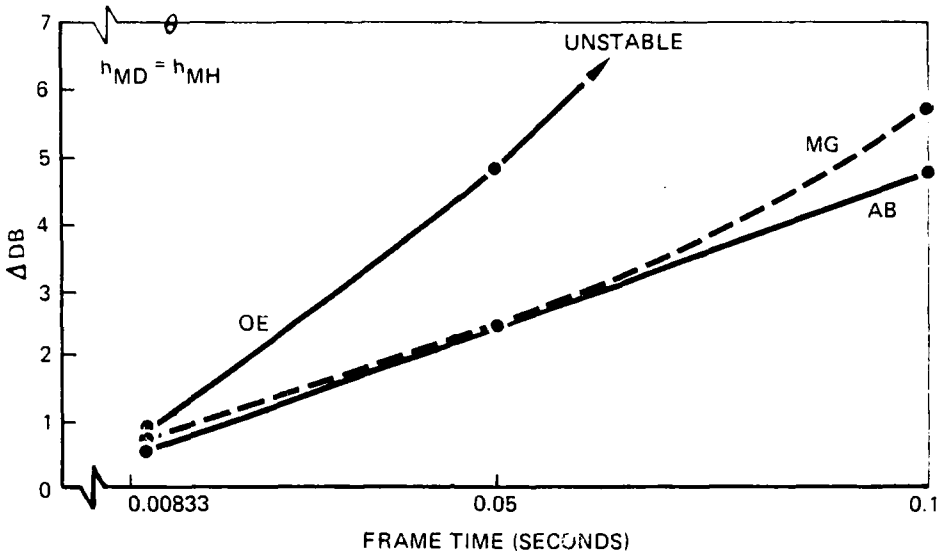

FIGURE 29. PEAK POWER MAGNITUDE SHIFT DUE TO FRAME TIME

method offered better results than the other methods, on the basis of peak power magnitude shift. However, if the frequency shift of the referenced frequency Δf_{ref}, is monitored at the various frame times, it can be seen that Mod Gurk offers less frequency distortion. This effect is shown in Figure 30.

In investigating the effects of the digital computer's frame time on solution accuracy, a timing chart of the airframe mechanization was constructed as shown in Figure 31. In this configuration, the Master Digital (MD) computer initially triggers (TRIG) the Master Hybrid (MH) computer, then proceeds into retrieving required data from common memory (INPUT). Numerical integration (INTEG) of the equations-of-motion is then executed with subsequent results being outputted (OUTPUT) to shared common memory. After this time, the theoretical time histories (THEORY) are computed as well as the error between the computer configuration solution and the theoretical airframe solution.

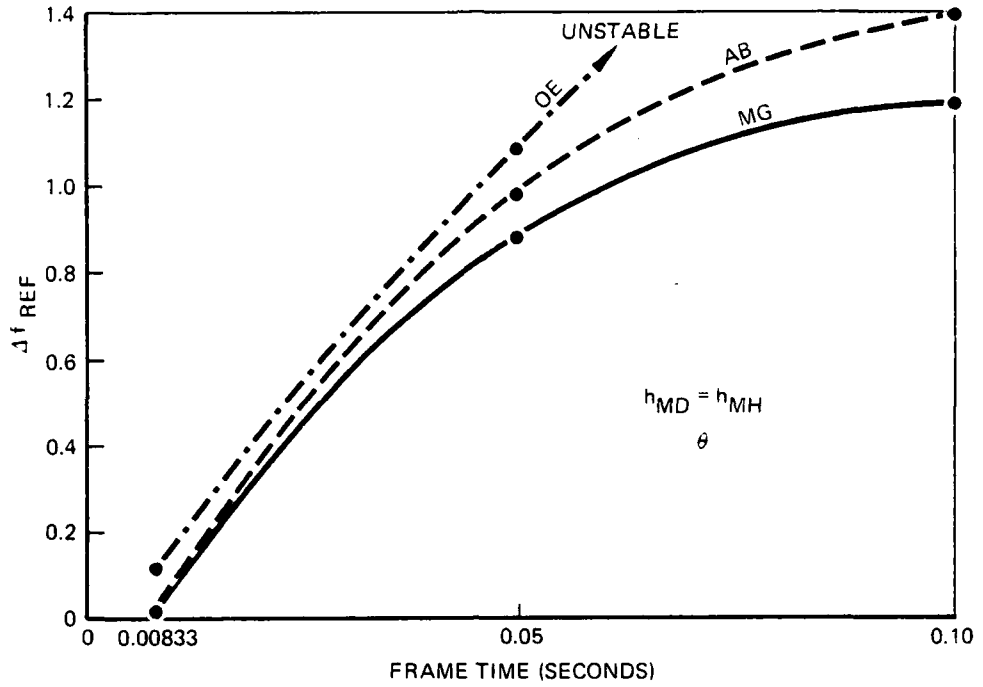

FIGURE 30. REFERENCE FREQUENCY SHIFT DUE TO FRAME TIME

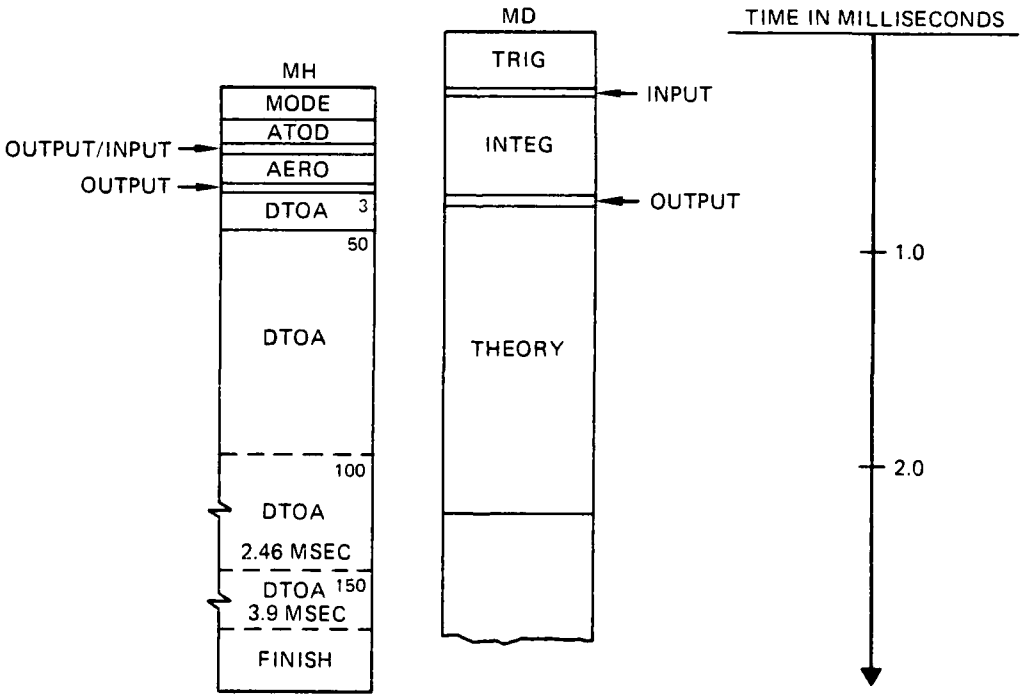

FIGURE 31. AIRFRAME MECHANIZATION TIMING CHART

After being triggered, the MH computer enters some mode checking logic (MODE) and then reads the A/D converters (ATOD). The results of the A/D conversion are then transferred to common memory at which time the results of the last numerical integration are retrieved from common memory (OUTPUT/INPUT). The aerodynamic buildup (AERO) is then accomplished with subsequent passing of results to common memory (OUTPUT). Finally, the D/A converter (DTOA) is accessed for varying numbers of channels. In Figure 31, the time required for 3, 50, 100 and 150 D/A channels is shown relative to the rest of the MH and MD programs. At this time, the MH program is formally terminated and waits until it is triggered again. The triggering process, however, is handled in a systematic and scheduled fashion.

When the MH frame time is held constant and the MD frame time is varied to increasing values, multiple A/D conversions and aerodynamic buildups are accomplished before the numerical integration of the vertical acceleration and pitch acceleration equations is carried out. In a similar fashion, if the MD frame time is held constant and the MH frame time is increased, multiple numerical integrations will be performed for each A/D transfer and aerodynamic buildup. For each of the above conditions, appreciable errors are induced into the solution as is shown in Figure 32, since a coupled set of equations is being solved.

As can be seen in Figure 32, the change in peak power magnitude increases negatively for an increasing Master Digital frame time while holding the Master Hybrid frame time at 0.00833 seconds. These results are for pitch attitude and Adams Bashforth integration although the trends are identical for angle of attack and the other integration techniques examined. In Figure 32, the numbers in parenthesis adjacent to the data points denote the frequency shift, relative to the 3.3 radians per second reference frequency.

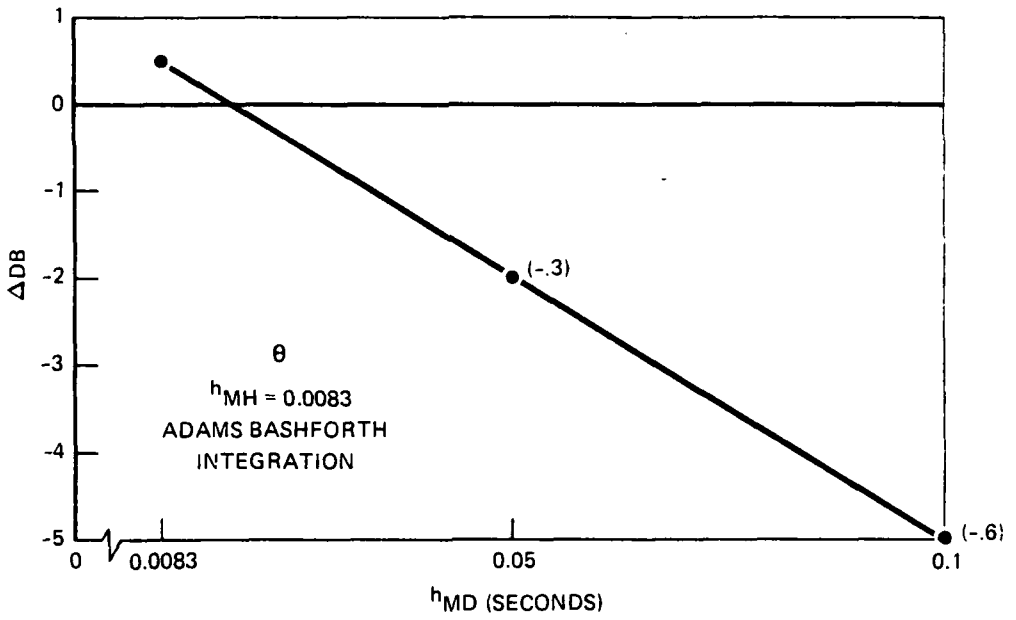

FIGURE 32. EFFECTS OF ASYNCHRONOUS FRAME TIMES

When the Master Hybrid frame time was increased with a constant Master Digital frame time, the power change at the reference frequency increased slightly up to a certain point. A further increase in the Master Hybrid frame time, however, offered improved results.

4.6 Hybrid-Dual CPUs With Input/Output Link Configuration

This configuration, as shown in Figure 33, utilizes all digital computation, except for the elevator surface forcing function. The aerodynamic buildup is contained in the Multiple System Interface (MSI) digital computer while the integration of the equations-of-motion were done in the Master Digital (MD) computer. The MD computer also provides for the A/D and D/A hybrid linkage requirements while the MSI and MD communicate through an Input/Output (I/O) link.

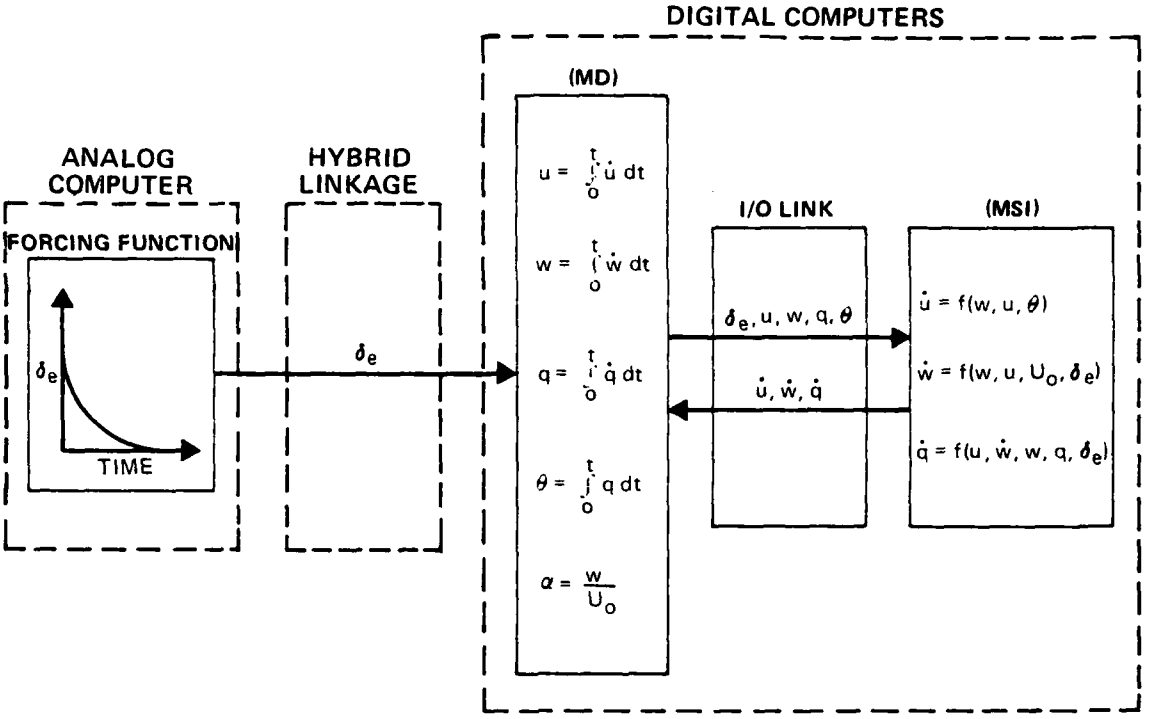

FIGURE 33. HYBRID-DUAL CPUS WITH I/O LINK CONFIGURATION

Controlled error sources utilized for tests with this computer configuration included:

1) Linkage time delay
2) Quantization resolution
3) Digital computer frame time
4) Numerical integration technique

In addition to the 3 numerical integration techniques presented in the Section 4.5 (see equations 4-14 through 4-16), a second order Runge Kutta (RK2) method was employed. This method is a predictor-corrector type as is shown below:

$$\dot{y}_n = f(y_n, t_n) \tag{4-17}$$

$$y^p_{n+1} = y_n + h\dot{y}_n \tag{4-18}$$

$$\dot{y}^p_{n+1} = f(y^p_{n+1}, t_{n+1}) \tag{4-19}$$

$$y_{n+1} = y_n + \frac{h}{2}(\dot{y}_n + \dot{y}^p_{n+1}) \tag{4-20}$$

Initially, an estimate of the integrated value is obtained by use of equation 4-18, which is nothing more than an Open Euler integration. The system rate (derivative) is this re-evaluated or predicted for the end of the interval. Using this predicted rate, along with the rate available at the top of the frame, computation with the trapezoidal integration method (equation 4-20) produces the final result. This method is somewhat more time consuming since multiple evaluations of the rates are required.

The effects of integration technique on this computer configuration are similar to the hybrid-dual CPUs with shared common memory configuration except that the peak power magnitude shift results tends to decrease with frame time rather than increase with frame time as was shown in Figure 29. For the shared common memory configuration, recall that the frame time of the Master Digital and Master Hybrid computers were varied together to show the effects of integration technique. The negative Δdb trend for the I/O link configuration and pitch attitude response is shown in Figure 34.

Although the Open Euler (OE) method looks attractive, it was the only method which distorted the reference frequency position under the test conditions shown in Figure 34. Second order Runge Kutta produced excellent results relative to the Adams Bashforth and Mod Gurk methods. The results are similar for the angle of attack response, however, for forward velocity a slight improvement at the 0.05 second frame time occasionally occurred.

The effects of quantization resolution resulted in the same trends as in the shared common memory configuration, but again with reversed direction. A decrease in word length (to 9 bits) continually decreased the magnitude change of the power spectra at the 3.3 radians per second reference frequency. As shown in Figure 35, this trend occurred for all integration techniques.

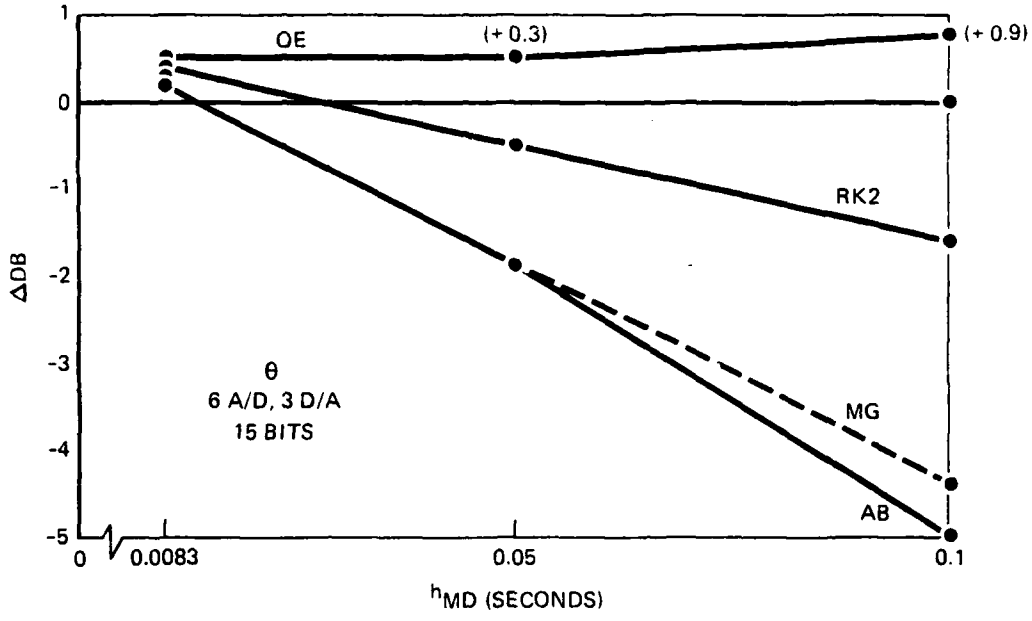

FIGURE 34. PEAK POWER MAGNITUDE SHIFT DUE TO FRAME TIME

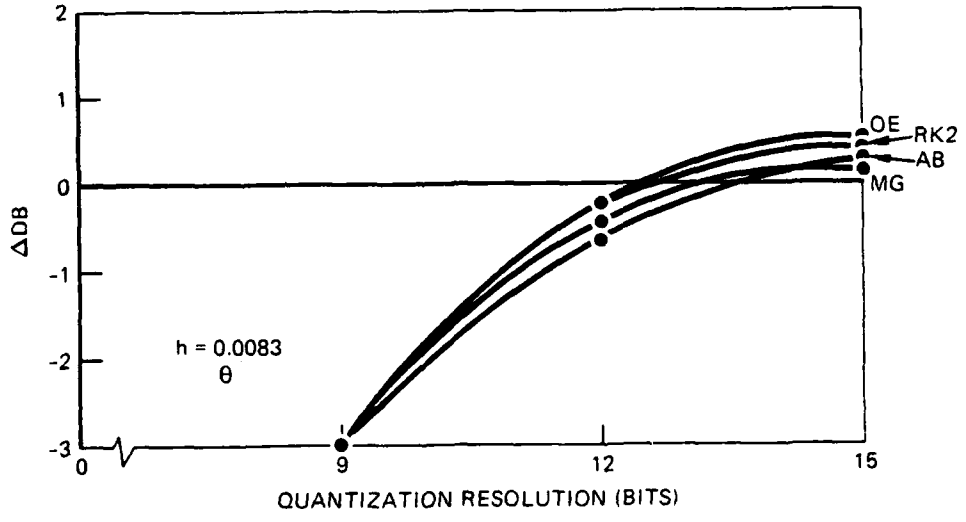

FIGURE 35. EFFECTS OF QUANTIZATION RESOLUTION

Although the trends shown in Figure 35 are for the pitch attitude response, the results are identical for forward velocity and angle of attack.

4.7 Concluding Remarks

The effects of error sources on the solution accuracy of an airframe model have been demonstrated with four separate computer configurations. The results cannot conclude which type of computer configuration must be employed for a given model. However, they can be used as a metric for the determination of probable effects of certain known error sources on low, high, and high/low combined frequency airframe equations when mechanized on a certain complement of computer equipment.

5. EFFECTS OF DIGITAL COMPUTER FRAME TIME

The effects of digital computer frame time were discussed in Section 4 for the hybrid-single CPU, hybrid-dual CPUs with shared common memory and hybrid-dual CPUs with I/O link computer configurations. In general, it was found that in all of these hybrid configurations, as the frame time goes up, the power spectra magnitude at the reference frequency changed relative to the analytical solution. However, in each of these configurations, other significant hybrid computer errors might have contaminated the results as they pertain to frame time effects.

Therefore, a special all digital mechanization was constructed which utilized a single CPU and a digital elevator forcing function. The aerodynamic buildup and integration of the equations-of-motion were computed sequentially without skewing. Furthermore, a fourth order Runge Kutta integration algorithm was employed which is as follows:

$$y^{P1} = y_n + \frac{h}{2}(\dot{y}_n) \tag{5-1}$$

$$\dot{y}^{P1} = f(y^{P1}, t_{n+\frac{1}{2}}) \tag{5-2}$$

$$y^{P2} = y_n + \frac{h}{2}(\dot{y}^{P1}) \tag{5-3}$$

$$\dot{y}^{P2} = f(y^{P2}, t_{n+\frac{1}{2}}) \tag{5-4}$$

$$y^{P3} = y_n + h\dot{y}^{P2} \tag{5-5}$$

$$\dot{y}^{P3} = f(y^{P3},\ t_{n+1})$$

$$y_{n+1} = y_n + h\left[\frac{1}{6}(\dot{y}_{n-1}) + \frac{1}{3}(\dot{y}^{P1}) + \frac{1}{3}(\dot{y}^{P2}) + \frac{1}{6}(\dot{y}^{P3})\right] \qquad (5\text{-}7)$$

In the fourth order Runge Kutta algorithm, an initial half-step prediction of the integrated result is made (equation 5-1). This prediction utilizes the past integration result and the derivative (rate) based on the previous frame. Next a re-evaluation of the rate is accomplished utilizing the initial half-step prediction (equation 5-2), which is then used for a second half-step prediction of the integrated value (equation 5-3). The derivatives are re-evaluated for the third time within the frame based on the second half-step predicted output (equation 5-4). The Open Euler integration method is then utilized for a full-step prediction to the end of the frame (equation 5-5) from which a fourth and final derivative evaluation is then performed (equation 5-6). A weighted sum of the derivative evaluations is then utilized with the past integrated value to construct the new, current frame integration result (equation 5-7). This integration method offers accurate results, but as can be expected is time consuming due to the necessary repeated derivative evaluations.

A Bode metric was utilized to measure the effects of the digital computer frame time with the aforementioned digital airframe mechanization. Bode magnitude and phase data were generated for a sinusoidally oscillating elevator input at 512 discrete constant frequencies for both the digital airframe mechanization and the theoretical airframe. Therefore, as the frame time was varied, the relative distortion or departure of the digital airframe model solution from the analytical solution could be measured. The variation in the Bode gain for the pitch attitude response as the digital frame time is varied from 0.00833 seconds to 0.1 seconds, is shown in Figure 36.

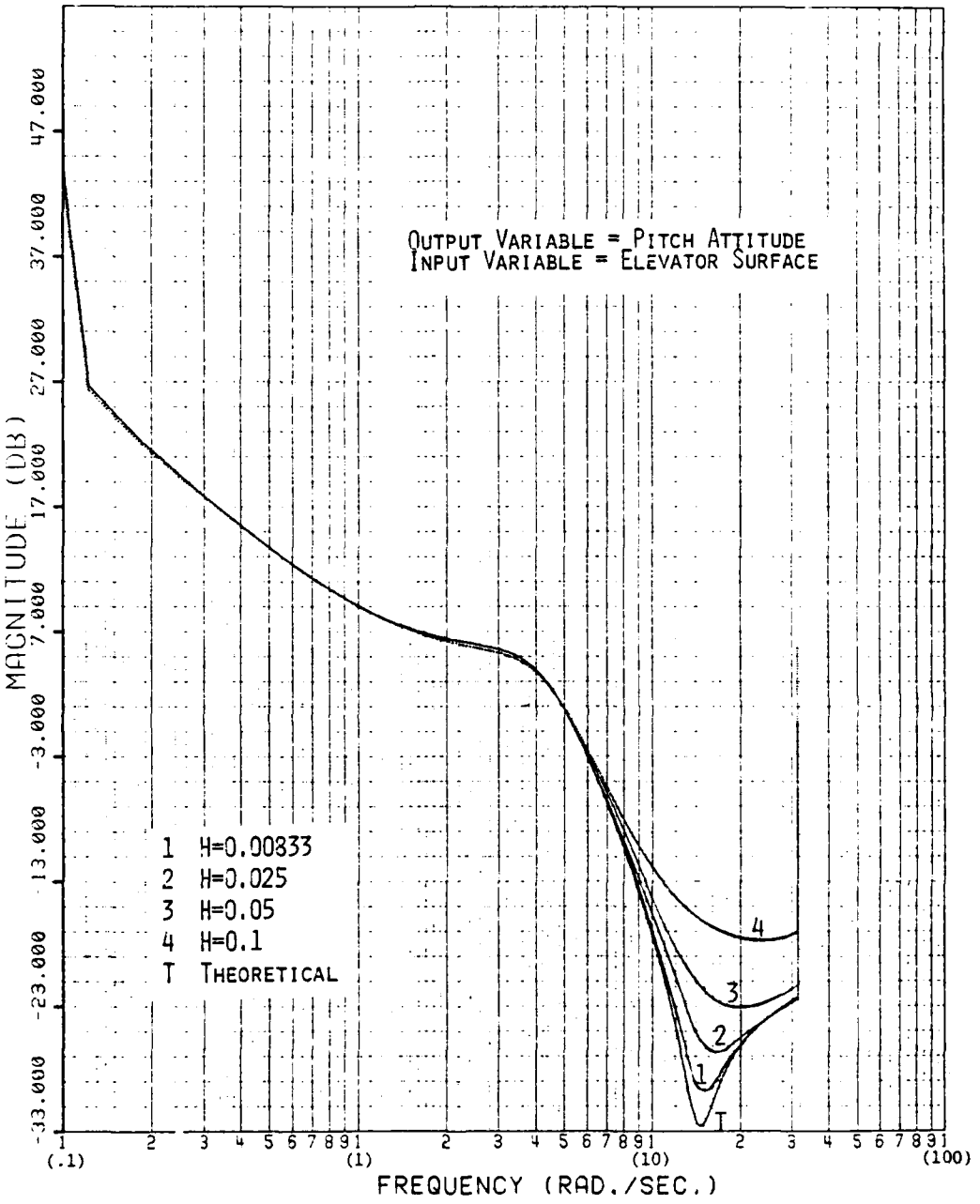

FIGURE 36. VARIATION IN BODE GAIN DUE TO FRAME TIME

In Figure 36, it can be seen that increasing the frame time produces an appreciable shift in gain in the system at the higher frequencies, relative to the theoretical solution. The theoretical solution represents the Bode plot as generated from the theoretical time history response. Similarly, as presented in Figure 37 for airframe pitch attitude, the Bode phase angle develops a significant amount of variation, especially at the higher frame times. The phase angle plot for frame times up to 0.05 seconds tends to distort primarily at frequencies above 2 radians per second. The 0.1 second frame time case, however, maintains a shift for all frequencies (in Figure 37, this curve is denoted by the dotted line at low frequencies).

The pitch attitude response is an excellant parameter to use to show the effects of frame time since it is influenced adequately by both the phugoid and short period dynamics of the airframe. The forward velocity variable produces responses which are of interest to the phugoid motion of the airframe. On the other hand, the angle of attack parameter generates responses which are dominated by short period dynamics.

During the investigation of the effects of digital computer frame time, it was found that the forward velocity Bode plot maintained an excellant match with the theory, even at the higher frame times. This fact is evident as shown in Figures 38 and 39, for the Bode gain and phase, respectively. These plots were generated from the forward velocity response at a frame time of 0.1 seconds. Since the simulated airframe utilized an all digital mechanization (including the forcing function) and no serious distortion occurred in the frequency domain plots, it can be concluded that frame times up to 100 milliseconds have little effect on phugoid-type solution accuracy. Furthermore, large power spectra shifts found during the tests reported on in Section 4 can be concluded to be caused by the hybrid linkage.

Short period dynamics, however, as typified by angle of attack variable are greatly affected by digital computer frame time. As shown in Figure 40,

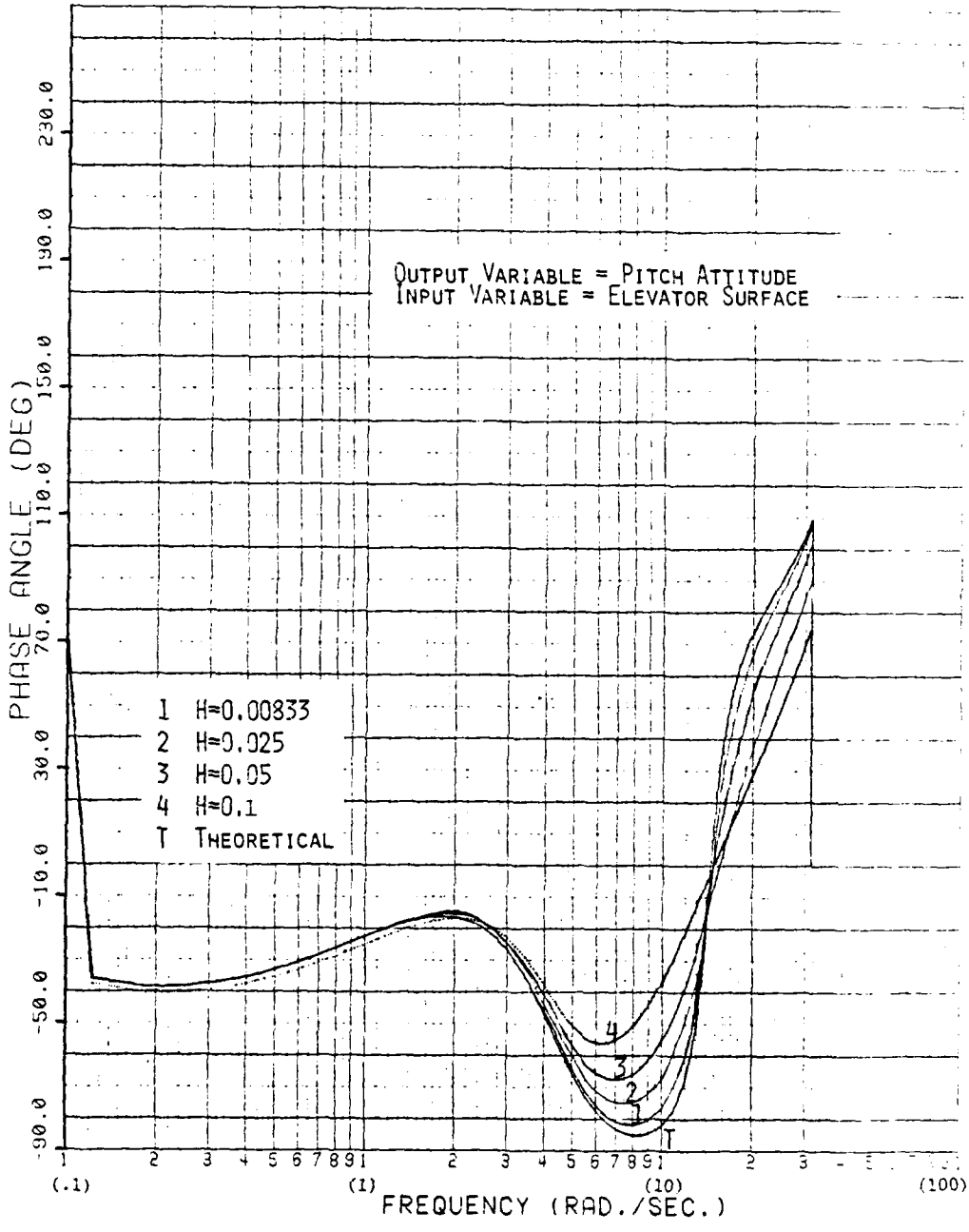

FIGURE 37. VARIATION IN BODE PHASE ANGLE DUE TO FRAME TIME

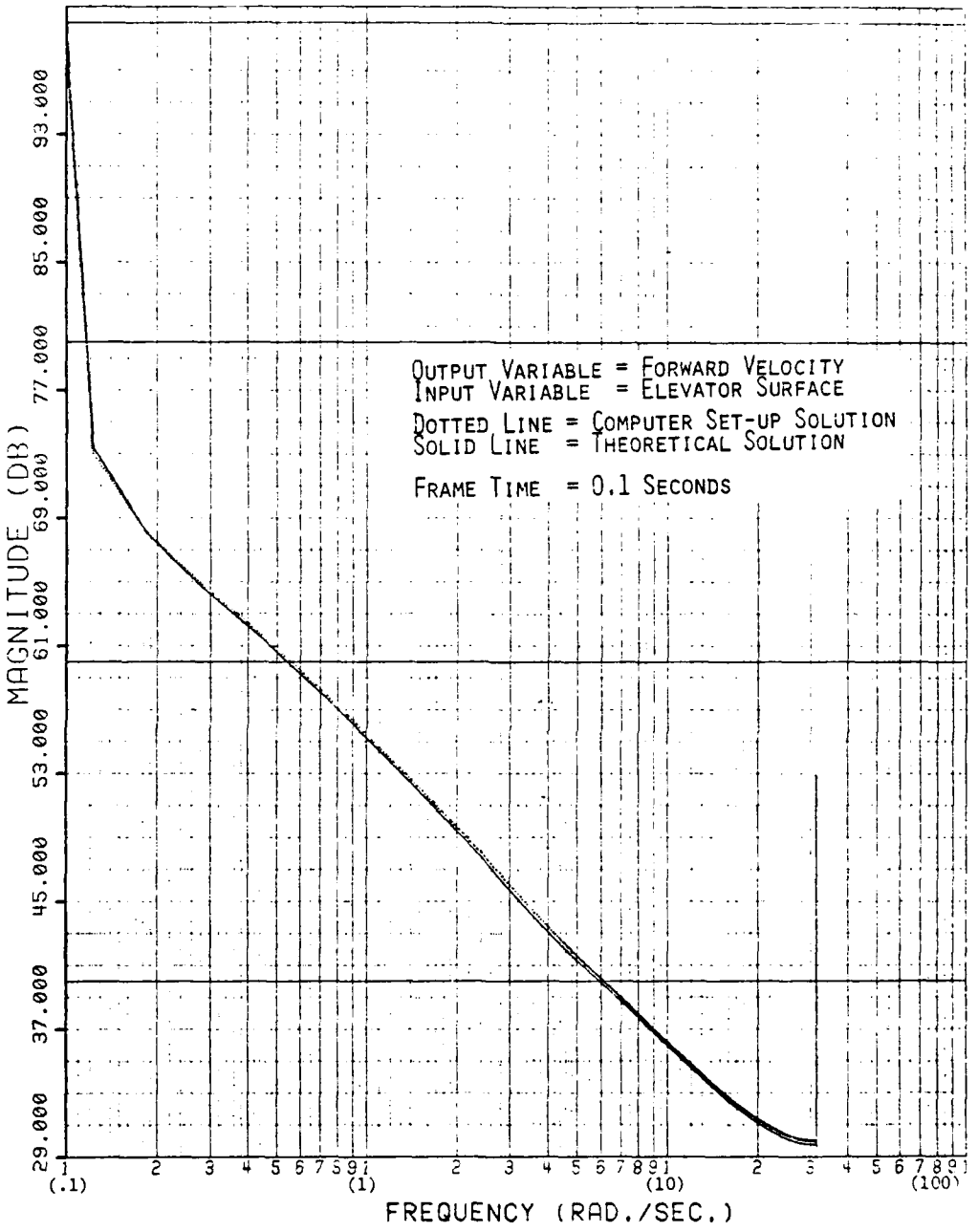

FIGURE 38. BODE GAIN FOR FORWARD VELOCITY, FRAME TIME = 0.1 SECONDS

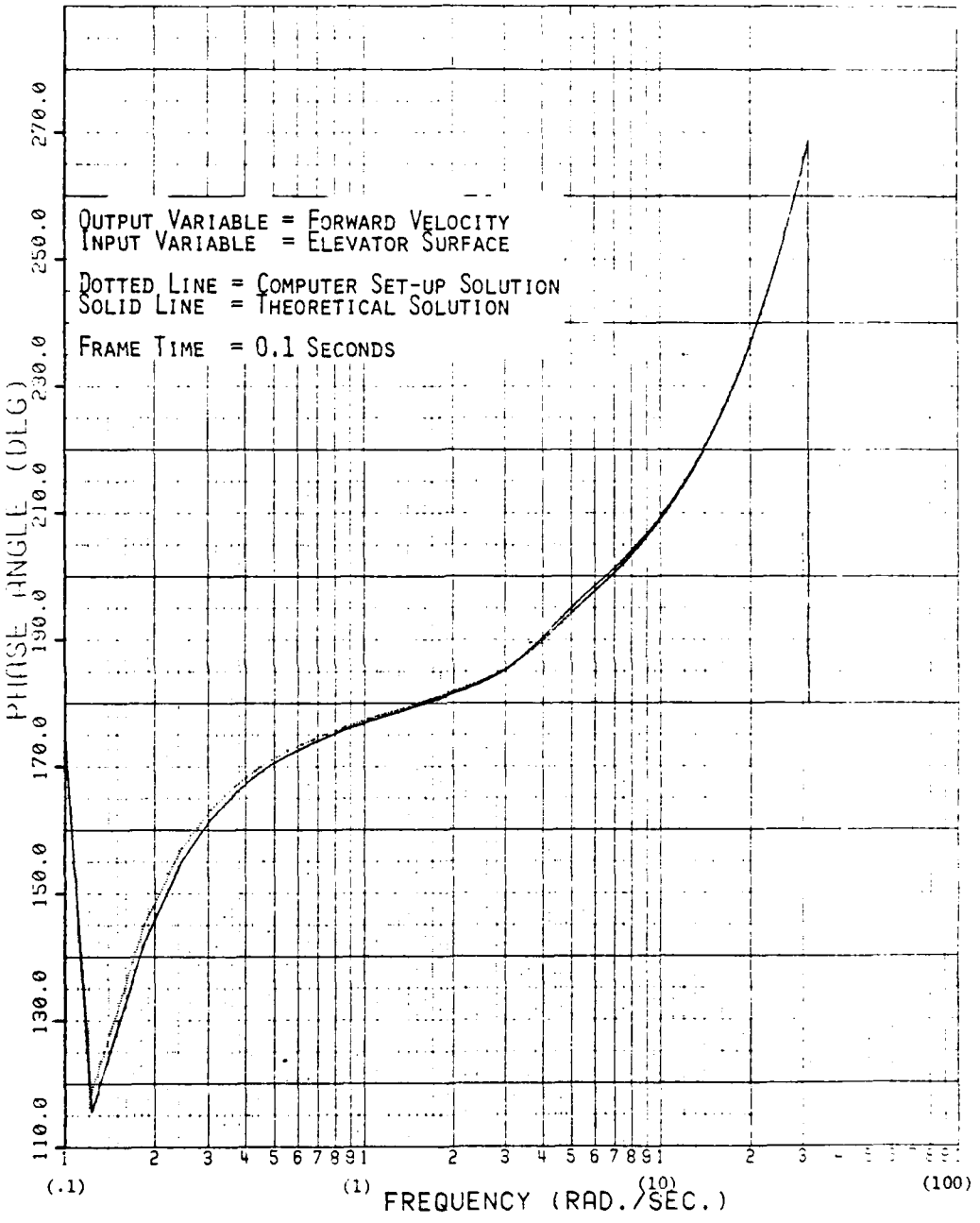

FIGURE 39. BODE PHASE ANGLE FOR FORWARD VELOCITY, FRAME TIME = 0.1 SECONDS

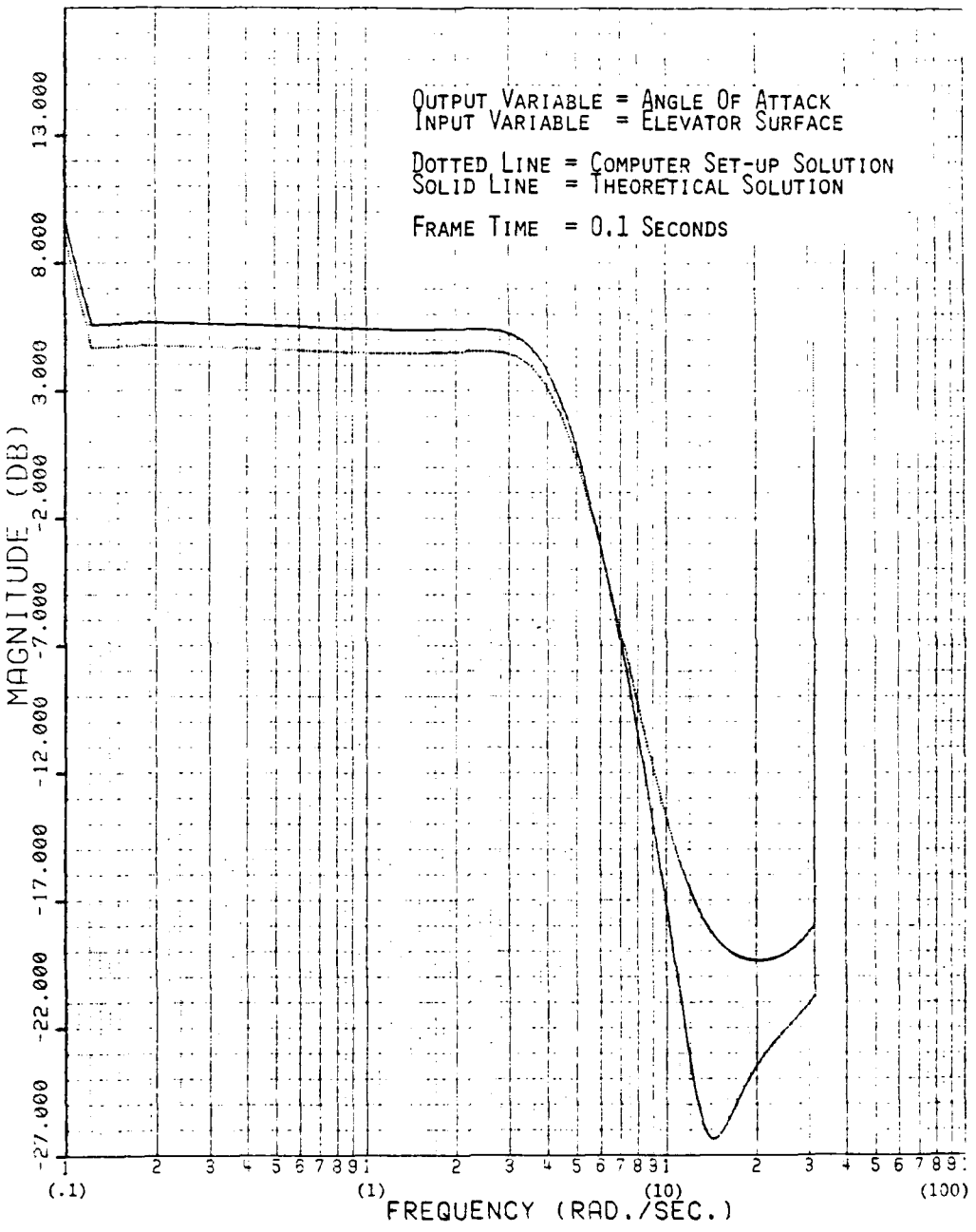

FIGURE 40. BODE GAIN FOR ANGLE OF ATTACK, FRAME TIME = 0.1 SECONDS

appreciable gain errors, relative to the theoretical case, are generated for angle of attack for the 100 millisecond frame time case shown. Similarly, the Bode phase plot for angle of attack is greatly distorted, even at very low frequencies, when the frame time is increased to 100 milliseconds. This can be seen in Figure 41. It is interesting to note that the pitch attitude variable resembles the forward velocity characteristics in the low frequency region and the angle of attack characteristics in the high frequency region.

Another metric used to investigate the effects of computer frame time on solution accuracy is the accuracy chart. As described in Appendix B, accuracy charts indicate the percent error of the complex gain in a system, relative to the analytical complex gain. Since it was shown that pitch attitude yields adequate information about both longitudinal dynamics modes, accuracy charts are presented for pitch attitude as the frame time is varied.

Figure 42 shows an accuracy chart for when the digital computer frame time is set at 0.00833 seconds. The airframe frequency response characteristics remain highly accurate up to around 10 radians per second. After that point, the error builds from a value of approximately 0.1 percent error to a peak value of 0.9 percent at 15 radians per second. As the frequency is increased past 15 radians per second, the solution accuracy improves drastically to better than 0.01 percent at 20 radians per second and beyond.

For the 0.025 second frame time case, the pitch attitude frequency response characteristic remains very accurate with a gradual increase to a peak error of 4 percent at 15 radians per second, as shown in Figure 43. A rapid error falloff is then experienced which eventually drops to a low value of 0.03 percent at 26 radians per second. As the frequency increases past 26 radians per second, the error once again begins to build up.

Figure 44 shows similar trends when the frame time is increased to 0.05 seconds. The peak error in this case, however, is 12 percent at 15 radians per second with a subsequent dropoff to 0.27 percent at 30 radians

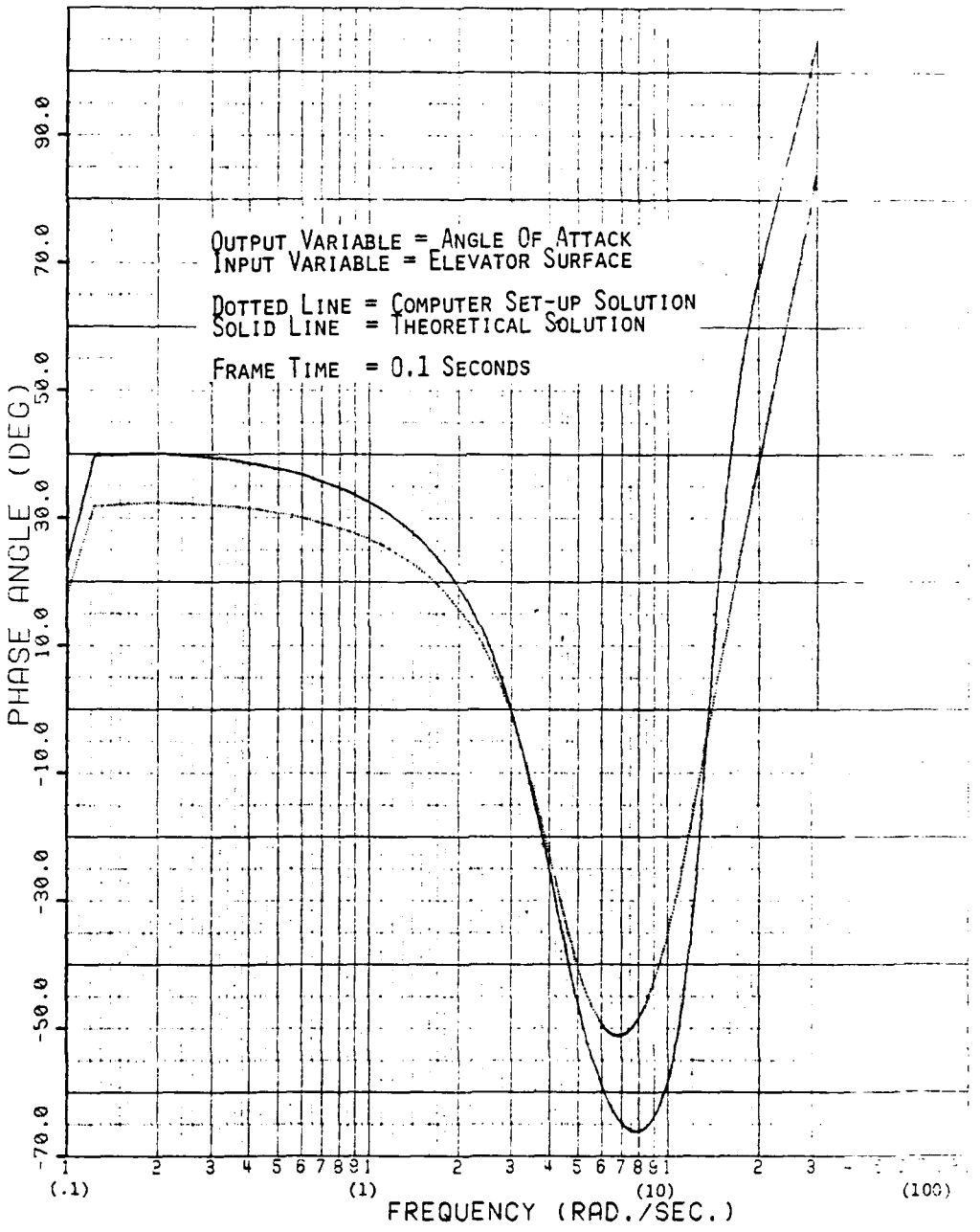

FIGURE 41. BODE PHASE ANGLE FOR ANGLE OF ATTACK, FRAME TIME = 0.1 SECONDS

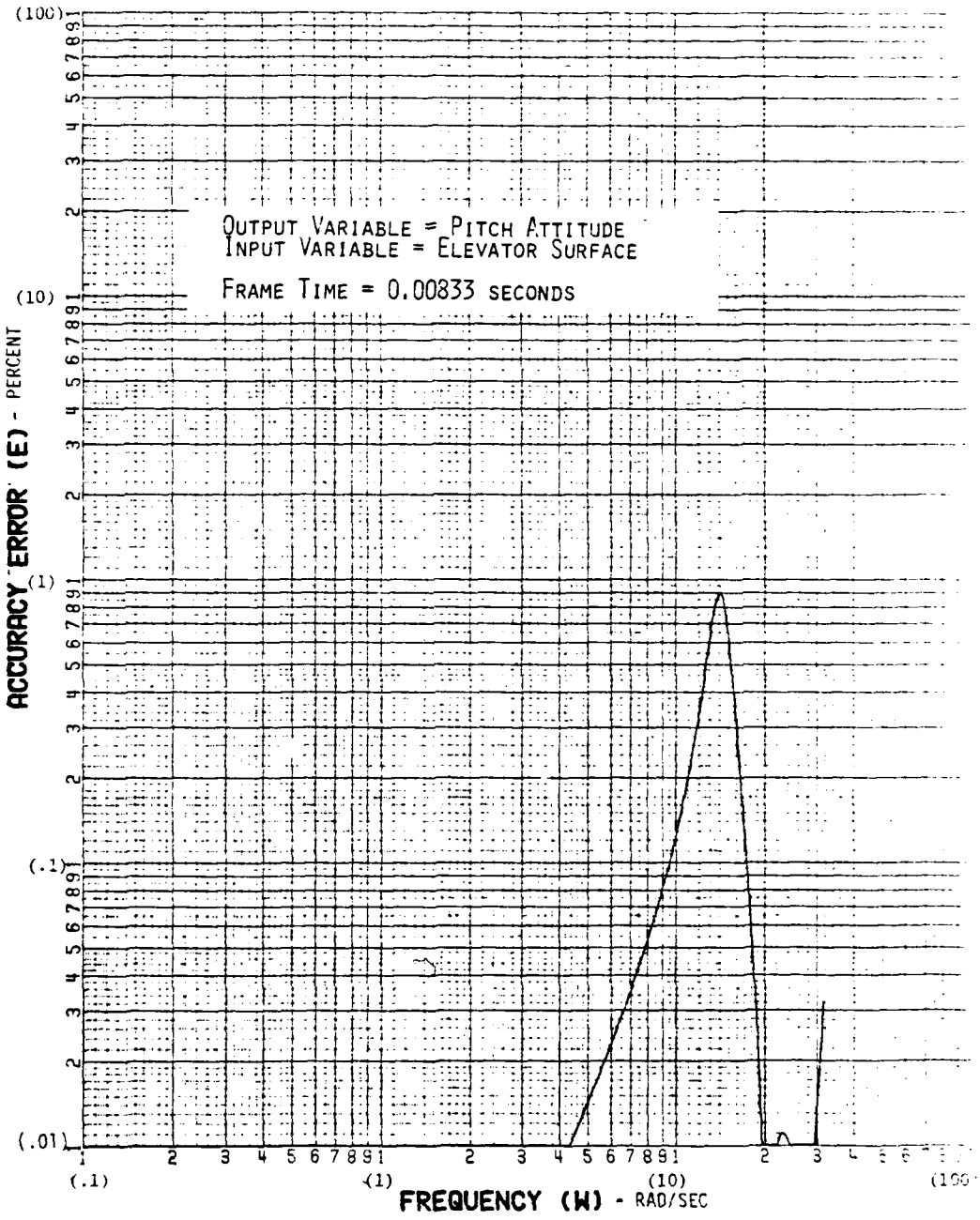

FIGURE 42. ACCURACY CHART - PITCH ATTITUDE, FRAME TIME = 0.00833 SECONDS

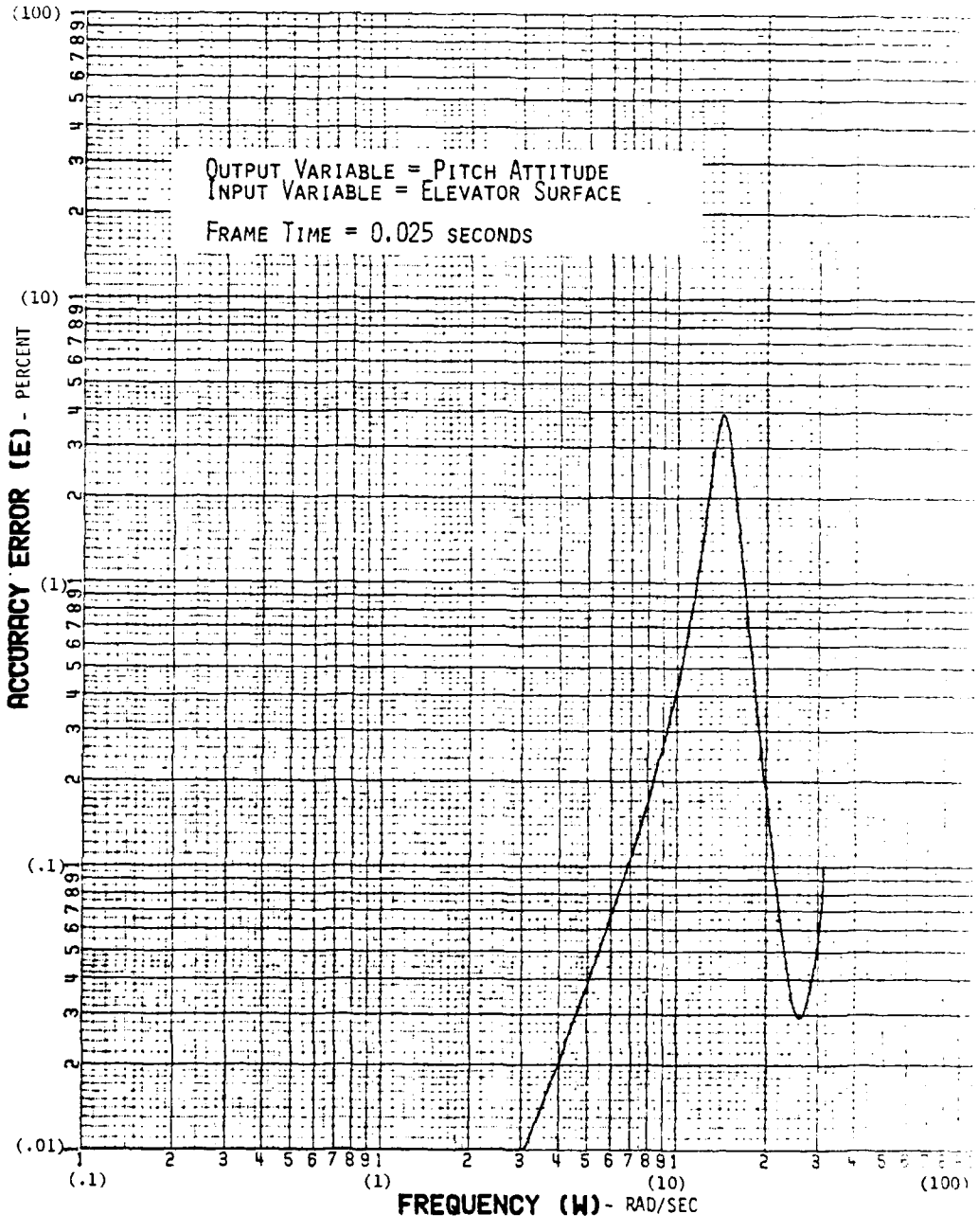

FIGURE 43. ACCURACY CHART - PITCH ATTITUDE,
FRAME TIME = 0.025 SECONDS

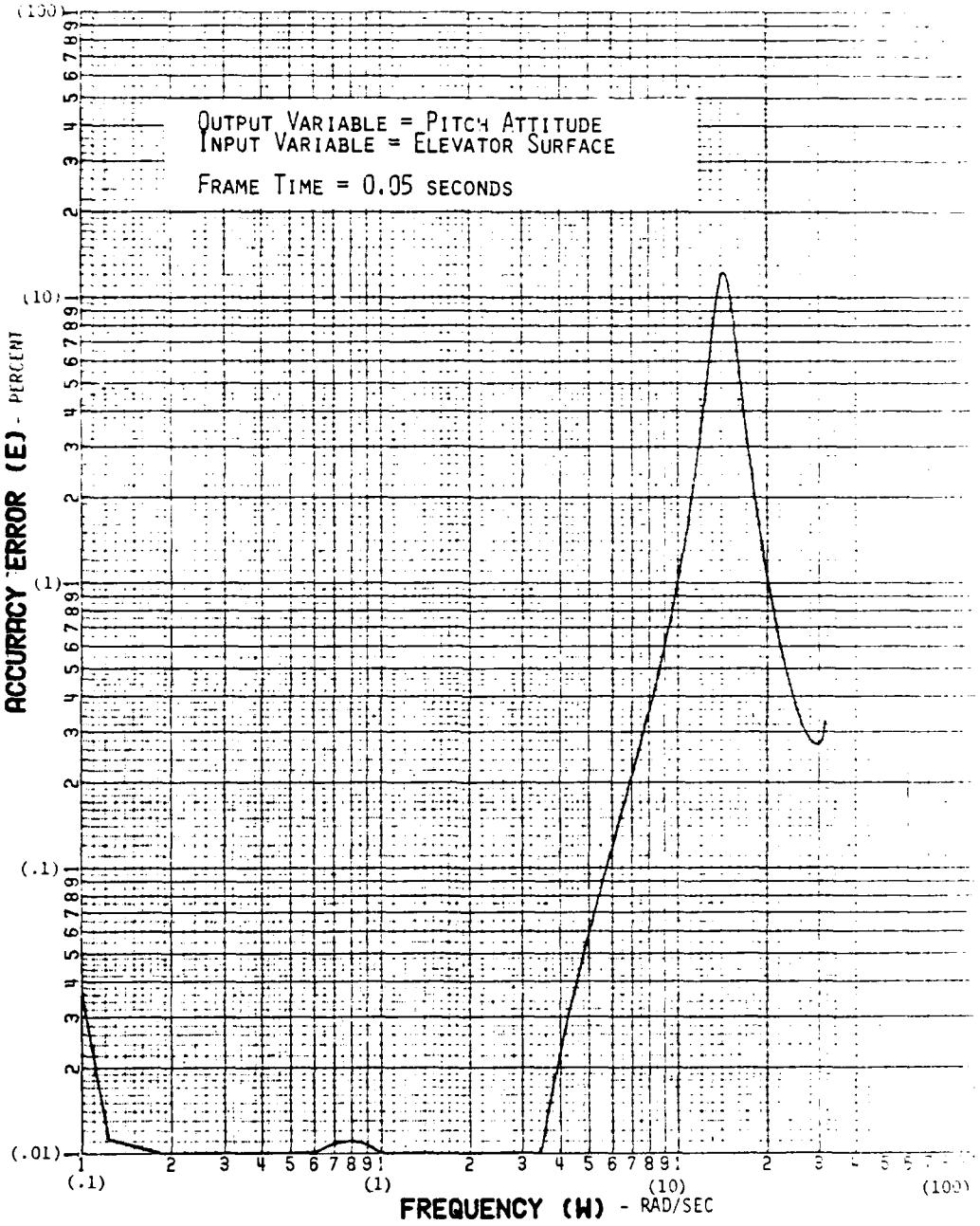

FIGURE 44. ACCURACY CHART - PITCH ATTITUDE, FRAME TIME = 0.05 SECONDS

per second. Also, it appears that some lower frequency errors (due to the phugoid motion inaccuracies) are starting to increase in size as magnitudes of 0.01 percent are experienced in the frequency band between 0.1 and 1.0 radians per second. Up to this point, most of the errors could be attributed to the sensitivities of the short period frequency response.

Finally, as the frame rate is decreased to 10 iterations per second (100 millisecond frame time), low frequency errors increase. However, as can be seen in Figure 45, these errors are 3 orders of magnitude lower than the high frequency errors which tend to peak at 45 percent error at 15.3 radians per second. This is in contrast to a .057 percent error peak at 3 radians per second under these conditions.

In conclusion, a Bode and Accuracy Chart metric was utilized to investigate the effects of digital computer frame time on airframe solution accuracy. The frequency responses shown in these plots were always related to the theoretical frequency response. Phugoid mode equations tend to have some inaccuracies induced as frame time is increased, but this effect is not so adverse as is the case with the high frequency (short period mode) related equations.

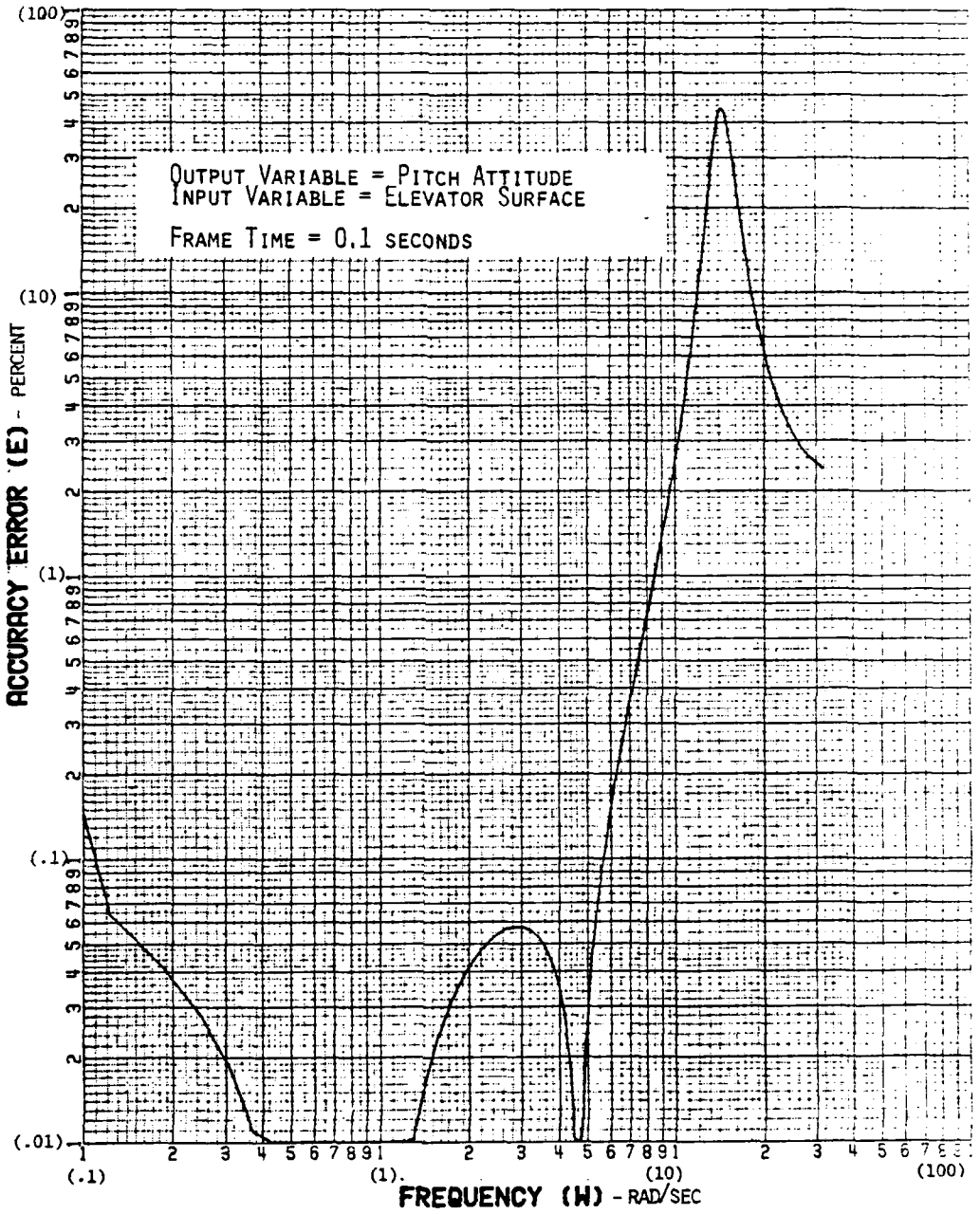

FIGURE 45. ACCURACY CHART - PITCH ATITTUDE,
FRAME TIME = 0.1 SECONDS

6. ERROR ACCUMULATION

As a result of errors induced by the various components in an analog, hybrid, or digital computing system, whether hardware or numerical in nature, the solution generated by the computer will deviate from the correct values as dictated by the analytical solution. This deviation can be expected to become larger and larger as time progresses and errors accumulate. When a computing system is operated over a specified time interval, it is desired to generate an estimate to understand what the greatest error or greatest deviation from the analytical solution will be as a result of the accumulated error. This accumulated error estimation constitutes the most difficult problem in the error analysis of hybrid computer systems. In most large scale simulations, it is virtually impossible to predict an overall absolute solution accuracy. This is especially true if a large time increment or number of computer cycles is involved.

The concept of error dominance can be used to gain insight into the effects of propagated or accumulated error. For hybrid computation, the accumulated error will be dominated by a particular error source if, while computing in a stable manner, the local per-step error committed by that error source is in magnitude much larger than the other errors contaminating the solution. This concept leaves an uncertain region where several or even all hybrid computer error sources are within an order of magnitude of each other. If this is the case, then all local per-step errors compete in forming the accumulated error and no one source dominates. To use error dominance as a basis for estimating error accumulation effects, the relative magnitude of each error source must be determined for the particular system of equations being mechanized.

To study the effects and trends of accumulated error with the linearized longitudinal airframe model described in Section 4.2, the most accurate mechanization of each computer configuration was established. Listed below are the particular test conditions/numerical methods which were utilized to study accumulated error effects for each computer configuration listed:

ANALOG

1) Potentiometer settings and amplifier gains on the Comcor 5000 were set such that component saturation did not occur and the majority of the full scale analog voltage was utilized.

HYBRID-SINGLE CPU

1) Potentiometer settings and amplifier gains on the Comcor 5000 were set such that component saturation did not occur and the majority of the full scale analog voltage was utilized.

2) The Master Hybrid CPU frame time was set at 8.333 milliseconds, which was the fastest schedulable frame time (without intra-program looping).

3) The minimum number of digital-to-analog converter channels (3) was utilized.

4) The minimum number of analog-to-digital converter channels (6) was utilized.

5) The hybrid linkage word length was set at its highest physical value of 15 bits.

HYBRID-DUAL CPUS WITH SHARED COMMON MEMORY

1) Potentiometer settings and amplifier gains on the Comcor 5000 were set such that component saturation did not occur and the majority of the full scale analog voltage was utilized.

2) The Master Hybrid CPU frame time was set at 8.333 milliseconds which was the fastest schedulable frame time (without intra-program looping).

3) The Master Digital CPU frame time was set at 8.333 milliseconds which was the fastest schedulable frame time (without intra-program looping).

4) The integration of the vertical and pitch acceleration equations in the Master Digital CPU utilized Mod Gurk numerical integration.

5) The minimum number of digital-to-analog converter channels (3) was utilized.

6) The minimum number of analog-to-digital converter channels (6) was utilized.

7) The hybrid linkage word length was set at its highest physical value of 15 bits.

HYBRID-DUAL CPUS WITH I/O LINK

1) Potentiometer settings and amplifier gains on the Comcor 5000 were set such that component saturation did not occur and the majority of the full scale analog voltage was utilized.

2) The Master Digital CPU frame time was set at 8.333 milliseconds, which was the fastest schedulable frame time (without intra-program looping).

3) The Multiple System Interface (MSI) CPU was left free-running to generate aerodynamic data. When the Master Digital CPU triggered the MSI through the I/O Link, it would wait until the MSI was completed with its computations before proceeding on. This eliminated time skewing over the I/O link.

4) The integration of the equations-of-motion was accomplished in the Master Digital CPU with the 2nd order Runge Kutta method.

5) The minimum number of digital-to-analog converter channels (3) was utilized.

6) The minimum number of analog-to-digital converter channels (6) was utilized

7) The hybrid linkage word length was set at its highest physical value of 15 bits.

Having established the most accurate airframe mechanization on each of the four computer configurations, the accumulated error or deviation of the model from the known zero condition trim point was monitored for a period of two hours.

For the analog configuration, a transient was induced when the computer was placed into the operate (computer) mode from the reset condition. This transient is sometimes referred to as "jump error". The jump-effect is a very small initial step displacement of an integrator output when the computer is placed into the operate mode. The jump error transient excites the phugoid motion of the airframe as can be seen in the forward velocity trace in Figure 46 (the frequency of oscillation of the forward velocity perturbation equals that of the airframe's phugoid frequency). The stair-stepped appearance of the analog trace shown in Figure 46 is due to the A/D converter (quantizer) which was required to record the data on the digital computer's magnetic tape. The size of the quantum levels for the 100 volt analog utilized system was 0.0061035 units.

As can be seen in Figure 46, after the initial transient subsides, the airframe responses maintain a slight bias relative to the zero trim condition with some high frequency noise signals superimposed. These accumulated errors retain this standoff condition throughout the 2 hour run. This is even true when a pitch attitude "glitch" was experienced at about the mid-test point. The exact cause of the glitch cannot be determined, although it is believed to be inherent in the computer hardware. In any case, the perturbed airframe reached approximately 70 percent of the amplitudes shown in Figure 46 but then returned to the standoff trim condition. This non-zero trim condition denotes the steady state values required by the computer solution due to the errors present in the mechanization to balance the airframe's forces and moments and drive the accelerations to zero. In summary,

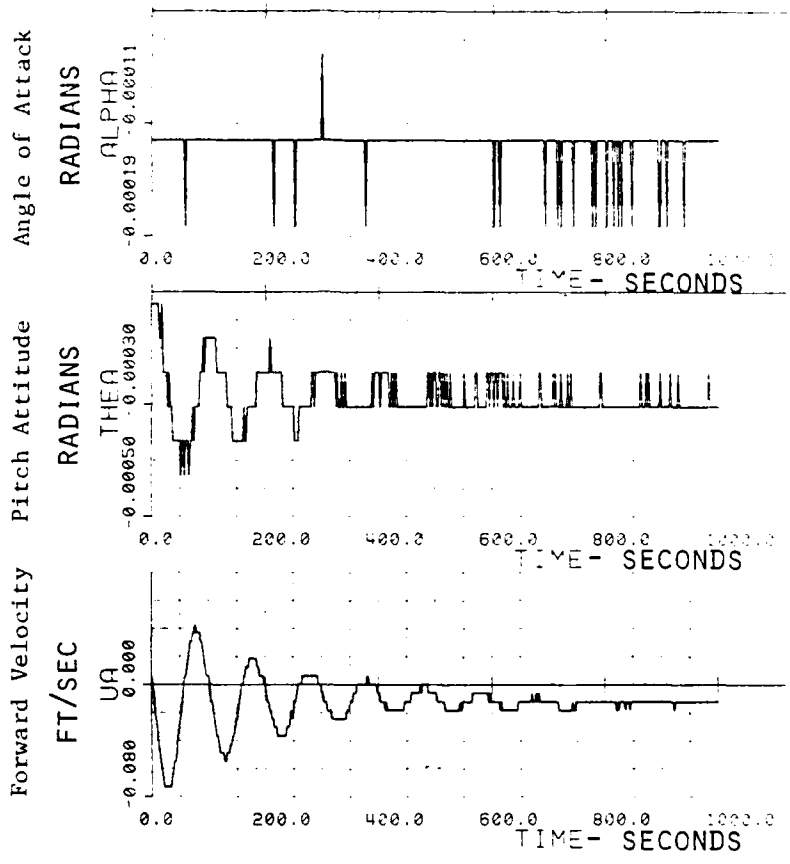

FIGURE 46. ANALOG CONFIGURATION ERROR ACCUMULATION

the analog computer mechanization trim conditions differed from their nominal zero values and were found to be:

Angle of Attack = -0.000122 radians
Pitch Attitude = -0.0003 radians
Forward Velocity = -0.012 feet/second

For the hybrid-single CPU computer configuration, a similar standoff condition from the zero trim condition occurs, but with increased severity for the forward velocity response. The initial response of the airframe in this error accumulation test is shown in Figure 47. Recall that in this configuration, the aerodynamic buildup was computed in the digital computer, whereas all integration of the equations-of-motion was accomplished on the

analog computer. As can be seen in Figure 47, the solution of equations mechanized in the hybrid-single CPU computer configuration established steady-state trim positions at:

Angle of Attack = 0.0 radians
Pitch Attitude = -.00006 radians
Forward Velocity = -1.05 feet/second

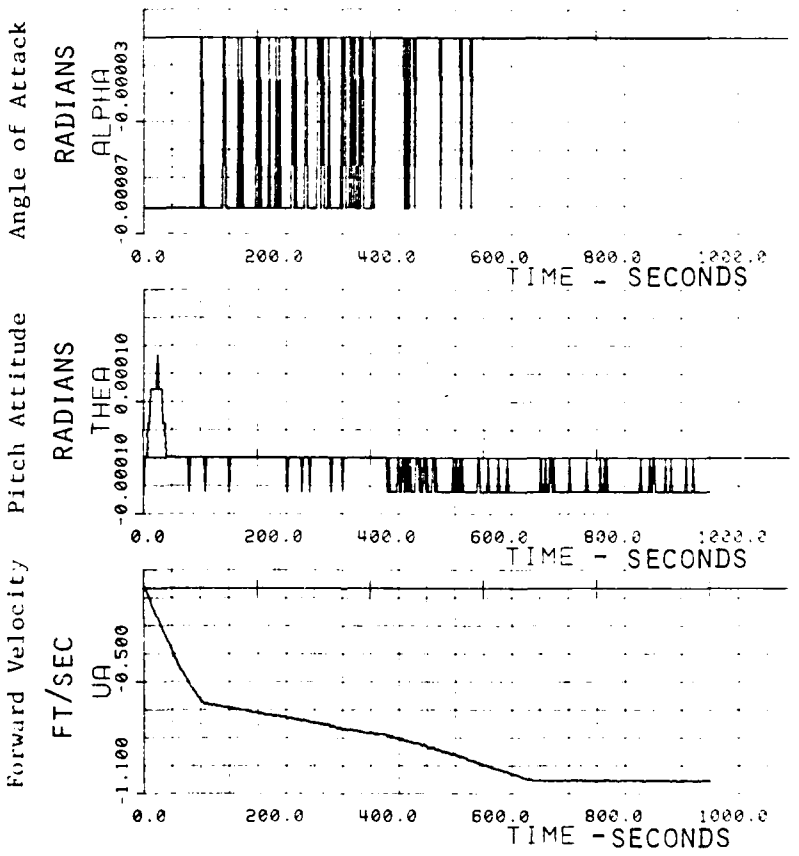

FIGURE 47. HYBRID-SINGLE CPU ERROR ACCUMULATION

The values for pitch attitude and angle of attack are found to relate closer to the true zero trim values (as specified by the analytical solution), relative to the analog computer configuration described earlier. exact cause for the large forward velocity trim change is not absolut

AD-A081 953 NORTHROP CORP HAWTHORNE CA AIRCRAFT GROUP F/G 20/4
HYBRID COMPUTER ERRORS IN ENGINEERING FLIGHT SIMULATION.(U)
AUG 79 R A WEEKS F33615-78-C-3608
UNCLASSIFIED NOR 79-89 AFFDL-TR-79-3091 NL

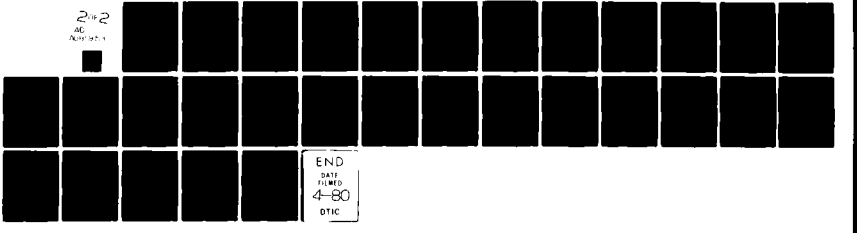

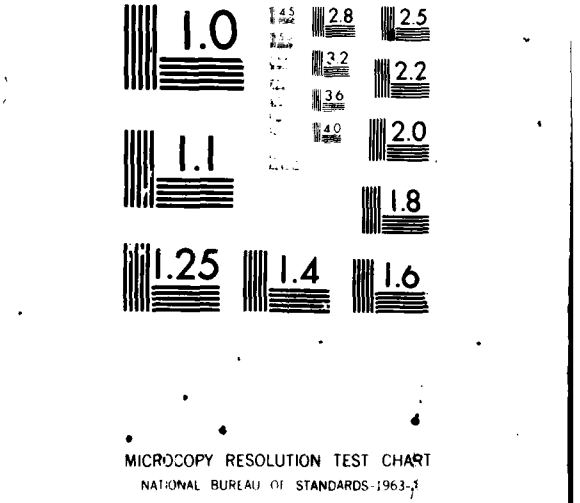
1.0
1.1
1.25
1.4
1.6
1.8
2.0
2.2
2.5
2.8
3.2
3.6
4.0
MICROCOPY RESOLUTION TEST CHART
NATIONAL BUREAU OF STANDARDS-1963-A

understood. However, it appears that at the initiation of the compute mode, a 3 quantum level elevator transient was experienced. The more immediate effect of this transient can be noted from the pitch attitude response. In any case, after approximately 11.2 minutes into the run, the computer mechanization of the equations-of-motion became balanced and no further long period transients were experienced. Furthermore, low magnitude short period transients appear to have virtually no effect on the airframe response.

Figure 48 shows the effect of accumulated error on the trim position of the airframe model in the hybrid-dual CPUs with shared common memory configuration.

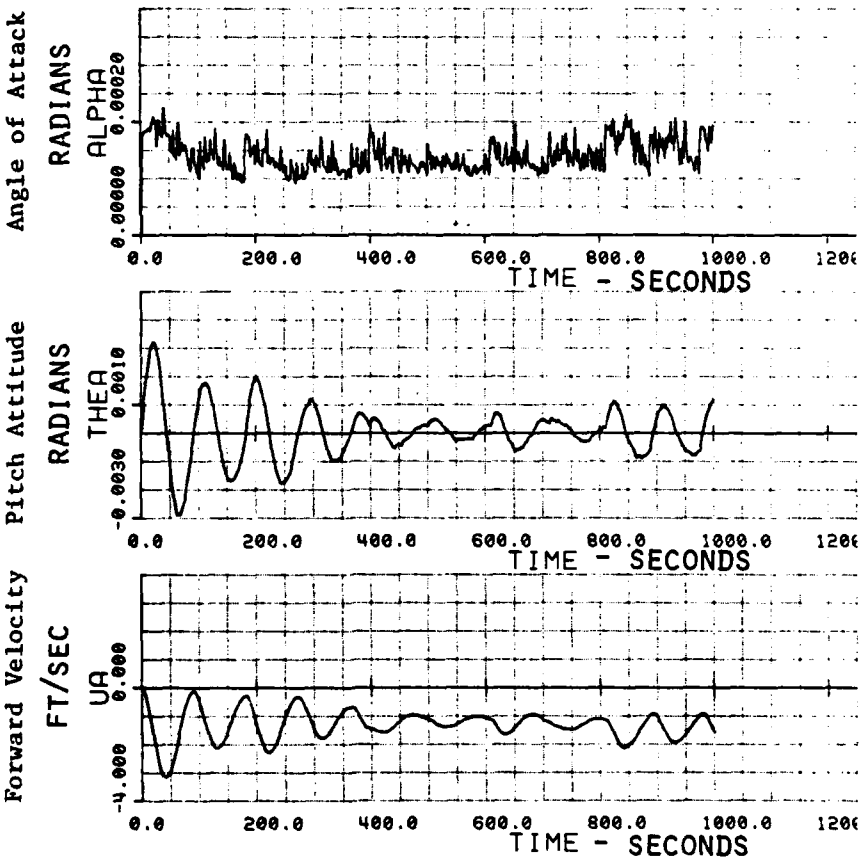

FIGURE 48. HYBRID-DUAL CPUS WITH SHARED COMMON MEMORY ERROR ACCUMULATION

As with the hybrid-single CPU configuration, a 3 quantum level initial elevator transient (caused by the reset-to-compute mode change) sets the computer mechanization into motion. Since this configuration utilizes much digital computation (only the forcing function and forward acceleration integrator are analog), the quantized elevator input has a much greater effect on the airframe response. This is due to the ability of the digital computer to handle extremely small values as valid data. Also, there is a lack of computing component damping which is found in analog circuits (transfer function characteristics of operational amplifiers were discussed in Section 3). This higher sensitivity which largely affects the airframe acceleration equations accounts for the nonlinearity appearance of the airframe responses, as shown in Figure 48.

The airframe perturbations attained a near steady-state condition after the data run had progressed approximately 74 minutes, at which time offset trim change values were found to be:

Angle of Attack = 0.0002 radians
Pitch Attitude = 0.0004 radians
Forward Velocity = -1.8 feet/second

Results of the accumulated error test at the airframe trim condition, for the hybrid-dual CPUs with an I/O link configuration, yielded much the same responses as found with the hybrid-dual CPUs with shared common memory configuration. Trim biases, as shown in Figure 49, were recorded as:

Angle of Attack = 0.00018 radians
Pitch Attitude = 0.0005 radians
Forward Velocity = -1.6 feet/second

Justification for the trend of these responses are basically the same as those described for the hybrid-dual CPUs with shared common memory configuration since the I/O link configuration was all digital except for the elevator surface forcing function.

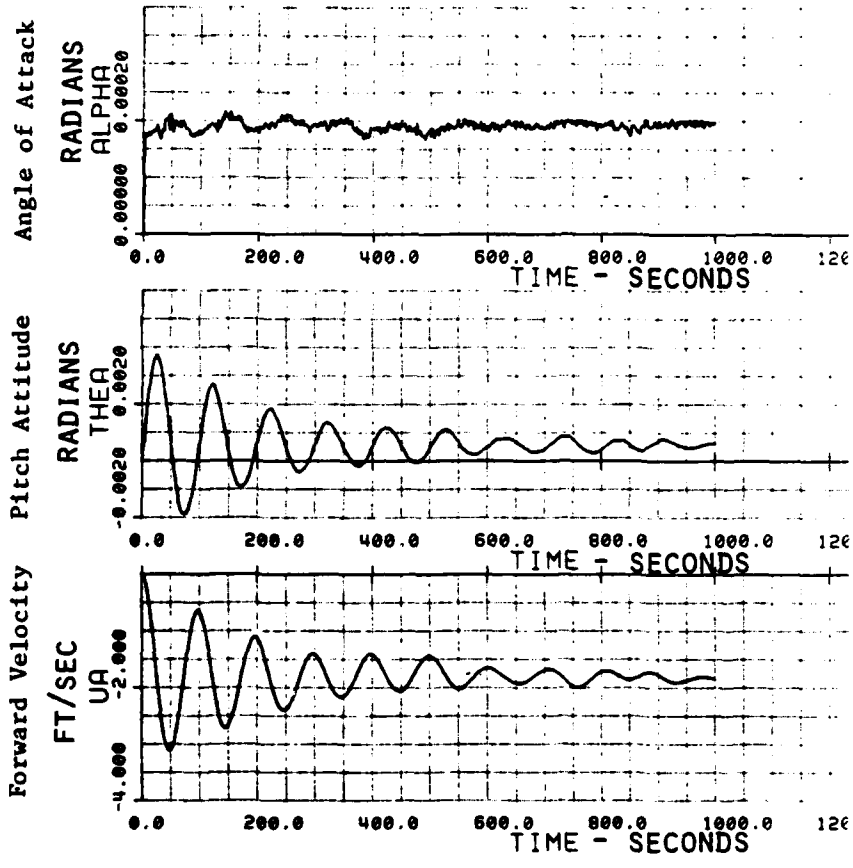

FIGURE 49. HYBRID-DUAL CPUS WITH I/O LINK ERROR ACCUMULATION

Hence, an evaluation of the ability of four separate computer configurations to hold a known trim condition was accomplished with the aforementioned results. It appears that the low frequency (phugoid) motion equation (forward velocity) is most sensitive to accumulated error. Furthermore, it was demonstrated that the hybrid linkage and analog mode transients induced a significant amount of accumulated errors into the airframe mechanization.

7. CONCLUSIONS AND RECOMMENDATIONS

A linear airframe simulation was constructed with an all analog, 3 hybrid, and all digital computer configuration so as to investigate the effects of controllable error sources on solution accuracy. In many instances, the analog mechanization provided for the most accurate results, but the program size capability is extremely limited. For the hybrid configurations, large peak power magnitude shifts at a reference frequency were observed for the phugoid mode variables. This result is attributed to the hybrid linkage time delay and word length. Short period dynamics were greatly affected by digital frame time and hybrid linkage quantization resolution. For digital mechanizations, choice of numerical integration technique directly influences the stability of the simulated system.

Since the complexity of aerospace simulation problems makes pure analog computation obsolete, attention should be focused on digital mechanizations. The multiple CPU configuration with an I/O link computer set-up looks promising for use with special purpose high-speed processors. It is recommended that further research be initiated to determine the effectiveness of Array Processors in manned aerospace simulations. Since higher-ordered numerical integration techniques offer improved results, further research should indicate the feasibility of the use of Array Processors for high-speed/high-order nonlinear numerical integration. Also since many simulations do require an analog interface, it is further recommended that high-speed hybrid linkage methods and hardware be investigated.

REFERENCES

1. Aaron, M. R. and Kaiser, J. F., On The Calculation Of Transient Response, Proceedings of the IEEE, Volume 53, 1966.

2. Allen, R. H., Numerically Stable Explicit Integration Techniques Using A Linearized Runge Kutta Extension, October 1969

3. Baxter, D. C., The Digital Simulation Of Transfer Functions, National Research Council of Canada, April 1964.

4. Beattie, M. L., et al, Redundant Flight Critical Control System Evaluation, FAA-SS-73-2-2, October 1974.

5. Bekey, George A., and Karplus, Walter J., Hybrid Computation, John Wiley & Sons, Inc., 1968.

6. Bekey, G. A. and Tomovic, R., Sensitivity Of Discrete Systems To Variation Of Sampling Interval, IEEE Transactions On Automatic Control, AC-11, April 1966

7. Bennett, W. R., Spectra Of Quantized Signals, Bell System Technical Journal, Volume 27, July 1948.

8. Benyon, P. R., A Review Of Numerical Methods For Digital Simulation, Simulation, November 1968.

9. Blum, E. K., A Modification Of The Runge-Kutta Fourth-Order Method, Mathematics of Computation, Volume 16, Number 78, April 1952.

10. Boxer, R. and Thaler, S., A Simplified Method Of Solving Linear And Nonlinear Systems, Proceedings of the IRE, January 1956.

11. Brandin, David H., Numerical Integration And Digital Simulation Of Continuous Systems (Technical Comment), Simulation, October 1967.

12. Brandon, Daniel M., Jr., A New Single-Step Implicit Integration Algorithm With A-Stability And Improved Accuracy, Simulation, July 1974.

13. Cahn, Lee, Accuracy Of An Analog Computer, IRE Transactions On Electronic Computers, Volume EC-2, Number 4, December 1953.

14. Chase, P. E., Stability Properties Of Predictor-Corrector Methods For Ordinary Differential Equations, Journal of the Association For Computing Machinery, Volume 9, Number 4, October 1962.

15. Corrington, Murlan S., Simplified Calculation Of Transient Response, Proceedings of the IEEE, March 1965.

16. Crask, Geoffrey J., Snare Those Elusive Aliasing Errors, Electronic Design 11, May 1977.

17. Dahlquist, Germund G., Stability Questions For Some Numerical Methods For Ordinary Differential Equations, Available from DDC as AD 276990 .

18. Davis, Philip J., Numerical Integration, Blaisdell Publishing Company, 1967.

19. Davis, S. A., Feedback And Control Systems, Simon and Schuster, Inc., 1974.

20. D'Azzo, J. J. and Houpis, C. H., Feedback Control System Analysis And Synthesis, 2nd Edition, McGraw-Hill, Inc., 1966.

21. Deiters, Robert M., and Nomura, Tamiya, Circle Test Evaluation Of A Method Of Compensating Hybrid Computing Error By Predicted Integral, January 1967.

22. Dill, Carl, University of Illinois, Report Number 295, A Computer Graphic Technique For Finding Numerical Methods For Ordinary Differential Equations, January 1969.

23. Dow, Paul C., Jr., An Analysis Of Certain Errors In Electronic Differential Analyzers I-Bandwidth Limitations, IRE Transactions On Electronic Computers, Volume EC-2, Number 4, December 1957.

24. Dow, Paul D., An Analysis Of Certain Errors In Electronic Differential Analyzers II-Capacitor Dielectric Absorption, IRE Transactions On Electronic Computers, March 1958.

25. Duffin, R. J., Algorithms For Classical Stability Problems, SIAM Review, Volume II, Number 2, April 1969.

26. Fehlberg, Erwin, Low-Order Classical Runge-Kutta Formulas With Stepsize Control And Their Application To Some Heat Transfer Problems, NASA TR R-315 .

27. Froese, Charlotte, An Evaluation Of Runge-Kutta Type Methods For Higher Order Differential Equations, Journal of the Association For Computing Machinery, Volume 8, Number 4, October 1961.

28. Fry, C. R., An Experimental Comparison Of Runge-Kutta And Predictor-Corrector Numerical Integration Processes, Carde TN 1713/66.

29. Gagne, R. E., Smoothing Of Digital-To-Analog Converted Data In Digital Data Systems, MK-12, April 1964.

30. Gagne, R. E., and Baxter, D. C., Techniques For The Design Of Linear Digital Simulations, Simulation, August 1968.

31. Garrett, Patrick, Optimize Transducer/Computer Interfaces Technology Note, Electronic Design 11, May 1977.

32. Gaskill, Roger A., Fact And Fallacy In Digital Simulation, Simulation, November 1965.

33. Gaston, Jerry A. and Rowland, James R., Realtime Digital Integration For Continuous Kalman Filtering In Nonlinear Systems, Computer And Electronic Engineering, Volume 2, 1975.

34. Gear, C. W., The Automatic Integration Of Ordinary Differential Equations, Communications of the ACM, Volume 14, Number 3, March 1971.

35. Gear, C. W., Hybrid Methods For Initial Value Problems In Ordinary Differential Equations, University of Illinois Report Number 164, June 1964.

36. Gleman, Robert, Corrected Inputs-A Method For Improved Hybrid Simulation, Proceedings of the 1963 Fall Joint Computer Conference.

37. Giese, Clarence, State Variable Difference Methods For Digital Simulation, Simulation, May 1967.

38. Gilbert, Elmer G., Dynamic-Error Analysis Of Digital And Combined Analog-Digital Computer Systems, Simulation, April 1966.

39. Gilliland, M. C., The Spectral Evaluation Of Iterative Differential Analyzer Integration Techniques, Proceedings of the Western Joint Computer Conference, May 1961.

40. Giloi, Wolfgang and Grebe, Hartmut, Construction Of Multistep Integration Formulas For Simulation Purposes, IEEE Transactions on Computers, Volume C-17, Number 12, December 1968.

41. Gilot, W. Dr., Error-Corrected Operation Of Hybrid Computer Systems, 5th International Analogue Computation Meetings.

42. Gray, Harry J. Jr., Numerical Methods In Digital Real Time Simulation, PhD Dissertation, 1953.

43. Gray, H. J. Jr., Propagation Of Truncation Errors In the Numerical Solution Of Ordinary Differential Equations By Repeated Closures, Association for Computing Machinery, Volume 52, Number 1, January 1955.

44. Green, Alan Irwin, Design Of A Special Purpose Digital System, Available from DDC as AD 607679, January, 1958.

45. Gurk, Herbert M., The Use Of Stability Charts In The Synthesis Of Numerical Quadrature Formulae, Quarterly of Applied Mathematics, Volume 13, Number 1, April 1955.

46. Hamming, R. W., Stable Predictor-Corrector Methods For Ordinary Differential Equations, Journal of the Association for Computing Machinery, Volume 6, Number 1, January 1959.

47. Hammond, Joseph L. Jr., and Alford, Cecil O., Sampling Errors In Closed-Loop Hybrid Computer Programs, Simulation, December 1969.

48. Henrici, P., Error Propagation For Difference Methods, John Wiley and Sons, Inc., 1963.

49. Hildebrand, F. B., Introduction To Numerical Analysis, 2nd Edition, McGraw-Hill, Inc., 1974.

50. Hindmarsh, A. C., Numerical Solution Of Ordinary Differential Equations: Lecture Notes, June 1964.

51. Holbrook, J. G., Laplace Transforms For Electronic Engineers, 1966.

52. Honeywell Inc., Digital Flight Control Systems For Tactical Fighters, AFFDL-TR-73-119, Volume I.

53. Howe, R. M., Fogarty, L. E., Error Analysis Of Computer Mechanization Of Airframe Dynamics.

54. Hull, T. E., et al., Comparing Numerical Methods For Ordinary Differential Equations, SIAM Journal of Numerical Analysis, Volume 9, Number 4, December 1972.

55. Hull, T. E. and Creemer, A. L., Efficiency Of Predictor-Corrector Procedures, Journal of the Association for Computing Machinery, Volume 10, Number 3, July 1963.

56. Hull, T. E. and Newberry, A.C.R., Integration Procedures Which Minimize Propagated Errors, SIAM Journal, Volume 9, Number 1, March 1961.

57. Hung, J. W., et al., Investigation Of Numerical Techniques As Applied To Digital Flight Control Systems, AFFDL-TR-66-68, February 1967.

58. Hurt, James M., New Difference Equation Technique For Solving non-linear Differential Equations, Proceedings - Spring Joint Computer Conference, 1964.

59. Huskey, H. D. and Korn, G. A., Computer Handbook, McGraw-Hill Book Co., Inc., 1962.

60. Jackson, Albert S., Analog Computation, McGraw-Hill Book Company, Inc., 1960.

61. Johnson, Clarence L., Analog Computer Techniques, McGraw-Hill Book Company, Inc., 1963.

62. Karplus, Walter J., PhD., Analog Simulation (Solution of Field Problems), McGraw-Hill Book Company, Inc., 1958.

63. Karplus, Walter J., Analog Subroutines For Digital Computer Programs, Simulation, March 1965.

64. Karplus, Walter J., Error Analysis Of Hybrid Computer Systems, Simulation, February 1966.

65. Karplus, Walter J., Random Thoughts On Hybrid Computation, Simulation, September 1964.

66. Katzenelson, Jacob, On Errors Introduced By Combined Sampling And Quantization, IRE, Volume AC-7, April 1962.

67. Kelly, L. G., Handbook Of Numerical Methods And Applications, Addition-Wesley Publishing Comapny, 1967.

68. Kemp, Nelson H., Extension And Analysis Of Use Of Derivatives For Compensation Of Hybrid Solution Of Linear Differential Equations, Fall Joint Computer Conference, 1969.

69. Klein, G. A., Software Tools For Evaluating The Effects Of Finite Wordlength, Master Thesis, December 1977.

70. Klophenstein, R. W. and Millman, R. S., Numerical Stability Of A One-Evaluation Predictor-Corrector Algorithm For Numerical Solution Of Ordinary Differential Equations, Mathematics of Computation, Volume 22, 1968.

71. Knowles, J. B. and Edwards, R., Effect Of A Finite-Word-Length Computer In A Sampled-Data Feedback System, Proceedings of the IEEE, Volume 112, Number 6, June 1965.

72. Korn, G. A. and Korn, T. M., Electronic Analog And Hybrid Computers, Second Edition, McGraw-Hill Book Company, 1972.

73. Krogh, Fred T., On Testing A Subroutine For The Numerical Integration Of Ordinary Differential Equations, Journal of the Association for Computing Machinery, Volume 20, Number 4, October 1973.

74. Macnee, A. B., Some Limitations On The Accuracy Of Electronic Differential Analyzers, proceedings of the IRE, Volume 40, Number 3, March 1952.

75. Magg, W. and Wehrli, R., A Survey On Rounding Effects In Floating-Point Arithmetic, 1977.

76. Mantey, Patrick E., State-Variable Selection For Efficient Computer Implementation Of Linear Discrete Systems, Proceeding of NEC, Chicago, 1967.

77. Marsocci, Velio A., An Error Analysis Of Electronic Analog Computers, IRE Transactions on Electronic Computers, Volume EC-5, Number 4, December 1956.

78. Martin, D. W., Runge-Kutta Methods For Integrating Differential Equations On High Speed Digital Computers, Computer Journal, Volume 1, Number 3, October 1958.

79. McCalla, Thomas Richard, Introduction To Numerical Methods And Fortran Programming, John Wiley & Sons, Inc., 1967.

80. McCollum, P. A. and Brown, B. F., Laplace Transform Tables and Theorems, Holt, Rinehart and Wilson Inc., 1965.

81. Miesser, Wayne W., Error Curves (Technical Comment), Simulation, May 1967.

82. Meissinger, H. F., Parameter Influence Coefficients And Weighting Functions Applied To Perturbation Analysis Of Dynamic Systems, Proceedings of the 3rd International Congress, AICA, 1961.

83. Miller, G. Kimball, Jr., and Riley, Donald R., Evaluation Of Several Secondary Tasks In The Determination Of Permissible Time Delays In Simulator Visual And Motion Cues, NASA Technical Paper 1214, 1978.

84. Miller, K. S. and Murray, F. J., A Mathematical Basis For An Error Analysis Of Differential Analyzers, MIT Journal of Mathematics and Physics, Volume 32, 1953.

85. Milne, W. E. and Reynolds, R. R., Fifth-Order Methods For The Numerical Solution Of Ordinary Differential Equations, Journal of the Association for Computing Machinery, January 1962.

86. Miura, T. and Iwata, J., Effects Of Digital Execution Time In A Hybrid Computer, AFIPS Conference Proceedings, Volume 24, 1963.

87. Miura, T. and Iwata, J., Study On Time-Shared Analog Computation Technique, Simulation, November 1965.

88. Murray, F. J., Mathematical Error Analysis For Continuous Computers, Project Cyclone Symposium II, Part 2.

89. Nelson, Don J., Digital Differential Analyzer Error Analysis Using Sampled Data Techniques, Proceedings, Spring Joint Computer Conference, Volume 21, 1962.

90. Nigro, Bart J., et al., A Digital Computer Program For Deriving Optimum Numerical Integration Techniques For Real Time Flight Simulation, 1967.

91. Nigro, Bart J., An Investigation Of Optimally Stable Numerical Integration Methods With Application To Real Time Simulation, Simulation, November 1969.

92. Nigro, B. J., Technical Note On Numerical Integration (Technical Note), Simulation, April 1968.

93. Nixon, F. E., Handbook Of LaPlace Transforms, Prentice-Hall, Inc., 1960.

94. Nordsieck, Arnold, On Numerical Integration Of Ordinary Differential Equations, Mathematics of Computation, Volume 16, 1962.

95. Northrop Corporation, Dynamics Of The Airframe, BuAer Report AE-61-4II, September 1952.

96. Northrop Corporation, Methods Of Analysis And Synthesis Of Piloted Aircraft Flight Control Systems, BuAer Report AE-61-4I, March 1952.

97. Piovoso, Michael Joseph, Digital Simulation Using Poisson Transform Sequences, June 1969.

98. Powell, David J. and Akhter, Mahboob, Multi-Calculation Rate Simulations, November 1977.

99. Precision Filters Inc. , Aliasing And Anti-Alias Filters-Application Note.

100. Rademacher, Hans A., On The Accumulation Of Errors In Processes Of Integration On High-Speed Calculating Machines, Process Of A Symposium On Large Scale Digital Calculating Machinery, 1948.

101. Rahme, H. S., A New Look At The Numerical Integration Of Ordinary Differential Equations, Grumman Research Department, Memo RM-310, February 1966.

102. Ralston, Anthony, Relative Stability In The Numerical Solution Of Ordinary Differential Equations, SIAM Review, Volume 7, Number 1, January 1965.

103. Rogers, A. E. and Connolly, T. W., Analog Computation In Engineering Design, McGraw-Hill Book Company, Inc., 1960.

104. Roskam, Jan, On Some Linear And Nonlinear Stability And Response Characteristics Of Rigid Airplanes And A New Method To Integrate Nonlinear Ordinary Differential Equations, PhD Thesis, May 1965.

105. Rubin, Arthur I., Hybrid Techniques For Generation Of Arbitarary Functions, Simulation, December 1966.

106. Rubinoff, Morris, Digital Computers For Real-Time Simulation, Association for Computing Machinery, Volume 1, Number 3, July 1955.

107. Sabin, Marc L., A Study Of Tunable Integration And Control Theory For The Analysis Of Differential Equation Solvers, SRL-TR-77-0006, May 1977.

108. Scarritt, Nathan S., A Generalized Predictor-Corrector Method For The Solution Of Systems Of Ordinary Differential Equations, September 1966.

109. Shinners, Stanley M., Which Computer....Analog, Digital, or Hybrid, Machine Design, January 1971.

110. Spicer, J. A., Solving Time Varying And Coupled Nonlinear Systems Of Differential Equations By The Self Starting Predictor Algorithm Of Arbitrary Order Using Exact Stability, Proceedings Of Hawaii International Conference on System Sciences, 1974.

111. Tracy, F.T. and Kirkland, J. L., Stability Analysis Of Linear And Nonlinear Dynamic Finite Element Method Programs, 1974.

112. Tustin, A., A Method Of Analysing The Behaviour Of Linear Systems In Terms Of Time Series, Institute of Electronic Engineers Journal, Volume 94, Part II, May 1947.

113. University of Michigan, Engineering Summer Conferences, Hybrid Computation, A One-Week Intensive Course For Engineers and Scientists, July 1965.

114. Van Der Houwen, P. J., One Step Methods For Linear Initial Value Problems 1 Polynominal Methods, Available from DDC as AD 883761.

115. Verwer, J. G., A Two-Step Runge-Kutta Method Of Third Order With Extended Stability Region, Available from DDC as AD 913350.

116. Vichnevetsky, Robert, Error Analysis In The Computer Simulation Of Dynamic Systems: Variational Aspects Of The Problem, Volume EC-16, Number 4, August 1967.

117. Vichnevetsky, R., A New Method Of Analyzing The Truncation Error In The Finite Representation Difference Of Partial Differential Operators, Simulation, March 1965.

118. Vidal, Jacques and Karplus, Walter J., Characterization And Compensation Of Quantization Errors In Hybrid Computer Sytems, Part III, March 1965.

119. Vidal, Jacques J., A Unified Approach To Deterministic And Random Errors In Hybrid Loops, Proceedings-Fall Joint Computer Conference, 1966.

120. Wait, John V., A Hybrid Analog-Digital Differential Analyzer System, Proceedings-Fall Joint Computer Conference, 1963.

121. Walli, C. R., Quantizing And Sampling Errors In Hybrid Computation, Proceedings-Fall Joint Computer Conference, 1964.

122. Westerwick, R. A., Transient Simulation Using The Transition Matrix Method.

123. Widrow, Bernard, A Study Of Rough Amplitude Quantization By Means Of Nyquist Sampling Theory, IRE Transactions PGCT, III, 1956.

124. Wilf, Herbert S., A Stability Criterion For Numerical Integration, Journal of the Association for Computing Machinery, Volume 6, Number 3, July 1959.

125. Wilkinson, J. H., Rounding Errors In Algebraic Processes, Prentice-Hall, Inc., 1963.

126. Wilson, John W. and Steinmetz, George G., Analysis Of Numerical Integration Techniques For Real-Time Digital Flight Simulation, NASA TN D-4900, November 1968.

127. Wylie, C. R., Advanced Engineering Mathematics, 4th Edition, McGraw-Hill, Inc., 1975.

128. Zondek, B. and Sheldon, J. W., On The Error Propagation In Adams' Extrapolation Method, Mathematics of Computers 13, 1959.

APPENDIX A.

THEORETICAL AIRFRAME

The longitudinal three-degree-of-freedom response of an airframe to an elevator input was considered in this study. The equations-of-motion representing this airframe are:

$$\dot{u} = X_w w + X_u u - g\theta \qquad \text{(A-1)}$$

$$\dot{w} = Z_w w + Z_u u + U_o q + Z_{\delta_e} \delta_e \qquad \text{(A-2)}$$

$$\dot{q} = M_u u + M_{\dot{w}} \dot{w} + M_w w + M_q q + M_{\delta_e} \delta_e \qquad \text{(A-3)}$$

Equation A-1 represents the forward velocity acceleration equation, while the vertical velocity acceleration and pitch acceleration equations are represented by equations A-2 and A-3, respectively.

This set of equations maintains the following assumptions:

1) The airframe is assumed to be a rigid body.
2) The earth is assumed to remain fixed in space. The earth's atmosphere is also fixed with respect to the earth.
3) The mass of the airframe is assumed to remain constant.
4) The x-z plane of the airframe is assumed to be a plane of symmetry.
5) The disturbances from the initial steady flight conditions are assumed to be small such that the products and squares of the change of velocities are negligible compared with the changes themselves. Also, the disturbance angles are assumed small enough such that the sines of these angles may be set equal to zero and the cosines set equal to one. Products of these angles are approximately zero and are therefore neglected. Air density remains a constant since the airframe perturbations are small.

6) Under steady flight conditions, the airframe is assumed to be in a wings level condition with all velocity components zero except the initial true airspeed, U_o. Stability axes are used as the reference axes; therefore, the initial vertical velocity, W_o, is zero.

7) The flow is assumed to be quasi-steady.

8) Stability derivatives whose magnitudes are small compared to the other stability derivatives are assumed to be negligible. These include:

   a) $X_{\dot{w}}$, X-force due to the rate of change of vertical velocity

   b) X_q, X-force due to pitch rate

   c) $Z_{\dot{w}}$, Z-force due to the rate of change of vertical velocity

   d) X_{δ_e}, X-force due to elevator deflection

   e) Z_q, Z-force due to pitch rate

   f) T_u, Thrust force due to the change in forward velocity

   g) $T_{\delta_{RPM}}$, Thrust force due to change of engine revolutions-per-minute

9) Under steady state conditions, the flight path is assumed to be horizontal, $\gamma_o = 0$

If equations A-1 through A-3 are considered to be a set of linear ordinary differential equations with constant coefficients, they can then be rewritten in Laplace form as:

$$(s-X_u)u(s) - X_w w(s) + g\theta(s) = 0 \qquad \text{(A-4)}$$

$$-Z_u u(s) + (s-Z_w)w(s) - sU_o\theta(s) = Z_{\delta_e}\delta_e \qquad \text{(A-5)}$$

$$-M_u u(s) - (sM_{\dot{w}}+M_w)w(s) + (s-M_q)s\theta(s) = M_{\delta_e}\delta_e \qquad \text{(A-6)}$$

Longitudinal transfer functions may then be written in determinant form for the response to an elevator deflection. For the forward velocity response,

$$\frac{u(s)}{\delta_e(s)} = \frac{\begin{vmatrix} 0 & -X_w & g \\ Z_{\delta_e} & (s-Z_w) & -sU_o \\ M_{\delta_e} & -(sM_{\dot{w}}+M_w) & (s-M_q)s \end{vmatrix}}{\begin{vmatrix} (s-X_u) & -X_w & g \\ -Z_u & (s-Z_w) & -sU_o \\ -M_u & -(sM_{\dot{w}}+M_w) & (s-M_q)s \end{vmatrix}} \qquad \text{(A-7)}$$

which reduces to the following linear transfer function form:

$$\frac{u(s)}{\delta_e(s)} = \frac{A_u s^2 + B_u s + C_u}{D_1} \qquad \text{(A-8)}$$

where:

$$A_u = Z_{\delta_e} X_w \qquad \text{(A-9)}$$

$$B_u = -Z_{\delta_e}(gM_{\dot{w}}+M_q X_w) + M_{\delta_e}(U_o X_w - g) \qquad \text{(A-10)}$$

$$C_u = g(M_{\delta_e} Z_w - M_w Z_{\delta_e}) \qquad \text{(A-11)}$$

Also,

$$D_1 = As^4 + Bs^3 + Cs^2 + Ds + E \tag{A-12}$$

where:

$$A = 1 \tag{A-13}$$

$$B = -(M_q + X_u + Z_w + U_o M_w) \tag{A-14}$$

$$C = M_q Z_w - U_o M_w + X_u (M_q + Z_w + U_o M_w) - X_w Z_u \tag{A-15}$$

$$D = -X_u (M_q Z_w - U_o M_w) - M_u U_o X_w + M_q X_w Z_u + g(M_w Z_u + M_u) \tag{A-16}$$

$$E = g(M_w Z_u - M_u Z_w) \tag{A-17}$$

For the vertical velocity response of the airframe, the determinant form yields:

$$\frac{w(s)}{\delta_e(s)} = \frac{\begin{vmatrix} (s-X_u) & 0 & g \\ -Z_u & Z_{\delta_e} & -sU_o \\ -M_u & M_{\delta_e} & (s-M_q)s \end{vmatrix}}{D_1} \tag{A-18}$$

which reduces to the following linear transfer function:

$$\frac{w(s)}{\delta_e(s)} = \frac{A_w s^3 + B_w s^2 + C_w s + D_w}{D_1} \tag{A-19}$$

where:

$$A_w = Z_{\delta_e} \tag{A-20}$$

$$B_w = -Z_{\delta_e}(M_q + X_u) + M_{\delta_e} U_o \tag{A-21}$$

$$C_w = X_u(Z_{\delta_e} M_q - M_{\delta_e} U_o) \tag{A-22}$$

$$D_w = g(Z_{\delta_e} M_u - M_{\delta_e} Z_u) \tag{A-23}$$

Similarly, for the pitch attitude response to an elevator surface input, the determinant form yields:

$$\frac{\theta(s)}{\delta_e(s)} = \frac{\begin{vmatrix} (s-X_u) & -X_w & 0 \\ -Z_u & (s-Z_w) & Z_{\delta_e} \\ -M_u & -(sM_{\dot{w}}+M_w) & M_{\delta_e} \end{vmatrix}}{D_1} \tag{A-24}$$

which reduces to:

$$\frac{\theta(s)}{\delta_e(s)} = \frac{A_\theta s^2 + B_\theta s + C_\theta}{D_1} \tag{A-25}$$

where:

$$A_\theta = Z_{\delta_e} M_{\dot{w}} + M_{\delta_e} \tag{A-26}$$

$$B_\theta = Z_{\delta_e} (M_w - M_{\dot{w}} X_u) - M_{\delta_e} (X_u + Z_w) \tag{A-27}$$

$$C_\theta = Z_{\delta_e} (M_u X_w - M_w X_u) + M_{\delta_e} (X_u Z_w - X_w Z_u) \tag{A-28}$$

Having established linear transfer functions representing the forward velocity, vertical velocity, and pitch attitude responses of the airframe, the following numerical values were used for the aircraft mechanization utilized in this study:

$$\left.\begin{aligned} X_w &= 0.0016 \\ X_u &= -0.0097 \\ Z_w &= 1.43 \\ Z_u &= -0.0955 \\ Z_{\delta_e} &= 69.8 \\ M_u &= 0.0 \\ M_w &= -0.0235 \\ M_q &= 1.92 \\ M_{\delta_e} &= 26.1 \\ M_{\dot{w}} &= -0.0013 \\ U_o &= 660.0 \\ g &= 32.1725 \end{aligned}\right\} \tag{A-29}$$

Combining equations A-29 with A-8 through A-28, the longitudinal transfer functions reduce to:

$$\frac{u(s)}{\delta e(s)} = \frac{1.54627073\ (s^2-7251.566697s-10295.4342)}{\left(\frac{s^2}{\omega_{n_p}^2}+\frac{2\zeta_p s}{\omega_{n_p}}+1\right)\left(\frac{s^2}{\omega_{n_{sp}}^2}+\frac{2\zeta_{sp} s}{\omega_{n_{sp}}}+1\right)} \qquad \text{(A-30)}$$

$$\frac{\Delta\alpha(s)}{\delta_e(s)} = \frac{1}{U_o}\left(\frac{w(s)}{\delta_e(s)}\right) = \frac{1.4640093\ (s^3+248.46705s^2+2.4126074s+1.1497135)}{\left(\frac{s^2}{\omega_{n_p}^2}+\frac{2\zeta_p s}{\omega_{n_p}}+1\right)\left(\frac{s^2}{\omega_{n_{sp}}^2}+\frac{2\zeta_{sp} s}{\omega_{n_{sp}}}+1\right)} \qquad \text{(A-31)}$$

$$\frac{\theta(s)}{\delta_e(s)} = \frac{360.0582073\ (s^2+1.38254518s+0.01346405)}{\left(\frac{s^2}{\omega_{n_p}^2}+\frac{2\zeta_p s}{\omega_{n_p}}+1\right)\left(\frac{s^2}{\omega_{n_{sp}}^2}+\frac{2\zeta_{sp} s}{\omega_{n_{sp}}}+1\right)} \qquad \text{(A-32)}$$

where:

$$\left.\begin{aligned} \omega_{n_p} &= 0.06292853 \quad \text{radians/second} \\ \zeta_p &= 0.07158915 \\ \omega_{n_{sp}} &= 4.27106544 \quad \text{radians/second} \\ \zeta_{sp} &= 0.49285126 \end{aligned}\right\} \qquad \text{(A-33)}$$

For an exponential elevator surface input of:

$$\delta_e(t) = e^{-ft} \Rightarrow \delta_e(s) = \frac{K_1}{s+f} \tag{A-34}$$

equations A-30 and A-32 then have the form of:

$$f(s) = \frac{K_1 K(s^2+a_1 s+a_o)}{(s+f)\left(\frac{s^2}{\omega_{n_1}^2} + \frac{2\zeta_1 s}{\omega_{n_1}} +1\right)\left(\frac{s^2}{\omega_{n_2}^2} + \frac{2\zeta_2 s}{\omega_{n_2}} +1\right)} \tag{A-35}$$

Taking the inverse Laplace transform of A-35, the time history response is obtained as:

$$f(t) = \omega_{n_1}^2 \omega_{n_2}^2 K_1 K \left[A\, e^{-ft} + \frac{1}{\omega_{n_1}\sqrt{1-\zeta_1^2}} \sqrt{B}\, e^{-\zeta_1 \omega_{n_1} t} \cos\left(\omega_{n_1}\sqrt{1-\zeta_1^2}\, t - \phi_1\right) \right.$$
$$\left. + \frac{1}{\omega_{n_2}\sqrt{1-\zeta_2^2}} \sqrt{C}\, e^{-\zeta_2 \omega_{n_2} t} \cos\left(\omega_{n_2}\sqrt{1-\zeta_2^2}\, t - \phi_2\right) \right] \tag{A-36}$$

where:

$$A = \frac{f^2 - a_1 f + a_o}{\left[(\zeta_1\omega_{n_1} - f)^2 + \omega_{n_1}^2(1-\zeta_1^2)\right]\left[(\zeta_2\omega_{n_2} - f)^2 + \omega_{n_2}^2(1-\zeta_2^2)\right]} \tag{A-37}$$

$$B = \frac{\left[\zeta_1^2\omega_{n_1}^2 - \omega_{n_1}^2(1-\zeta_1^2) - a_1\zeta_1\omega_{n_1} + a_o\right]^2 + \omega_{n_1}^2(1-\zeta_1^2)(a_1 - 2\zeta_1\omega_{n_1})^2}{\left[(f-\zeta_1\omega_{n_1})^2 + \omega_{n_1}^2(1-\zeta_1^2)\right]\left\{\left[(\zeta_2\omega_{n_2} - \zeta_1\omega_{n_1})^2 + \omega_{n_1}^2(1-\zeta_1^2) - \omega_{n_2}^2(1-\zeta_2^2)\right]^2 + 4\omega_{n_2}^2(1-\zeta_2^2)(\zeta_2\omega_{n_2} - \zeta_1\omega_{n_1})^2\right\}} \tag{A-38}$$

$$C = \frac{\left[\zeta_2^2\omega_{n_2}^2 - \omega_{n_2}^2(1-\zeta_2^2) - a_1\zeta_2\omega_{n_2} + a_o\right]^2 + \omega_{n_2}^2(1-\zeta_2^2)(a_1 - 2\zeta_2\omega_{n_2})^2}{\left[(f-\zeta_2\omega_{n_2})^2 + \omega_{n_2}^2(1-\zeta_2^2)\right]\left\{\left[(\zeta_2\omega_{n_2} - \zeta_1\omega_{n_1})^2 + \omega_{n_1}^2(1-\zeta_1^2) - \omega_{n_2}^2(1-\zeta_2^2)\right]^2 + 4\omega_{n_2}^2(1-\zeta_2^2)(\zeta_2\omega_{n_2} - \zeta_1\omega_{n_1})^2\right\}} \tag{A-39}$$

$$\phi_1 = \tan^{-1}\left[\frac{\zeta_1^2\omega_{n_1}^2 - \omega_{n_1}^2(1-\zeta_1^2) - a_1\zeta_1\omega_{n_1} + a_o}{\omega_{n_1}\sqrt{1-\zeta_1^2}\,(a_1-2\zeta_1\omega_{n_1})}\right] + \tan^{-1}\left(\frac{\omega_{n_1}\sqrt{1-\zeta_1^2}}{f-\zeta_1\omega_{n_1}}\right)$$

$$+ \tan^{-1}\left[\frac{2\omega_{n_1}\sqrt{1-\zeta_1^2}(\zeta_2\omega_{n_2}-\zeta_1\omega_{n_1})}{(\zeta_2\omega_{n_2}-\zeta_1\omega_{n_1})^2 + \omega_{n_2}^2(1-\zeta_2^2) - \omega_{n_1}^2(1-\zeta_1^2)}\right] \qquad \text{(A-40)}$$

$$\phi_2 = \tan^{-1}\left[\frac{\zeta_2^2\omega_{n_2}^2 - \omega_{n_2}^2(1-\zeta_2^2) - a_1\zeta_2\omega_{n_2} + a_o}{\omega_{n_2}\sqrt{1-\zeta_2^2}\,(a_1-2\zeta_2\omega_{n_2})}\right] + \tan^{-1}\left(\frac{\omega_{n_2}\sqrt{1-\zeta_2^2}}{f-\zeta_2\omega_{n_2}}\right)$$

$$+ \tan^{-1}\left[\frac{2\omega_{n_2}\sqrt{1-\zeta_2^2}\,(\zeta_1\omega_{n_1}-\zeta_2\omega_{n_2})}{(\zeta_2\omega_{n_2}-\zeta_1\omega_{n_1})^2 + \omega_{n_1}^2(1-\zeta_1^2) - \omega_{n_2}^2(1-\zeta_2^2)}\right] \qquad \text{(A-41)}$$

Substituting the numerator coefficients of equation A-32:

$a_o = 0.01346405$

$a_1 = 1.38254518$

$K = 360.0582073$

and $f = 5.0$

along with equations A-33 into equations A-36 through A-41, the theoretical pitch attitude response is obtained as:

$$\theta(t) = 26.01K_i\left[0.03267941e^{-5t}\right.$$
$$+ 0.01509994e^{-.004505t}\cos(0.06276707t-0.06548318) \qquad \text{(A-42)}$$
$$\left.+ 0.0506577e^{-2.10499998t}\cos(3.71631202t-2.80095432)\right]$$

Substituting the numerator coefficients of equations A-30:

$$a_o = -10295.4342$$
$$a_1 = -7251.566697$$
$$K = 1.54627073$$
$$\text{and } f = 5.0$$

along with equations A-33 into equations A-36 through A-41, the theoretical forward velocity perturbation response is obtained as:

$$u(t) = 0.1117K_i\left[46.91813685e^{-5t}\right.$$
$$+1797.934575e^{-.004505t}\cos(0.06276707t-4.69510339) \qquad \text{(A-43)}$$
$$\left.+85.9481544e^{-2.10499998t}\cos(3.71631202t-1.75616825)\right]$$

For the angle-of-attack perturbation, if the elevator surface input described by equation A-34 is combined with equation A-31, the Laplacian response then takes the form:

$$f(s) = \frac{K_i K(s^3+a_2s^2+a_1s+a_o)}{(s+f)\left(\frac{s^2}{\omega_{n_1}^2}+\frac{2\zeta_1 s}{\omega_{n_1}}+1\right)\left(\frac{s^2}{\omega_{n_2}^2}+\frac{2\zeta_2 s}{\omega_{n_2}}+1\right)} \qquad \text{(A-44)}$$

Taking the inverse Laplace transform of A-44, the time history response is obtained as:

$$f(t) = \omega_{n_1}^2 \omega_{n_2}^2 K_i K \left[A\, e^{-ft} + \frac{1}{\omega_{n_1}\sqrt{1-\zeta_1^2}} \sqrt{B}\, e^{-\zeta_1 \omega_{n_1} t} \cos\left(\omega_{n_1}\sqrt{1-\zeta_1^2}\, t - \phi_1\right) \right. \tag{A-45}$$

$$\left. + \frac{1}{\omega_{n_2}\sqrt{1-\zeta_2^2}} \sqrt{C}\, e^{-\zeta_2 \omega_{n_2} t} \cos\left(\omega_{n_2}\sqrt{1-\zeta_2^2}\, t - \phi_2\right) \right]$$

where:

$$A = \frac{-f^3 + a_2 f^2 - a_1 f + a_o}{\left[(\zeta_1\omega_{n_1} - f)^2 + \omega_{n_1}^2(1-\zeta_2^2)\right]\left[(\zeta_2\omega_{n_2} - f)^2 + \omega_{n_2}^2(1-\zeta_2^2)\right]} \tag{A-46}$$

$$B = \frac{\left\{\zeta_1\omega_{n_1}\left[3\omega_{n_1}^2(1-\zeta_1^2) - \zeta_1^2\omega_{n_1}^2\right] + a_2\left[\zeta_1^2\omega_{n_1}^2 - \omega_n^2(1-\zeta_1^2)\right] - a_1\zeta_1\omega_{n_1} + a_o\right\}^2 + \omega_{n_1}^2(1-\zeta_2^2)\left[3\zeta_1^2\omega_{n_1}^2 - \omega_{n_1}^2(1-\zeta_1^2) - 2a_2\zeta_1\omega_{n_1} + a_1\right]^2}{\left[(f-\zeta_1\omega_{n_1})^2 + \omega_{n_1}^2(1-\zeta_1^2)\right]\left\{\left[(\zeta_2\omega_{n_2} - \zeta_1\omega_{n_1})^2 + \omega_{n_1}^2(1-\zeta_1^2) - \omega_{n_2}^2(1-\zeta_2^2)\right]^2 + 4\omega_{n_2}^2(1-\zeta_2^2)(\zeta_2\omega_{n_2} - \zeta_1\omega_{n_1})^2\right\}} \tag{A-47}$$

$$C = \frac{\left\{\zeta_2\omega_{n_2}\left[3\omega_{n_2}^2(1-\zeta_2^2) - \zeta_2^2\omega_{n_2}^2\right] + a_2\left[\zeta_2^2\omega_{n_2}^2 - \omega_{n_2}^2(1-\zeta_2^2)\right] - a_1\zeta_2\omega_{n_2} + a_o\right\}^2 + \omega_{n_2}^2(1-\zeta_2^2)\left[3\zeta_2^2\omega_{n_2}^2 - \omega_{n_2}^2(1-\zeta_2^2) - 2a_2\zeta_2\omega_{n_2} + a_1\right]^2}{\left[(f-\zeta_2\omega_{n_2})^2 + \omega_{n_2}^2(1-\zeta_2^2)\right]\left\{\left[(\zeta_2\omega_{n_2}-\zeta_1\omega_{n_1})^2 + \omega_{n_1}^2(1-\zeta_1^2) - \omega_{n_2}^2(1-\zeta_2^2)\right]^2 + 4\omega_{n_2}^2(1-\zeta_2^2)(\zeta_2\omega_{n_2}-\zeta_1\omega_{n_1})^2\right\}} \quad \text{(A-48)}$$

$$\phi_1 = \tan^{-1}\left\{\frac{\zeta_1\omega_{n_1}\left[3\omega_{n_1}^2(1-\zeta_1^2) - \zeta_1^2\omega_{n_1}^2\right] + a_2\left[\zeta_1^2\omega_{n_1}^2 - \omega_{n_1}^2(1-\zeta_1^2)\right] - a_1\zeta_1\omega_{n_1} + a_o}{\omega_{n_1}\sqrt{1-\zeta_1^2}\left[3\zeta_1^2\omega_{n_1}^2 - \omega_{n_1}^2(1-\zeta_1^2) - 2a_2\zeta_1\omega_{n_1} + a_1\right]}\right\}$$

$$+ \tan^{-1}\left[\frac{2\omega_{n_1}\sqrt{1-\zeta_1^2}\,(\zeta_2\omega_{n_2}-\zeta_1\omega_{n_1})}{(\zeta_2\omega_{n_2}-\zeta_1\omega_{n_1})^2 - \omega_{n_1}^2(1-\zeta_1^2) + \omega_{n_2}^2(1-\zeta_2^2)}\right] \quad \text{(A-49)}$$

$$+ \tan^{-1}\left[\frac{\omega_{n_1}\sqrt{1-\zeta_1^2}}{f-\zeta_1\omega_{n_1}}\right]$$

$$\phi_2 = \tan^{-1}\left\{\frac{\zeta_2\omega_{n_2}\left[3\omega_{n_2}^2(1-\zeta_2^2) - \zeta_2^2\omega_{n_2}^2\right] + a_2\left[\zeta_2^2\omega_{n_2}^2 - \omega_{n_2}^2(1-\zeta_2^2)\right] - a_1\zeta_2\omega_{n_2} + a_o}{\omega_{n_2}\sqrt{1-\zeta_2^2}\left[3\zeta_2^2\omega_{n_2}^2 - \omega_{n_2}^2(1-\zeta_2^2) - 2a_2\zeta_2\omega_{n_2} + a_1\right]}\right\}$$

$$+ \tan^{-1}\left[\frac{2\omega_{n_2}\sqrt{1-\zeta_2^2}\,(\zeta_1\omega_{n_1} - \zeta_2\omega_{n_2})}{(\zeta_2\omega_{n_2} - \zeta_1\omega_{n_1})^2 - \omega_{n_1}^2(1-\zeta_1^2) + \omega_{n_2}^2(1-\zeta_2^2)}\right] \qquad \text{(A-50)}$$

$$+ \tan^{-1}\left[\frac{\omega_{n_2}\sqrt{1-\zeta_2^2}}{f-\zeta_2\omega_{n_2}}\right]$$

Now, substituting the numerator coefficients of equation A-31:

$$a_o = 1.1497135$$

$$a_1 = 2.4126074$$

$$a_2 = 248.46705$$

$$K = 1.4640093$$

and $f = 5.0$

along with equations A-33 into equation A-45 through A-50, the theoretical angle-of-attack response is obtained as:

$$\Delta\alpha(t) = 0.1057576K_i\left[10.969296e^{-5t}\right. \qquad \text{(A-51)}$$

$$+ 0.028947501e^{-.004505t}\cos(0.06276707t - 1.5332583)$$

$$\left. + 14.071923e^{-2.10499998t}\cos(3.71631202t - 2.4648131)\right]$$

Hence, closed-form solutions to linearized longitudinal equations-of-motion have been derived utilizing Laplacian methods and are depicted in equations A-42, A-43, and A-51 for the pitch attitude, forward velocity, and angle-of-attack responses, respectively.

APPENDIX B.

SIGNAL ANALYSIS FOR THE INVESTIGATION OF COMPUTER ERRORS

The Bode analysis program generates Power Spectral Densities Bode gain and phase angle plots and Accuracy Charts for arbitrary time histories. The program is totally user interactive and contains many plot options. In the Bode program, the gain and phase angle generated is plotted relative to a specific sinusoidal forcing function at various frequencies. The same results however can be generated by measuring the system output as a function of a sum-of-sines forcing function. In this study, 512 sine waves (with various frequencies) were summed for each cycle of the digital computer to create the airframe forcing function. Airframe response due to this sum-of-sines surface input then constituted a valid output response for a Bode analysis.

The Bode analysis itself utilizes Fast Fourier Transforms to create a Power Spectral Density (PSD) from a time history response. Initially, the time history vector is transformed to a complex frequency vector. For a system input variable (such as elevator surface), the process is defined as:

$$x_t = X_\omega \tag{B-1}$$

Similarly, for an output variable (such as pitch attitude, angle of attack, and forward velocity), the process is defined as:

$$y_t = Y_\omega \tag{B-2}$$

The PSD is then defined as:

$$G_{xx} = X_\omega X_\omega^* \tag{B-3}$$

$$G_{yy} = Y_\omega Y_\omega^* \tag{B-4}$$

Where:

X_ω^* = complex conjugate of X_ω

Y_ω^* = complex conjugate of Y_ω

The parameter G_{yy} was the main variable of interest in the investigation of the effects of error sources on airframe solution accuracy, as presented in Section 4. The variable Δdb, as defined in Section 4, was the difference between the power of the simulated (numerical) system and the power of the theoretical (analytical) solution.

For Bode plot generation, the cross-spectra was obtained as:

$$G_{xy} = X_\omega Y_\omega \tag{B-5}$$

The Bode gain and Phase, respectively were then generated by:

$$|G| = \frac{G_{yy}}{G_{xx}} \tag{B-6}$$

and

$$\phi = \tan^{-1} \left(\frac{\text{Imaginary Part of } G_{xy}}{\text{Real Part of } G_{xy}}\right) \tag{B-7}$$

In Section 5, which discusses the effects of digital computer frame time, $|G|$ and ϕ were plotted against frequency, ω.

After Bode gain and phase information is generated for both the numerical and theoretical systems, the accuracy error is generated by:

$$e = \frac{\left| G^{th}_{(j\omega)} - G_{(j\omega)} \right|}{G^{th}_{(j\omega)}} \qquad \text{(B-8)}$$

where $G^{th}_{(j\omega)} \equiv$ complex gain of theoretical system

and

$G_{(j\omega)} \equiv$ complex gain of numerical system.

In Section 5, the accuracy chart plotted e as a function of frequency ω.